

Project No:
764697

Project acronym:
CHEERS

Project full title:
Chinese-European Emission-Reducing Solutions

Type of Action: **RIA**

Call/Topic:
European Horizon 2020 Work Programme 2016 – 2017, 10. 'Secure, Clean and Efficient Energy',
under the low-carbon energy initiative LCE-29-2017: *CCS in Industry, including BioCCS*

Start-up: 2017-10-01

Duration: 60 months

**Deliverable D3.3:
Oxygen-carrier validation
in CLC pilot units**

Due submission date: 2021-05-31

Actual delivery date: 2021-05-31

Organisation name of lead beneficiary for this deliverable:
SINTEF Energi AS

Project funded by the European Union's Horizon 2020 research and innovation programme under grant agreement No 764697, and co-funded by the Chinese Ministry of Science and Technology (MOST)		
Dissemination Level		
PU	Public	X
CO	Confidential, only for members of the consortium (including the Commission Services and MOST)	
INT	Confidential, only for members of the consortium	

Deliverable number:	D3.3
Deliverable title:	Oxygen-carrier validation in CLC pilot units
Deliverable description:	
Work package:	WP3 Oxygen carriers and characterisation of fuel conversion phenomena
Lead participant:	SINTEF ER

Revision Control (only when a submitted deliverable is revised)			
Revision	Date	Author(s)	Comments

Quality assurance, status of deliverable		
Action	Performed by	Date
Delivered	Jointly by all authors mentioned below	2021-05-31
Verified (Work Package leader)	Øyvind Langørgen (SINTEF ER)	2021-05-31
Approved (Management Support Team)	By e-mail	2021-06-15
Endorsed (Executive Board)	By e-mail	2021-06-30
Submitted to the European Commission	Nils Haugen (SINTEF ER)	2021-06-30

Author(s)		
Name	Organisation	E-mail address (optional)
Nicolas Vin	IFPEN	
Arnold Lambert	IFPEN	
Kristina Bakoc	IFPEN	
Stéphane Bertholin	IFPEN	
Zuoan Li	SINTEF MK	
Yngve Larring	SINTEF MK	
Inge Saanum	SINTEF ER	
Roger Khalil	SINTEF ER	
Øyvind Langørgen	SINTEF ER	

Table of Contents

	Page
0 PREFACE	10
0.1 Disclaimer.....	10
1 EXECUTIVE SUMMARY	11
2 PILOT UNITS.....	12
2.1 Pilot unit at SINTEF.....	12
2.1.1 Reactor system.....	12
2.1.2 Modifications to the reactor system.....	14
2.1.3 Evaluation of process and oxygen carrier performance	14
2.1.4 Uncertainties in results evaluation	17
2.2 Pilot unit at IFPEN	19
2.2.1 Reactor system.....	19
2.2.2 Evaluation of fuel conversion and oxygen carrier reduction degree.....	20
3 OXYGEN CARRIERS	23
3.1 First oxygen carrier – Ilmenite T1	23
3.2 Second oxygen carrier – Mn ore LY	24
3.3 Third oxygen carrier – Ilmenite T2	28
4 FUELS	29
4.1 Petcoke.....	29
4.2 Biomass	30
5 RESULTS WITH FIRST OXYGEN CARRIER – ILMENITE T1	31
5.1 SINTEF ER	31
5.1.1 Overview of tests	31
5.1.2 Summary of main test results	31
5.1.3 FR gas conversion efficiency and capture rate	32
5.1.4 Solid circulation and oxygen carrier conversion	37
5.1.5 Oxygen carrier characterisation.....	38
5.1.6 Agglomeration tests.....	43
5.2 IFPEN	47
5.2.1 Operating conditions.....	47
5.2.2 Ilmenite agglomeration.....	49
5.2.3 Ilmenite activation	51
5.2.4 Petcoke reactivity tests.....	53
5.2.5 OC characterization.....	57
5.2.6 Lessons learned from unit operation.....	62
5.3 Discussion and conclusions of Ilmenite T1	64

6	RESULTS WITH SECOND OXYGEN CARRIER – MN ORE LY.....	65
6.1	IFPEN	65
6.1.1	Performance tests in batch unit.....	65
6.1.2	Performance tests in 10 kW continuous pilot unit with LY Mn ore.....	67
6.1.3	After petcoke injection (end of campaign)	77
6.1.4	Fines production	79
6.1.5	Agglomeration phenomena	80
6.1.6	Lessons learned from unit operation.....	81
6.2	SINTEF ER	83
6.2.1	Main test results	83
6.2.2	Oxygen carrier characterisation.....	86
6.2.3	Agglomeration and operability	91
6.2.4	Summary from operation of Mn-ore LY in 150 kW unit	92
7	RESULTS WITH THIRD OXYGEN CARRIER – ILMENITE T2.....	94
7.1	IFPEN	94
7.1.1	Ageing tests results	94
7.1.2	Kinetic screening	98
7.1.3	Ilmenite T2 test with water addition	99
7.2	SINTEF MK.....	103
7.2.1	Attrition testing of ilmenite T2 (vs Mn-ore LY)	103
7.2.2	Kinetics of ilmenite T2 vs other candidate materials.....	105
7.3	SINTEF ER	106
7.3.1	Main test results	106
7.3.2	Oxygen carrier characterisation.....	107
7.3.3	Agglomeration and operability	110
7.3.4	Summary from operation of ilmenite T2 in 150 kW unit.....	111
8	CONCLUSIONS.....	113
9	REFERENCES.....	115
A	MODIFICATIONS DONE AT SINTEF ER PILOT UNIT	116
B	SUMMARY OF MAIN RESULTS SINTEF ER PILOT UNIT	119

Table of Figures

	Page
Figure 2-1: Schematic overview of CLC pilot unit system at SINTEF ER.	12
Figure 2-2: CLC pilot unit at SINTEF ER placed in tent hall, control room and new fuel screw feeder.	13
Figure 2-3: Typical reactor temperatures history for one day test (January 28 th , 2021).	14
Figure 2-4: 3D scheme of the pilot unit at IFPEN.	19
Figure 3-1: Ilmenite T1 particle size distribution.	23
Figure 3-2: Fresh ilmenite, size fraction 38 – 122 μm as delivered to SINTEF ER after sieving.	24
Figure 3-3: Cross-section SEM pictures of LY-Mn ore.	25
Figure 3-4: SEM pictures of LY-Mn ore powder.	26
Figure 3-5: Particle size distribution of the original Ly Mn ore shipped to IFPEN.	26
Figure 3-6: PSD of Mn-ore LY after sieving at SINTEF ER.	27
Figure 3-7: Mn-ore LY batch SINTEF ER as received (left) and after sieving (right).	27
Figure 3-8: Particle size distribution of ilmenite T2 compared to ilmenite T1.	28
Figure 3-9: Picture of ilmenite T2.	28
Figure 4-1: Petcoke, here shown size fraction 315 – 500 μm	30
Figure 4-2: Arbaflame wood pellets. Whole (left), milled and sieved > 800 μm (mid), milled and un-sieved (right).	30
Figure 5-1: CO ₂ capture rate.	33
Figure 5-2: Fuel reactor gas conversion efficiency.	33
Figure 5-3: Reactor temperatures, test with biomass pellets (September 21st, 2018).	34
Figure 5-4: Exhaust gas composition from FR and AR, test with biomass pellets (September 21st, 2018).	35
Figure 5-5: Reactor temperatures, test with biomass powder (milled and sieved pellets), mix 50/50 biomass powder/petcoke 315-500 μm , and only petcoke 315 – 500 μm (June 7 th , 2019).	35
Figure 5-6: Exhaust gas composition, biomass powder (June 7 th , 2019).	36
Figure 5-7: Exhaust gas composition, mix 50/50 biomass powder/petcoke (June 7 th , 2019).	36
Figure 5-8: Exhaust gas composition, only petcoke (June 7 th , 2019).	36
Figure 5-9: Pressure profile up along reactor height from experiment.	38
Figure 5-10: Fresh ilmenite T1. SEM atomic mass contrast (left) and EDS Fe, Mn, Ti oxides (right). Analysed in May 2018. NOTE! This is from a larger size fraction than used in the present tests.	39
Figure 5-11: Sample from FR bucket. SEM atomic mass contrast (left) and EDS Fe, Mn, Ti oxides (right).	40
Figure 5-12: Sample from FR chamber. SEM atomic mass contrast (left) and EDS Fe, Mn, Ti oxides (right).	40
Figure 5-13: Sample from AR bucket. SEM atomic mass contrast (left) and EDS Fe, Mn, Ti oxides (right).	41
Figure 5-14: Sample from AR chamber. SEM atomic mass contrast (left) and EDS Fe, Mn, Ti oxides (right).	41
Figure 5-15: Optical images, bright field. FR bucket (upper left), FR chamber (bottom left), AR bucket (upper right), AR chamber (lower right).	42

Figure 5-16: Reactor temperatures during agglomeration test, day 1	43
Figure 5-17: Reactor temperatures during agglomeration test, day 2	44
Figure 5-18: Small agglomerates taken out from reactors after agglomeration test day 2. Easily broken and crushed with the fingers.....	45
Figure 5-19: SEM (left) and EDS (right) of agglomerates	45
Figure 5-20: SEM (left) and EDS (right) of agglomerates, higher magnification.....	46
Figure 5-21: Relation between solid flow rate and lift pressure drop for Ilmenite before and after the campaign, perovskite, and copper-based material.	48
Figure 5-22: (a) reconstitution of an agglomerate retrieved on the distribution plate of the fuel reactor and (b) agglomerates remaining in the fuel reactor at the end of the campaign.....	49
Figure 5-23: SEM cross-cut section of the FR agglomerate formed during the first oxidation of the OC.	50
Figure 5-24: SEM cross-cut section of the FR agglomerate recovered after the complete test.....	50
Figure 5-25: Methane conversion and $R_0\Delta X$ as a function of time and methane flow rate.	52
Figure 5-26: Methane conversion and $R_0\Delta X$ as a function of number of cycles.	53
Figure 5-27: Evolution of petcoke conversion and oxygen carrier $R_0\Delta X$ at different (a) temperature, (b) petcoke flowrate, (c) oxygen carrier flow rate, (d) bed height and (e) steam inlet fraction.....	56
Figure 5-28: X-ray diffractograms of OC samples extracted from AR2 : a) oxidized at 800°C; b) after 23h methane activation; c) after petcoke tests, recovered oxidized powder.....	58
Figure 5-29: Mass of fines recovered as a function of circulation time. Petcoke combustion was not performed on a continuous basis.....	59
Figure 5-30: SEM cross-section analysis of OC during methane activation.	60
Figure 5-31: Evolution of particles porosity during methane activation measured by mercury porosimetry.....	61
Figure 5-32: SEM cross-section analysis of OC after petcoke tests	61
Figure 5-33: SEM cross-section analysis of particles collected at filter candles – top:AR2, bottom: FR.	62
Figure 6-1: Methane conversion rate and oxygen mobilization for different materials tested in the CHEERS project	65
Figure 6-2: Photo of the agglomerates recovered at the end of the ageing test.	66
Figure 6-3: SEM pictures of LY-Mn ore particles after 250 redox cycles (left: direct observation; right: polished cross-section).....	66
Figure 6-4: X-ray diffractogram of LY Mn ore after methane ageing in batch unit	67
Figure 6-5: Correlation between oxygen carrier flowrate and pressure drop in lift leading to fuel reactor.....	68
Figure 6-6: Evolution of methane conversion during LY Mn ore activation cycles in comparison to Ilmenite T1 behaviour.....	70
Figure 6-7: Evolution of $R_0\Delta X$ during LY Mn ore activation cycles in comparison to Ilmenite T1.....	70
Figure 6-8: Effects of (a) Temperature in fuel reactor, (b) steam content in inlet gas to fuel reactor, (c) petcoke flowrate and (d) oxygen carrier flowrate on petcoke conversion in petcoke tests with LY Mn ore.....	72
Figure 6-9: Effects of (a) Temperature in fuel reactor, (b) steam content in inlet gas to fuel reactor, (c) petcoke flowrate and (d) oxygen carrier flowrate on $R_0\Delta X$ value in petcoke combustion tests with LY Mn ore	73

Figure 6-10: X-Ray Diffractogram of LY-Mn ore after methane activation	74
Figure 6-11: SEM pictures of LY-Mn ore powder after methane activation	75
Figure 6-12: Cross-section SEM pictures of LY-Mn ore particles after methane activation	76
Figure 6-13: X-Ray Diffractogram of LY-Mn ore after test campaign.....	77
Figure 6-14: SEM pictures of LY-Mn ore powder after the test campaign	78
Figure 6-15: Cross-section SEM pictures of LY-Mn ore particles after test campaign	78
Figure 6-16: Evolution of fines production during the campaign	79
Figure 6-17: Left : agglomerates formed in the L-valve of AR2 ; right : agglomerates formed at the outlet of FR (around 5 cm of diameter).....	80
Figure 6-18: X-Ray diffractogram of agglomerates formed at the outlet of FR.....	81
Figure 6-19 : Cross-section SEM pictures of agglomerates formed at the outlet of FR.....	81
Figure 6-20: CO ₂ capture rate, SINTEF-ER with Mn-ore LY as OC.	86
Figure 6-21: FR gas conversion efficiency, SINTEF ER with Mn-ore LY as OC.	86
Figure 6-22: Fresh Mn-ore LY about 60 – 200 μm. SEM (left) and EDS of Fe, Mn, Ti oxides (right).	87
Figure 6-23: SEM (left) and EDS (right) of Mn-ore sample from AR reactor after last test with petcoke (top), from AR bucket (middle), and from AR chamber (bottom).	88
Figure 6-24: SEM (left) and EDS (right) of Mn-ore sample from FR reactor after last test with petcoke (top), from FR bucket (middle), and from FR chamber (bottom).	89
Figure 6-25: SEM (left) and EDS (right) of Mn-ore sample from FR reactor (same as above but larger magnification).....	90
Figure 6-26: Enlarged SEM of Mn-ore sample from FR chamber, showing many small and hollow fuel particles.....	90
Figure 6-27: Metallic lump taken out from FR after last test with Mn-ore LY.....	91
Figure 6-28: Optical view (bright field) of metallic lump taken out from FR.	91
Figure 6-29: SEM (left) and EDS (middle and right) of lump from FR.	92
Figure 7-1: Experimental results of the ageing tests performed on ilmenite materials. (a) evolution of the methane conversion with the number of cycles, (b) evolution of the oxygen carrier's R ₀ ΔX value over the cycle number for the 10 tests performed with ilmenite oxygen carriers	94
Figure 7-2: Agglomerated ring of ilmenite T2.	95
Figure 7-3: Particle size distribution of fresh ilmenite T1 (batch delivered to IFPEN, i.e., after sieving to 180-300 μm) and T2 (directly delivered after drying), measured by laser granulometry.	95
Figure 7-4: SEM pictures of fresh ilmenite T1 particles (left: direct observation; right: polished cross-section)	96
Figure 7-5: SEM pictures on polished cross-section of fresh ilmenite T2 particles	96
Figure 7-6: SEM pictures of T1 after 250 redox cycles (left: direct observation; right: polished cross-section)	97
Figure 7-7: SEM pictures of T2 after 250 redox cycles (left: direct observation; right: polished cross-section)	97
Figure 7-8: SEM (left) and EDS (right) pictures of T1 after 250 redox cycles, showing Fe and Ti distribution.....	98
Figure 7-9: CO ₂ and CO concentration evolution at the reactor outlet during petcoke conversion in the batch fluidized bed reactor.	98

Figure 7-10: Impact of temperature and steam concentration on petcoke conversion in the batch fluidized bed unit. Test with petcoke from TOTAL and Ilmenite T2 as oxygen carrier.....	99
Figure 7-11: Flow rates during each phase of a cycle (inerting, reduction and oxydation).....	100
Figure 7-12: Evolution of methane conversion and oxygen mobility of ilmenite T2 over the number of cycles with 0 % (triangle), 8.6 % (red squares) and 30 % addition of steam (diamonds).	100
Figure 7-13: Comparison of the evolution of methane conversion and oxygen mobility of ilmenite T1 and T2 over the number of cycles with 0 % and 8.6 % steam addition.....	101
Figure 7-14: Left : outlet of the reactor (upper part) ; right : bottom part of the reactor after the test of ilmenite T1 with water addition.....	102
Figure 7-15: 3 kW rig with dual filter system to measure fines in filters. The system is also combined with a pressurised air system to return separated OCM back into the reactor to maintain mass circulation.	103
Figure 7-16: Accumulated fines for LY-Mn and ilmenite T2 as a function of time.	104
Figure 7-17: Agglomeration of LY-Mn fines in a filter.	105
Figure 7-18: Oxygen release rate of Ilmenite T1 and T2 in size fraction range 210-300 μm , between 5% H_2 and 20% O_2 as a function of temperature, compared to other and similar minerals in size range 125-180 μm	105
Figure 7-19: Fresh ilmenite T2 used in pilot unit at SINTEF ER, SEM (left) and EDS (right).	108
Figure 7-20: SEM and EDS of samples from AR reactor taken out after test.....	108
Figure 7-21: SEM and EDS of sample from FR bucket (top) and FR chamber (bottom) after petcoke test.	109
Figure 7-22: Magnified SEM picture of sample from FR bucket after petcoke test.	110
Figure 7-23: SEM and EDS of lump from FR reactor (top), with magnified view (bottom).	111

Table of Tables

	Page
Table 2-1: Evolution of petcoke CHONS composition for various petcoke conversion.....	21
Table 3-1: Studied ilmenite T1 properties.	24
Table 3-2: Main compounds and elements of Mn ore from XRF analysis provided by Tsinghua University.	24
Table 4-1: Petcoke composition (wt-% dry) and lower heating value.....	29
Table 4-2: Biomass composition (wt-%) and lower heating value. All values based on fuel as received (a.r.).....	30
Table 5-1: Overview of tests at SINTEF ER with ilmenite T1 as oxygen carrier.	31
Table 5-2: Summary of main operating conditions and performance results, SINTEF ER with ilmenite T1.	32
Table 5-3: Evaluation of oxygen carrier mass flow rates.	37
Table 5-4: Operating conditions of the first 60 hours of activation period.	51
Table 5-5: Reference operating conditions for Ilmenite.....	53
Table 5-6: Range of variation of operating conditions.	54
Table 5-7: Operating conditions of tests performed with petcoke.	54
Table 5-8: Petcoke tests experimental results.....	55
Table 5-9: Crystallographic phases detected by XRD during methane activation and petcoke combustion.	58
Table 6-1: Typical operating conditions during unit circulation start-up with LY Mn ore.....	67
Table 6-2: Operating conditions in 10 kW pilot unit over LY Mn ore activation period.....	68
Table 6-3: Operating conditions and performance for all the mass balances during the activation with methane.	69
Table 6-4: An overview of petcoke combustion performance test results with LY Mn ore.....	71
Table 6-5: Overview of tests at SINTEF ER with Mn-ore LY as oxygen carrier.....	83
Table 6-6: Main operating conditions, SINTEF ER with Mn-ore LY.	84
Table 6-7: Main performance results, SINTEF ER with Mn-ore LY.....	85
Table 7-1: Main operating conditions SINTEF ER pilot unit test with ilmenite T2.....	106
Table 7-2: Main performance results from SINTEF ER pilot unit test with ilmenite T2.....	107

0 PREFACE

CHEERS conforms to the European Horizon 2020 Work Programme 2016 – 2017, 10. 'Secure, Clean and Efficient Energy', under the low-carbon energy initiative (*LCE-29-2017: CCS in Industry, including BioCCS*). The ambition is to improve the efficacy of CO₂ capture in industry, and help ensuring sustainable, secure, and affordable energy.

The action involves a 2nd generation chemical-looping technology tested and verified at laboratory scale (150 kW_{th}). Within the framework of CHEERS, the core technology will be developed into a 3 MW_{th} system prototype for demonstration in an operational environment. This constitutes a major step towards large-scale decarbonisation of industry, offering a considerable potential for retrofitting industrial combustion processes.

The system prototype is based on a fundamentally new fuel-conversion process synthesised from prior research and development actions over more than a decade. The system will include heat recovery steam generation with CO₂ separation and purification, and it will comply with industrial standards, specifications, and safety regulations. Except for CO₂ compression work, the innovative concept can remove 96% of the CO₂ while eliminating capture losses to almost zero.

The CHEERS project is financed by the European Union's Horizon 2020 research and innovation programme under grant agreement No 764697, and co-funded by the Chinese Ministry of Science and Technology (MOST).

0.1 Disclaimer

The sole responsibility of this publication lies with the authors. Neither the European Union nor the MOST is responsible for any use that may be made of the information contained herein.

1 EXECUTIVE SUMMARY

A main objective of WP3 is to ensure that proper oxygen carriers (OCs) will be available for Chemical Looping Combustion (CLC) of petcoke and biomass in the 3 MWth demonstration unit to be developed within the project. There is a close coupling between the oxygen carrier properties and the design and sizing of the demonstration unit. In this project, the aim is to have a high air utilization giving lean air with less than 2 % O₂ out of the air reactor, to ensure high energetic efficiency. The fuel reactor will be a turbulent bed with high residence time due to the slow gasification of petcoke. To prevent the residence time from being exceedingly high, the average temperature in the fuel reactor will be at least around 950°C. If the selected oxygen carrying materials will cause an endothermic reaction in the fuel reactor, the oxygen carrier will also have to provide enough heat to ensure 950 °C in the fuel reactor. Consequently, the outlet temperature of the air reactor might go up to 1050 °C. The operating conditions described above are tough to meet for an oxygen carrier material.

The present deliverable D3.3, is the summary report of Task 3.3 in WP3. It summarizes the pilot unit testing performed, being the last validation step before choosing a suitable oxygen carrier for use in the 3 MW demo unit. Three different OC's have been tested in the pilot units. They were chosen among many candidates that were evaluated in Task 3.1 and described in detail in D3.1. The first candidate was a Norwegian ilmenite, a relatively cheap natural mineral that is well-known as OC in CLC, however, not so much with petcoke as fuel. The second candidate was a synthetic perovskite material, i.e., a material made from the bottom based on raw materials containing calcium, manganese, titanium, and iron, hence the short name CMTF. This will be much more costly and should show better performance to be competitive. The third material was a manganese ore from China, Mn-ore LY, that was delivered as small stones which were calcined and thereafter crushed, milled, and sieved.

During testing in a batch fluidised bed unit with petcoke, it showed up that the CMTF material became deactivated by fuel sulfur, even though it is a low-sulfur petcoke (~ 0.8 wt-% dry). For the demo unit and operation on petcoke it was concluded it could not be used. A second ilmenite material was then chosen as the third candidate for pilot testing.

The CHEERS project has two pilot units available in WP3: The 10 kW_{th} unit at IFPEN and the 150 kW_{th} unit at SINTEF ER, both being able to operate on solid fuels such as petcoke and biomass. They are quite different in design and way of operation, but together they cover the needed window of operating conditions.

Studies at IFPEN of the performance of oxygen carrier (OC) materials were done in two different reactors: a batch fluidised unit and the 10 kW pilot unit. Combustible conversion performances have been determined for each OC, and their structural evolution was monitored. Studies at IFPEN have shown that agglomeration issues observed during tests with the second ilmenite could be limited by adding steam throughout the test.

Results from SINTEF ER 150 kW unit show equal performance of the two ilmenites for both biomass and petcoke fuels. Mn LY gives a slightly higher petcoke conversion than the ilmenites, but the fuel reactor gas conversion efficiency is generally lower.

Hot attrition testing by SINTEF MK show that Mn LY has higher attrition rate and fines production than the ilmenites. I.e., lifetime will be shorter. This is also confirmed from the 10 kW unit tests at IFPEN.

Due to their performance and interesting price, ilmenites have been selected as the most promising candidates to be used in the 3 MW demonstration unit. The first ilmenite requires an additional sieving step to be in the correct particle size range, which is not the case with the second ilmenite. Finally, as long as the agglomeration issues can be controlled by steam addition and careful fluidization of low-velocity and dense zones, the second ilmenite is the best candidate to be used in the demonstration unit.

2 PILOT UNITS

2.1 Pilot unit at SINTEF

2.1.1 Reactor system

The CLC reactor system consists of two circulating fluidized bed reactors as shown in Figure 2-1. The two reactors, the air reactor (AR) and fuel reactor (FR) respectively, are interconnected through particle loop seals that works as gas locks to ensure that only the oxygen carrier (OC) particles are transferred between the reactors. In addition, particles are also transferred from the fuel reactor to the air reactor through the lifter, which is fed from the bottom of the fuel reactor. The system was originally designed for operation on methane as fuel gas, at a maximum fuel power of 150 kW ([1], [2]). Later it has been modified to allow operation on solid fuels [3]. Further improvements have been made in the CHEERS project to make the system more suited for feeding petcoke fuel. It should be noted that this pilot unit does not contain a carbon stripper to help reduce any loss of char from FR to AR.

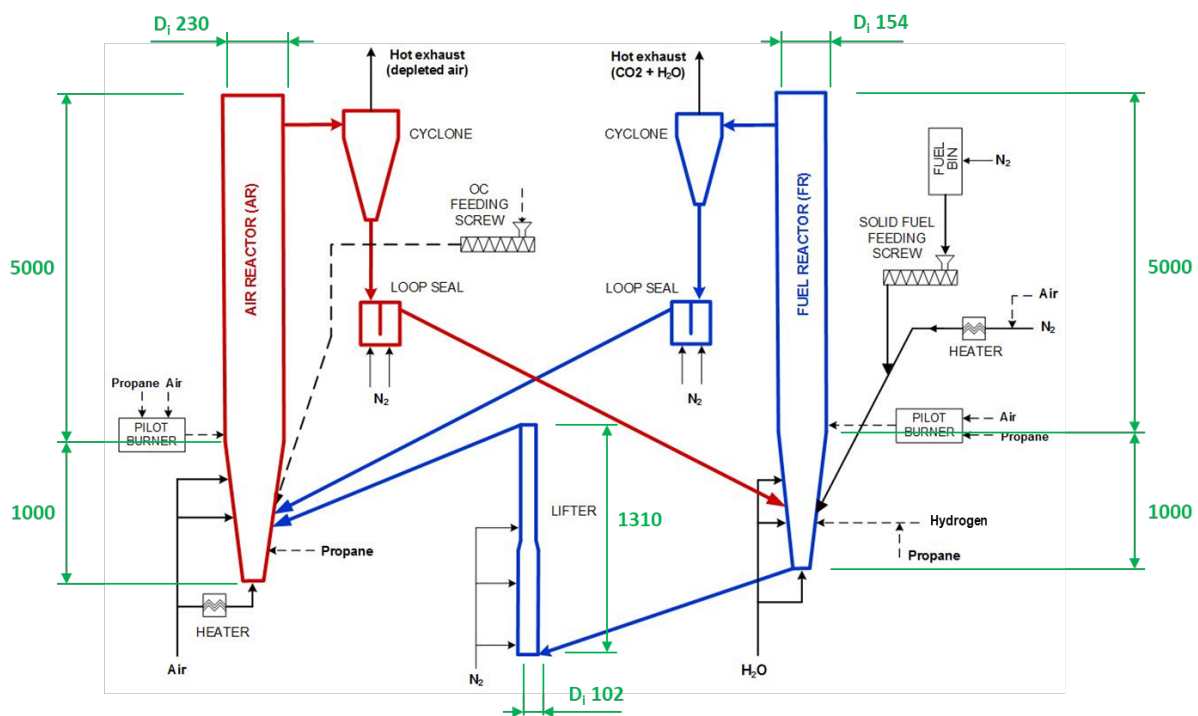


Figure 2-1: Schematic overview of CLC pilot unit system at SINTEF ER.

Both reactors are 6 m tall of which the first 1 m is a conical bottom section. The remaining 5 m cylindrical sections have internal diameters of 230 mm (AR) and 154 mm (FR). The system has a solid fuel feeding screw from which the fuel particles fall into the fuel inlet pipe and are injected into the FR with N₂ as a fuel carrying gas. There is an oxygen carrier feeding screw which makes it possible to refill particles during operation. At start-up, both reactors are first heated by hot air through two 30 kW electric heaters. Then fuel gas (propane and hydrogen) is introduced into the particle beds through fuel gas lances in each reactor. Pilot burners are mounted above the bed to ensure safe ignition of the injected fuel. In addition, a 10-kW electric heating wire is wound around each of the two reactors. The heating wires are in operation before and during the heat-

up sequence and if the reactor temperature gets too low. However, under normal CLC operation, the reactor temperature is controlled by the CLC process itself, i.e., auto-thermal operation, plus the possibility of adjusting the primary air preheat temperature to the air reactor. If this is not enough, it is possible to inject propane into the air reactor, but this is generally not necessary.

Each reactor has 6 pressure transmitters mounted up along the reactor height, with most of them in the bottom part. There are also pressure recordings in the bottom and top of the lifter, around the cyclones, in the loop-seals as well as in the main air and steam supply lines. There are 5 temperature transmitters in each reactor, plus temperature measurements in the lifter, in the exhaust system and in each of the pre-heated inlet streams and in the fluidisation steam line to the FR.

The composition of the outlet exhaust gas streams from the cyclones are monitored with on-line gas analysers. The CO₂, CO and O₂ concentrations of the fuel reactor exhaust is measured with an Emerson Rosemount X-stream IR analyser. A Varian CP4900 Micro-GC is also connected to the fuel reactor exhaust. It measures gases such as H₂, CH₄, N₂, C₂ hydrocarbons and helium. Helium is fed to the fuel reactor as a trace gas and its concentration in the exhaust is used for mass balance evaluation. The Micro-GC also measures CO₂ and CO and therefore serves as a check for the IR analyser. The air reactor gas outlet is monitored with a Horiba PG-250 IR analyser, measuring CO₂, CO and O₂ concentrations.



Figure 2-2: CLC pilot unit at SINTEF ER placed in tent hall, control room and new fuel screw feeder.

The pilot unit is placed in a tent hall together with a separate control room as shown in Figure 2-2. The unit is operated on a daily basis and is stopped at nights. During night, the 10-kW heating cable on each reactor is maintaining some temperature level in the reactor system, reducing the time for the heat-up sequence the next day. An example of a normal temperature history during a day of operation is shown in Figure 2-3. The

only additional heat provided is the pre-heat of the AR primary air (here mostly at 750 °C), except this the process is auto-thermal.

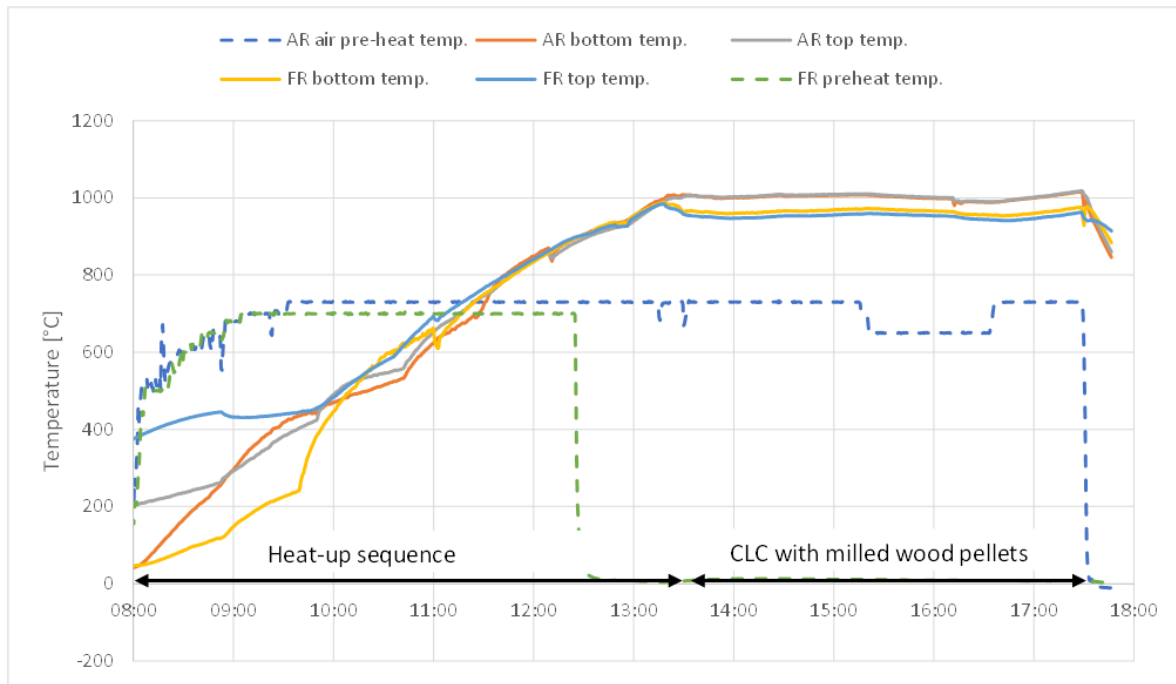


Figure 2-3: Typical reactor temperatures history for one day test (January 28th, 2021).

2.1.2 Modifications to the reactor system

The CLC reactor system was originally designed for gaseous fuels, and modifications have been done to be able to use solid fuels. Most of these were made before the CHEERS project. However, during the first part of the CHEERS project, additional improvements have been made to better suit the use of petcoke as fuel. This involves a new volumetric screw fuel feeder, installation of a small steam boiler, thermal mass flow controllers for better controlling loop-seals and lifter fluidisation (re-installing some old MFC's from another lab unit), particle settling chambers to better separate particles from the exhaust stream, and some other smaller modifications. This is described in more detail in Appendix A.

2.1.3 Evaluation of process and oxygen carrier performance

Fuel carbon conversion

The fuel carbon conversion (X_{fuel-C}) is calculated as the ratio between the carbon leaving as gas from the FR and the carbon fed to FR with the petcoke fuel,

$$X_{fuel-C} = \frac{(x_{CO_2,FR} + x_{CO,FR} + x_{CH_4,FR} + 2x_{C_2H_2,FR}) F_{total,dry}^{FR}}{\text{carbon in fuel feed to FR}},$$

where $F_{total,dry}^{FR}$ is the total dry molar flow rate of gas out of FR (kmol/h), and x_i is the mole fraction of carbon-containing gaseous species in the dry gas out of FR.

Fuel carbon conversion represents the percentage of fuel carbon that is leaving the FR in gaseous form by devolatilization, gasification and combustion in the FR. The remaining carbon will leave in particulate form, either following the FR outlet gas, or following the OC over to the AR (contributing to CO₂ loss from the AR and thereby CO₂ capture rate being less than 100 %).

If the fuel composition does not change with conversion, X_{fuel-C} is also equal to the percentage of fuel being converted in the FR. This is the case for the petcoke fuel being used in this study as shown in Table 2-1. For biomass fuels with higher share of volatile components, the carbon content will generally increase with fuel conversion.

Oxygen demand and fuel reactor gas conversion efficiency

The gases leaving the fuel reactor will normally not be fully converted, causing the need for an "oxygen polishing" step just downstream of the fuel reactor. I.e., pure oxygen is fed to the hot exhaust stream to completely burn out remaining unconverted gases. The needed oxygen for polishing is commonly calculated by the oxygen demand Ω_{OD} . It represents the ratio of the additional oxygen needed to completely convert the unconverted gases leaving the FR, to the stoichiometric amount of oxygen needed to fully convert all the gases in the FR to CO₂ and H₂O. In our case it is calculated as

$$\Omega_{OD} = \frac{0.5x_{CO,FR} + 2x_{CH_4,FR} + 0.5x_{H_2,FR} + 3x_{C_2H_y,FR}}{\Phi_0 (x_{CO_2,FR} + x_{CO,FR} + x_{CH_4,FR} + 2x_{C_2H_y,FR})},$$

where Φ_0 represents the molar amount of O₂ needed for full conversion of the fuel per mole of carbon in the fuel, x_i represents the mole fractions of the different species in the fuel reactor dry outlet gas, and the parenthesis in the denominator gives the total mole of carbon in the FR outlet gas. The Micro-GC gives the sum of some C₂ molecules. It is here assumed they are C₂H₄ in average so that the oxygen demanded is calculated using 3 moles O₂ per mole C₂H₄.

This way of calculating the oxygen demand is a very convenient parameter as it can be calculated only from the gas analysis of the FR exhaust. However, in solid fuel CLC, fuel conversion is generally not 100 % and there might be some losses of unconverted fuel particles out from the FR. They should be converted in the oxygen polishing step as well, to reduce fuel losses and increase the CO₂ capture rate of the system. The above oxygen demand calculation does not include this potential fuel loss, which would increase the oxygen demand to a higher value than given by the formula. Carbon particles have been observed in the exhaust system, especially when using petcoke as fuel. Petcoke is a slow reacting fuel compared to biomass, and less carbon is observed in the exhaust when using biomass. The calculation does not take heavier hydrocarbons and tars into account either. This would also increase the oxygen demand compared to calculated. The influence of these is considered small, which was confirmed by visual inspection of the exhaust system and filter, and FTIR gas analysis used in some of the experiments.

The above calculated oxygen demand may also differ from the actual oxygen demand when the composition of the original fuel is shifted in direction of carbon in the char. Φ_0 represents the O₂ needed for full conversion of the fuel per carbon atom in the fuel. This is calculated from the solid fuel composition (C_xH_yO_z). However, for this Φ_0 to be strictly valid for the gas-based calculation of oxygen demand, the gaseous mixture from devolatilization and gasification should have the same composition as the original solid fuel. For a biomass fuel with larger fraction of hydrogen and oxygen in the fuel, this gas mixture will likely contain more hydrogen than the original fuel (thereby increasing Φ_0 and reducing the actual oxygen demand), and also more oxygen from the fuel (thereby decreasing Φ_0 and increasing the actual oxygen demand). For a typical biomass the molar content of oxygen will be nearly half of hydrogen and then this should more or less outweigh each other. For a fuel with much more carbon and less volatile components, as petcoke, such deviations will be less relevant to consider.

From the oxygen demand calculation, the fuel reactor gas conversion efficiency can be defined as

$$\eta_{gas} = 1 - \Omega_{OD}.$$

This represents the efficiency of the conversion of the fuel gases being produced in the FR by devolatilization and gasification. It is a quality measure of the FR gas combustion and should be as high as possible, ideally 100 %.

CO₂ capture rate

In addition to char leaving out with FR exhaust, there may also be a loss of char particles from FR to AR, following the oxygen carrier particle stream. These char particles will immediately burn out to CO₂ in the high temperature, oxygen-rich atmosphere in the AR and leave with the AR exhaust. Since only the CO₂ out of the FR will be separated and available for permanent storage, this represents a loss of CO₂ that will cause the overall CO₂ capture rate to be lower than 100%. The CO₂ capture rate can then be calculated as

$$\eta_{CO_2 \text{ capture}} = \frac{\text{carbon in fuel feed to FR} - \text{carbon out from AR}}{\text{carbon in fuel feed to FR}}.$$

The carbon in fuel feed is calculated from the carbon content of the fuel and the fuel feed given by the screw feeder when it has been calibrated for the actual fuel. The carbon out from the AR is calculated from the total mole flow out from AR and the measured CO₂ concentration. The total mole flow out from AR is calculated from the total N₂ mole flow out of AR, being equal to N₂ fed to AR with air and fluidisation gases, and the concentrations of O₂ and CO₂ at the outlet, since they will be the only gases in addition to N₂. The capture rate calculated this way gives how large share of the total fuel carbon that leaves the FR in gaseous and char form. When all unburnt gaseous components and char is converted to CO₂ in the oxygen polishing step, this will represent the real capture rate of the system.

The pilot unit at SINTEF ER, originally designed for gaseous fuels, does not have a carbon stripper and some char will be lost from FR to AR, especially through the lifter. CLC systems for solid fuels will normally be equipped with a carbon stripper to convert most of these char particles before they reach the AR, thereby increasing the capture rate of the system. Especially for slow reacting fuels as petcoke this is important. A carbon stripper is an essential element of the CHEERS demo unit to be built at Dongfang Boiler facility in Deyang.

Oxygen carrier circulation and inventory

There is no direct way of measuring the oxygen carrier circulation rate between the reactors in the SINTEF pilot unit. One way to estimate it, is to use the reactor pressure recordings in the AR riser. An analytical theoretical riser mass flow can be estimated by the pressure difference (Δp) between the two upper pressure transducers, the difference in height between the transducers (Δh), the superficial gas velocity (u_0), the terminal velocity of the OC particles (u_t), and the reactor riser flow area (A) and gravitational acceleration (g):

$$\dot{m}_{riser} = \frac{A \Delta p}{g \Delta h} (u_0 - u_t).$$

This theoretical riser OC mass flow is not the same as the actual oxygen carrier circulation rate, as only a fraction of the particles flowing upwards in the AR riser follows the gas flow into the cyclone and is transferred to the fuel reactor. As the flow is in the turbulent to fast fluidisation regime and not in the transport regime, a large share of the particles falls downwards along the reactor wall forming an internal recirculation. Studies by Chalmers report that the share of particles leaving the reactor was about 29 % in one case and as low as 8 % in another case (Markström et al. [3], [4]). They point out that this fraction is expected to be different for

different reactor designs, superficial velocity, and concentration. However, the calculated theoretical AR riser mass flow can be used as a good indication of the relative differences in solid circulation between different cases tested on the SINTEF pilot unit.

The oxygen carrier inventory in the two reactors and lifter is estimated by calculating the average solid-gas mixture density between subsequent pressure transducers using the pressure difference (Δp) and height between the transducers (Δh). The densities are multiplied by the volume between the pressure transducers and summed to give the OC inventory of each reactor and the lifter.

Oxygen carrier sampling and analysis

The OC sampling is done only downstream of the cyclones. Each reactor has a bucket just after the cyclone where part of the OC's leaving the cyclone with the exhaust gas are collected. Shortly after this bucket is a larger low-velocity chamber, where the remaining OCs in the exhaust gas are collected. These buckets and chambers can be emptied during operation, and this is done rather often to weigh OC losses and have control of total inventory. The OC samples from the buckets and the chambers will have smaller size than the particles within the system, especially in the low-velocity chambers where OC fines are able to settle. Samples from within the reactor system is available only when the system is stopped, and OC samples can be taken out from the bottom of the AR and FR.

The oxygen carrier samples were analysed by SINTEF MK. Samples were first made into polished cross-sections. Next, they were analysed with microscopy, both bright field and dark field illumination. Finally, they were investigated by SEM-EDS (scanning electron microscopy - energy dispersive spectrometer) for microstructure and elemental analysis.

2.1.4 Uncertainties in results evaluation

Instrument uncertainties

Thermal mass flow controllers (MFC's) are used for feeding inlet gases to the system, except for steam. The MFC's in the system have been checked with a portable flow calibration unit. However, the largest MFC's delivering air to AR have capacity larger than the calibration unit that may introduce uncertainties in inlet air flow.

Gas analysis is done on-line by IR and GC analysers. They are calibrated before and during tests using calibration gases. The gas sampling lines contain heated filters, heated hoses and condensation and filter units. However, very small fuel particles following the FR exhaust stream have caused problem by clogging the sampling lines and filters on some occasions, especially with petcoke fuel where a large amount of very small fuel particles seem to follow the FR exhaust stream.

The pressure transmitters (PT's) are used to evaluate inventory and OC balance within the system. They have been checked with a portable calibration unit. The PT measurement lines were earlier flushed manually with some time interval between in order to prevent plugging because of particles. Some lines could then be partly plugged before it was detected. More recently, a continuous flushing system was installed to maintain a small flow that prevent any plugging.

Fuel feeding and composition

Fuel feeding is done with a volumetric screw feeder. The feeding rate of the different fuels are calibrated by running the screw at different rpm's, with the outlet pipe dismantled allowing feeding into a bucket which is weighed using an accurate scale. The pressure level upstream and downstream of the fuel screw are balanced with each other, and the pressure downstream is close to the FR pressure. This should ensure even feed rate

independent of pressure in the FR. However, it still some uncertainty in how the feed rate can be affected by the rather large and rapid pressure variations in the FR. As a check, all fuel fed to the system are weighed and checked against the integrated value of the fuel feed screw to ensure good match.

The temperature of the feeding line after the screw will be different in CLC operation than when doing the calibration. This may also have some effect on feed rate.

The fuel size and composition may not be completely homogeneous. Especially for the biomass cases using milled bio-pellets a lot of fuel had to be pre-processed in rather small batches. A new big-bag of Arbaflame pellets was received during the tests. The composition should be equal to the first big-bag but some variations might occur since it was not produced at the same time as the first one.

Gas flow out of reactors

A N₂ balance can be used to calculate the outlet gas flows of the reactors. In our case, the fluidisation of the loop seals and lifter is with N₂. A share of this N₂ will flow into the AR and the rest into the FR. It is assumed that half the flow to AR and FR loop seals plus 2/3 of the amount to lifter bottom, will go to the AR. This may not be fully correct, however, these N₂ flows are very small compared to the total N₂ with the air inlet to the AR and will have very limited effect on the balance. Out from AR it is assumed that only CO₂, O₂, and N₂ are the dry gases, and since CO₂ and O₂ concentrations are measured, the remaining is N₂. From the N₂ concentration, the total gas flow out of AR can be calculated.

The same principle is also used for the FR. The amount of N₂ fed to the FR is known and the GC measures the N₂ concentration at FR outlet. From this the total dry gas flow out of FR is known. The N₂ flow to FR is much smaller than the AR and the uncertainty in the distribution of the loop-seals and lifter flows will become more important. In the tests from October 2019 onwards a more accurate Helium tracer gas system has been used for the FR. A known quantity of He is fed to the upper part of FR (to ensure all is leaving out the FR) and the GC is measuring the He concentration in the FR exhaust. From this the total dry gas flow rate out of FR can be calculated.

The uncertainty of the above approach is mainly related to inaccuracies of the MFC's and the gas analysis, while the distribution of N₂ flows to loop-seals and lifter will have less significance.

Carbon balance

A carbon balance is performed on each test interval to check the amount of carbon leaving as gas out of FR plus carbon leaving AR as CO₂, in relation to carbon fed with the fuel. The remaining carbon will ideally be the fraction leaving the FR in particulate form. However, we have no quantitative way to check the amount of fuel particles leaving the FR during a test sequence in the SINTEF pilot unit. Only qualitative information can be obtained by SEM analysis of the OC samples taken regularly from FR exhaust. In addition, we have evaluated the amount of organic compounds in dried samples from the FR wet scrubber using a muffle oven.

2.2 Pilot unit at IFPEN

2.2.1 Reactor system

A schematic view of IFPEN's 10 kW_{th} CLC pilot unit used in this study is shown in Figure 2-4. The pilot is composed of three interconnected bubbling fluidized bed reactors and a carbon stripper. Two fluidized bed reactors (AR1 and AR2) are dedicated to the oxygen carrier oxidation and the third one (FR) is dedicated to fuel combustion, therefore performing OC reduction. In the fuel reactor, gaseous fuel or petcoke can be injected to react with the oxygen carrier and reduce it. The reduced particles go through the carbon stripper (CS) before entering the air reactor AR1. This CS has been implemented to separate unburnt carbon compounds from the OC in the case of solid fuels combustion (herein, petcoke combustion).

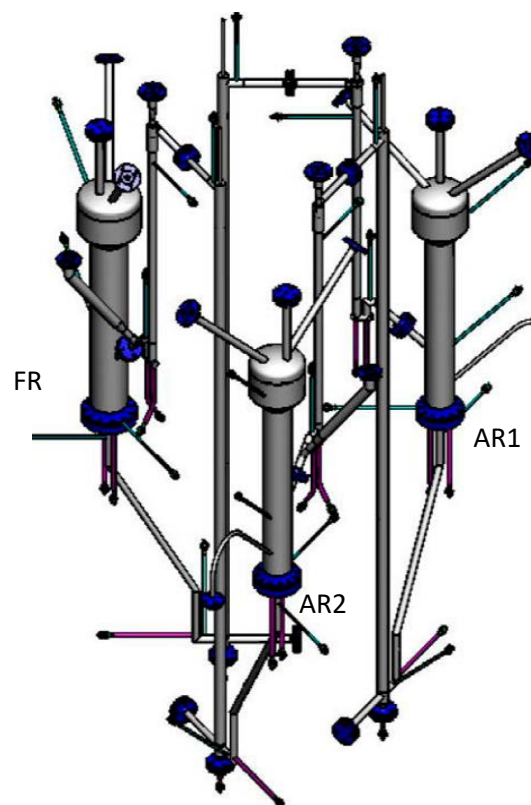


Figure 2-4: 3D scheme of the pilot unit at IFPEN

The solid circulation systems are identical from AR1 to AR2 and from AR2 to FR. The oxygen carrier leaving the reactors (AR1 or AR2) by the bottom enters a pneumatic L-valve of 0.017 m i.d. and 1.1 m height. From that point, the solid is transported through a lift with 0.02 m i.d. and 2.25 m height and then enters a horizontal dilute phase conveying line. Finally, the conveying gas and solid are separated in a cyclone. Then, the OC particles go through a loop seal upstream the next reactor (AR2 or FR). This loop seal, fluidized with nitrogen, allows to avoid any gas transfer between the reactor gas phase and the conveying gas transporting the solid to the cyclone. Between the FR and AR1 the solid leaving the reactor by the bottom goes through a pneumatic L-valve and is transported to the carbon stripper through a lift. The carbon stripper separates the particles according to their volume and density, the lightest particles get entrained by the gas, while the

heaviest fall down, leave the carbon stripper by the bottom and enter a loop seal connected to the air reactor AR1.

The fuel reactor (FR) has an internal diameter of 0.13m and is fluidized with nitrogen and methane in gas combustion mode, or nitrogen and water vapour in solid combustion mode. The total flow rate of the fluidizing gas is chosen in order to operate at 3 times the minimum fluidization velocity of the OC to ensure a sufficient fluidisation. Both air reactors (AR1 and AR2) can be fed with air or nitrogen. As in the fuel reactor, the total flow rates used are chosen to obtain a good fluidisation of the particles.

The CLC pilot unit is equipped with three multi-gas online analysers. CH₄, CO and CO₂ concentrations are continuously measured at the outlet of the FR by non-dispersive (NDIR) infrared analyzers (ABB-URAS 26), while H₂ concentration is analysed by a thermal conductivity detector (ABB-Aldos 27). In AR1, CO, CO₂ and O₂ concentrations are determined by a combined NDIR-paramagnetic analyser (ABB-Uras 26 /Magnos 206). Finally, in AR2, O₂ is measured by an electrochemical cell analyzer (Siemens – Ultramat 23). All data are collected by means of a PLC which is connected to a computer.

2.2.2 Evaluation of fuel conversion and oxygen carrier reduction degree

The reactivity of the oxygen carrier and its performances can be well represented by three parameters:

- The quantity of oxygen released in the fuel reactor $R_0\Delta X$ (wt%),
- The methane or petcoke conversion X_{CH_4} or $X_{petcoke}$ (%),
- The CO/CO₂ ratio, which is linked to the oxygen carrier efficiency.

The quantity of oxygen released by the material is represented by the $R_0\Delta X$ value, where ΔX corresponds to the conversion of the oxygen carrier in the fuel reactor and R_0 corresponds to the full oxygen transfer capacity of the fresh material (see Equation 1).

$$R_0 = \frac{m_{Oavailable}}{m_{solid}} \quad 1$$

The oxygen transfer capacity of the oxygen carriers used in this study were measured by TGA cycling. E.g., for Ilmenite material $R_0 = 5.2$ wt%.

The $R_0\Delta X$ parameter can be calculated in two different ways (Equations 2 and 3) if the oxygen mass balance is performed on the fuel or the oxygen reactors.

$$R_0\Delta X_{FR} = \frac{\left(\int_{t_0}^{t_f} (2F_{CO_2,out}^{FR} + F_{CO,out}^{FR} - F_{H_2O,in}^{FR}) dt + \frac{m_{H_2O}^{condenser}}{M_{H_2O}} \right) M_O - (Q_{petC,in}^{FR} - Q_{petC,out}^{FR}) O_{petC,in}}{\int_{t_0}^{t_f} Q_{m,s} dt} \quad 2$$

$$R_0\Delta X_{AR} = \frac{\left(\int_{t_0}^{t_f} (2F_{O_2,in}^{AR1} + 2F_{O_2,in}^{AR2} - 2F_{CO_2,out}^{AR1} - F_{CO,out}^{AR1} - 2F_{O_2,out}^{AR1} - 2F_{O_2,out}^{AR2}) dt \right) M_O + Q_{petC,in}^{AR1} O_{petC,in}}{\int_{t_0}^{t_f} Q_{m,s} dt} \quad 3$$

with $t_f - t_0$ standing for the duration of the mass balance (s), F_j^i the molar flow rate of component j at the outlet of reactor i (mol s⁻¹), $m_{H_2O}^{condenser}$ the mass of water obtained at the condenser of the fuel reactor during

the duration of the mass balance (kg), $Q_{petC,in\ or\ out}^{unit}$ the mass flowrate of petcoke at unit inlet or outlet (kg s^{-1}), $O_{petC,in}$ the oxygen content of the inlet petcoke (kg/kg) and $Q_{m,s}$ the solid flow rate (kg s^{-1}).

The values of $R_0\Delta X_{FR}$ and $R_0\Delta X_{AR}$ are similar for each mass balance, and the values of $R_0\Delta X$ presented in this work correspond to the average between these two $R_0\Delta X_j$ values.

The petcoke flowrate leaving the fuel reactor ($Q_{petC,out}^{FR}$) is divided in two flows. The petcoke dragged away with the gases ($Q_{petC,out,g}^{FR}$) and the petcoke leaving with the oxygen carrier by the reactor's bottom ($Q_{petC,out,OC}^{FR}$). Using the samples collected at the fuel reactor outlet, which contain petcoke and oxygen carrier, it is possible to calculate the unburnt petcoke flowrate leaving the reactor with the gases ($Q_{petC,out,g}^{FR}$). Indeed, these samples are calcined in an oven and, correcting for ilmenite weight gain during reoxidation using the $R_0\Delta X$ value, the variation of mass before ($m_{red+P,out}^{FR}$) and after the combustion ($m_{ox,out}^{FR}$) is linked to the petcoke content. The amount of petcoke dragged away with the gas flowrate is calculated as presented in equation 4 and 5, with $m_{petC,out,g}^{FR}$ being the mass of petcoke retrieved at the fuel reactor filter (kg).

$$m_{petC,out,g}^{FR} = m_{red+P,out}^{FR} - m_{ox,out}^{FR}(1 - R_0\Delta X) \quad 4$$

$$Q_{petC,out,g}^{FR} = \frac{m_{petC,out,g}^{FR}}{(t_f - t_0)} \quad 5$$

The flow rate of petcoke leaving the reactor with the oxygen carrier is calculated from the mass balance with equation 6.

$$Q_{petC,out,OC}^{FR} = \frac{\left(\int_{t_0}^{t_f} Q_{petC,in}^{FR} dt - m_{petC,out,g}^{FR}\right) C_{petC,in} - \left(\int_{t_0}^{t_f} (F_{CO_2,out}^{FR} + F_{CO,out}^{FR}) dt\right) M_C}{(t_f - t_0) C_{petC,in}} \quad 6$$

with $C_{petC,in}$ the proportion of carbon in the petcoke (kg/kg). In equation 6, it is assumed that petcoke composition is not impacted by its conversion, which is confirmed by analytical data shown in Table 2-1.

Table 2-1: Evolution of petcoke CHONS composition for various petcoke conversion.

$X_{petcoke}$ (%)	C (%)	H (%)	O (%)	N (%)	S (%)
0	96.5±0.7	0.92±0.1	0.31±0.1	1.36±0.1	0.74±0.1
20	96.6±0.7	0.65±0.1	0.49±0.1	1.31±0.1	0.93±0.1
50	96.1±0.7	0.51±0.1	0.43±0.1	1.26±0.1	1.03±0.1

A similar equation is used to calculate the flow rates of petcoke entering air reactor 1 (equation 7).

$$Q_{petC,in}^{AR1} = \frac{\left(\int_{t_0}^{t_f} Q_{petC,in}^{FR} dt - m_{petC,out}^{FR} - m_{petC,out}^{CCS} \right) C_{petC,in} - \left(\int_{t_0}^{t_f} (F_{CO_2,out}^{FR} + F_{CO,out}^{FR}) dt \right) M_C}{(t_f - t_0) C_{petC,in}} \quad 7$$

with $m_{petC,out}^{CCS}$ being the mass of petcoke retrieved at the carbon stripper cyclone (kg).

Methane conversion (X_{CH_4}) in the fuel reactor can be calculated from Equation 8. It is largely impacted by the solid and gas residence time in the reactor.

$$X_{CH_4} = \frac{(F_{gas,in}^{FR} * x_{CH_4,in}^{FR} - F_{gas,out}^{FR} * x_{CH_4,out}^{FR})}{F_{gas,in}^{FR} * x_{CH_4,in}^{FR}} \quad 8$$

$F_{gas,in}^{FR}$ is the FR inlet total molar flow rate of the gas phase (mol/s), $x_{CH_4,in}^{FR}$ the fraction of methane at the inlet of the FR (-), $F_{gas,out}^{FR}$ the FR outlet total molar flow rate of the gas phase (mol/s), and $x_{CH_4,out}^{FR}$ the fraction of methane at the outlet of the FR (-).

Petcoke conversion ($X_{petcoke}$) can be calculated from Equation 9.

$$X_{petcoke} = \frac{\left(\int_{t_0}^{t_f} (F_{CO_2,out}^{FR} + F_{CO,out}^{FR}) dt \right) M_C}{Q_{petC,in}^{FR} (t_f - t_0) C_{petC,in}} \quad 9$$

The ratio between CO and CO₂ (CO/CO₂) representing a quality of combustion is calculated from Equation 10. If the combustion is total, this ratio equals zero, but if the oxygen carrier is not able to oxidize all the carbon monoxide or hydrogen produced by the fuel conversion, this ratio increases and a mixture of CO, H₂, CO₂ and H₂O is obtained at the fuel reactor outlet. At similar fuel conversion, the operating conditions leading to a lower CO/CO₂ ratio must be favored.

$$\frac{CO}{CO_2} = \frac{F_{gas,out}^{FR} * x_{CO,out}^{FR}}{F_{gas,out}^{FR} * x_{CO_2,out}^{FR}} = \frac{x_{CO,out}^{FR}}{x_{CO_2,out}^{FR}} \quad 10$$

3 OXYGEN CARRIERS

Several oxygen carrier materials have been evaluated as possible candidates for the pilot unit testing, and subsequently, for the demo unit operation at the Dongfang Boiler site in Deyang in China. Screening tests and experimental validation at lab scale have been performed. This is described in detail in deliverable D3.1. Three different OCs were chosen for further pilot testing and delivered by SINTEF MK in proper size fractions to the pilot unit sites at IFPEN and SINTEF ER, as described in D3.2. The three OCs are from natural minerals and ores. A fourth OC was also heavily evaluated, a more refined synthetic OC with several favourable properties, except that it turned out to be de-activated by sulfur. It can therefore not be used with the sulfur-containing petcoke fuel, however, it may be relevant for some of the Chinese tests to be done with coal. Below is a short description of the three OCs chosen for pilot unit testing in this deliverable.

3.1 First oxygen carrier – Ilmenite T1

The first oxygen carrier that was selected for pilot unit testing is a Norwegian ilmenite (FeTiO_3), hereafter called ilmenite T1. The reasoning behind this choice is described in detail in deliverable D3.1 together with all the results from the screening tests at lab scale. The material was delivered by the project partner SINTEF MK (cf. D3.2). The ilmenite particle size distribution is shown in Figure 3-1.

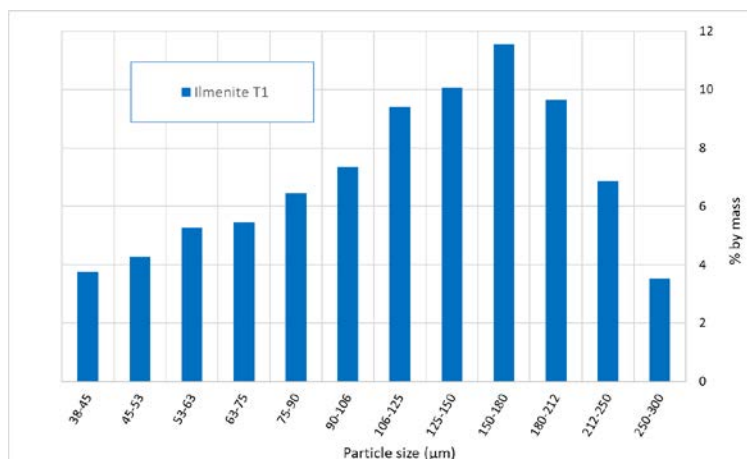


Figure 3-1: Ilmenite T1 particle size distribution.

The pilot units at IFPEN and SINTEF ER require different particle size due to the different designs. The ilmenite was therefore sieved at the particle lab of NTNU in Trondheim before being shipped to the pilot unit sites:

- 180 kg of 180-300 μm sieve size was shipped to IFPEN, Lyon, France
- 300 kg of 38-122 μm sieve size was shipped to SINTEF ER, Trondheim, Norway (see Figure 3-2).

Other main characteristics of the ilmenite T1 oxygen carrier:

- Maximum oxygen transfer capacity $R_0 = 5.2$ wt% (measured by TGA cycling at IFPEN).
- Bulk density is ~ 2600 kg/m³.

Table 3-1: Studied ilmenite T1 properties.

Name	Composition (measured by XRD)	Porosity (%)	Grain density (kg/L)
Ilmenite T1	TiFeO ₃ Fe ₂ O ₃ NiSi ₃ AlO ₈ (minor)	~0	4.77

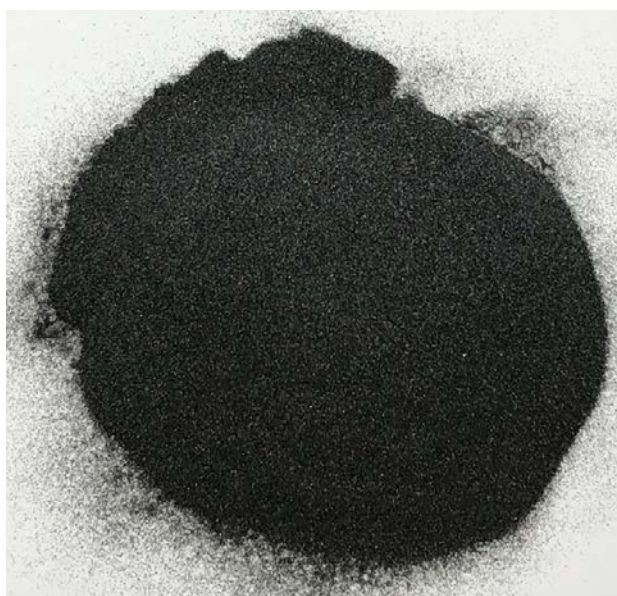


Figure 3-2: Fresh ilmenite, size fraction 38 – 122 μm as delivered to SINTEF ER after sieving.

3.2 Second oxygen carrier – Mn ore LY

The Mn ore LY is an oxygen carrier made from a Chinese manganese ore. The material was originally in form of small stones that were calcined at 1100 °C, then crushed, milled, and sieved to the size required by IFPEN and SINTEF ER. All this were done in China, with Tsinghua University helping to arrange. A batch of 530 kg was shipped to IFPEN, and 1360 kg to SINTEF ER. The main compounds and elements are given in Table 3-2.

Table 3-2: Main compounds and elements of Mn ore from XRF analysis provided by Tsinghua University.

Compound	Wt-%	StdErr		Element	Wt-%	StdErr
MnO	65.16	0.24		Mn	50.47	0.18
Fe ₂ O ₃	12.92	0.17		Fe	9.04	0.12
SiO ₂	12.06	0.16		Si	5.64	0.08
Al ₂ O ₃	3.73	0.09		Al	1.98	0.05
BaO	2.35	0.08		Ba	2.11	0.07
K ₂ O	0.996	0.05		K	0.827	0.041

Na ₂ O	0.533	0.087		Na	0.396	0.064
SrO	0.344	0.017		Sr	0.291	0.014
MgO	0.224	0.02		Mg	0.135	0.012
TiO ₂	0.217	0.011		Ti	0.13	0.006

A semi-quantitative X-Ray Fluorescence measurement shows that the ore contains mainly Mn and Fe as potentially redox active metals, as well as silicon, aluminum, and other trace elements (see Table 3-2).

X-Ray Diffraction analysis indicates that the ore contains large amounts of tephroite (Mn₂(SiO₄)) and pyrolusite (MnO₂) as well as some jacobsonite (MnFe₂O₄) and some quartz (SiO₂), along with other ill-defined and less abundant phases. Cross-section SEM analysis of the particles (Figure 3-3) shows the presence of highly crystalline precipitates in a matrix that contains dendrites which are usually formed during crystallization of metal alloys upon solidification. It is unclear whether this structure was initially present in the ore, or if it developed upon calcination.

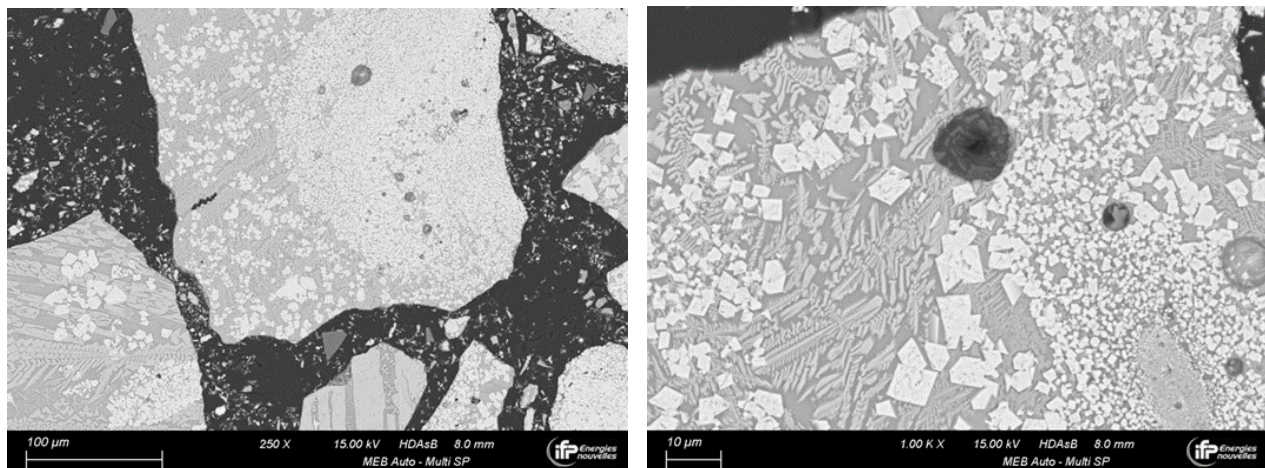


Figure 3-3: Cross-section SEM pictures of LY-Mn ore

SEM pictures of the powder clearly show that the crushed ore contains large amounts of fine particles (Figure 3-4). The particle size distribution of the material should be in the range 180 – 300 µm for the 10 kW unit to allow for good circulation. Additional manual sieving of the ore was therefore performed to remove fines. It appears that about 30 % of the total mass of the original material is below 100 µm (Figure 3-5), which is a significant fine percentage that could interfere with inter-reactor circulation in the 10 kW unit.

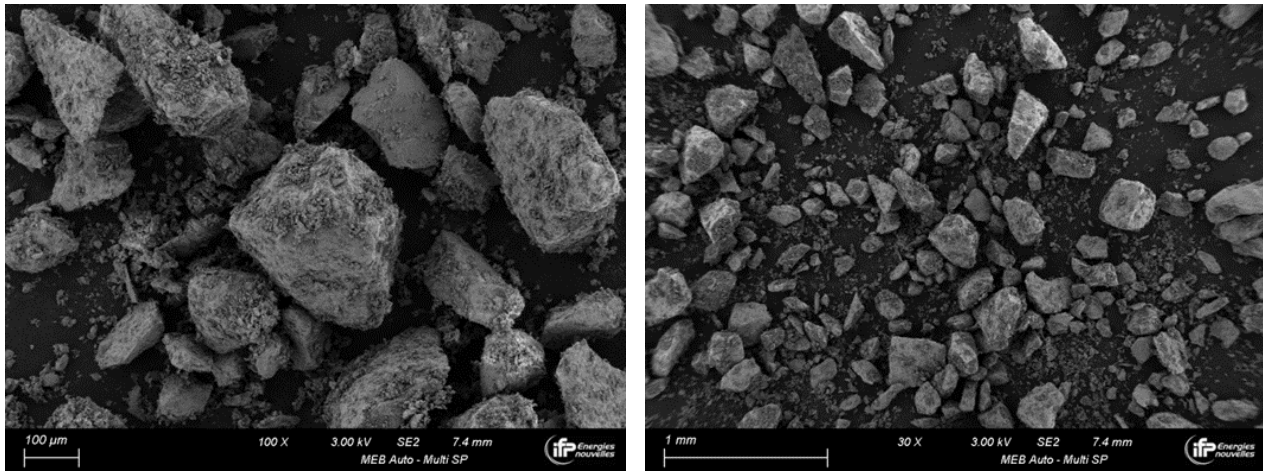


Figure 3-4: SEM pictures of LY-Mn ore powder

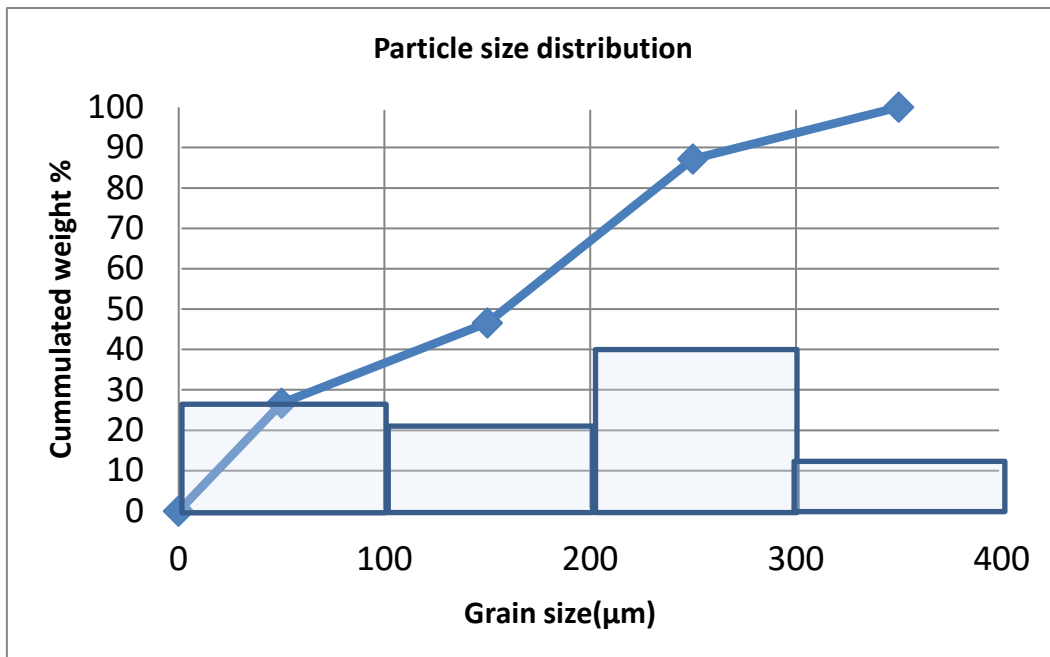


Figure 3-5: Particle size distribution of the original Ly Mn ore shipped to IFPEN

The same issue with fines were also encountered by the SINTEF ER 150 kW unit. Target range were 50 – 150 µm particle size. However, it turned out that the received material contained a lot of fines, plus a significant fraction with particles larger than 150 µm in the SINTEF ER batch. It was first made a trial to use the material as received, since sieving of this amount represents a large extra cost. Operation turned out to be difficult due to all the fines and it was decided that additional sieving was necessary, as was done also at IFPEN. Dry sieving was chosen to avoid another heating of the material. At SINTEF ER, cut size was set to 70 µm and it was sieved two times since it was hard to get rid of the fines. Even after the second sieving some fines were still present as seen in Figure 3-6. The figure shows that the resulting size fraction to be used in the pilot tests at SINTEF ER was mainly in range 60 – 200 µm with about 15 wt-% of material <60 µm diameter and about 10 wt-% material > 200 µm diameter.

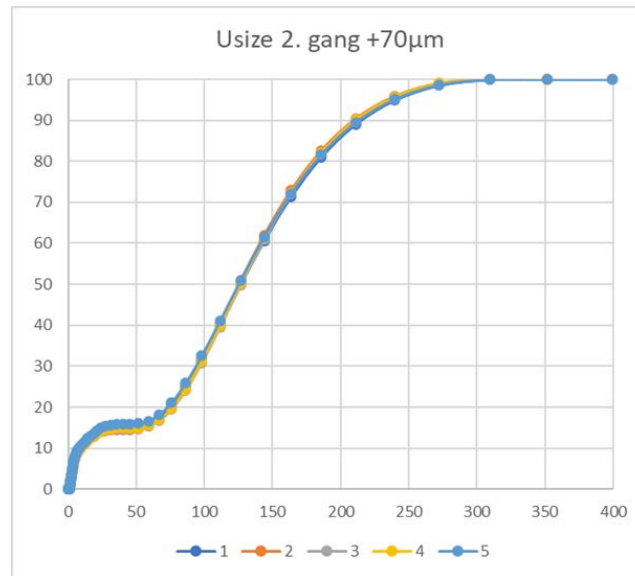


Figure 3-6: PSD of Mn-ore LY after sieving at SINTEF ER.

It was concluded that removing the fines from the Mn-ore is difficult, at least when dry sieving is used. Wet sieving could have been beneficial, but for the large amounts needed in the demo unit, the additional heating up and drying process is an extra step, adding further costs to the OC. However, removing the fines was needed to be able to operate with this OC material. A large improvement was obtained as can be seen in Figure 3-7, showing the material as received at SINTEF ER, and the material after sieving away most of the fines.



Figure 3-7: Mn-ore LY batch SINTEF ER as received (left) and after sieving (right).

The bulk density (poured) of the Mn-ore LY was about 1800 kg/m³.

3.3 Third oxygen carrier – Ilmenite T2

This is also a Norwegian ilmenite but compared to the first ilmenite (T1), this one (hereafter called ilmenite T2) has a larger particle size. The size fraction of this material is much more beneficial with respect to particle size for the 3 MW demo unit, since about 85 wt-% is larger than 180 μm as shown in Figure 3-8. It has almost exactly same composition as the T1 ilmenite, except it was completely dried before being used in the pilot units.

Early-stage testing of T2 showed serious problems with agglomeration and it was in fact rejected as a candidate. However, more recent tests at IFPEN showed that adding a small steam flow during heating up and OC activation could potentially avoid the agglomeration issue. The benefit of the more optimal particle size distribution is large and further testing was decided, as will be described later in the report.

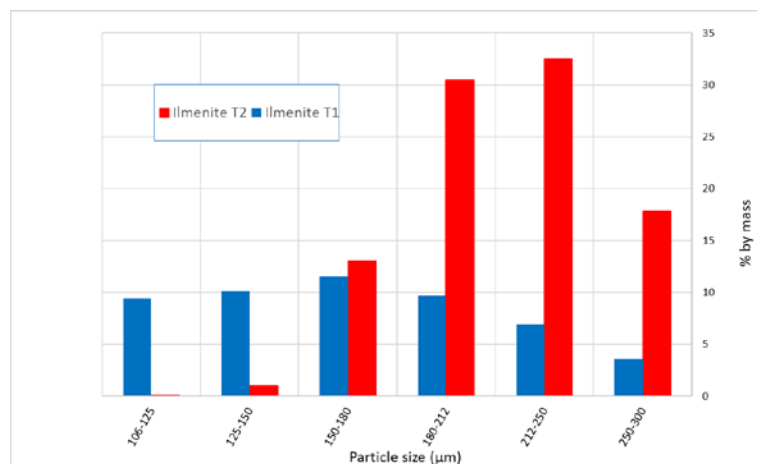


Figure 3-8: Particle size distribution of ilmenite T2 compared to ilmenite T1.



Figure 3-9: Picture of ilmenite T2.

4 FUELS

Fuels to be used in the European tests in the demo unit will be mainly petcoke plus some limited number of tests with biomass. The same fuels have therefore been used in the pilot unit tests. Their properties and supply are described below. Since the demo unit will require large amounts of fuel, it was decided to look for Chinese suppliers, especially for the petcoke, being the main fuel.

4.1 Petcoke

The chosen petcoke is a low-sulphur Chinese petcoke. It was chosen based on screening tests of three different candidates at IFPEN as described in the internal deliverable D3.1b (not public). Two tonnes of raw petcoke were shipped from Tianjin Mingxintai Petrochemical Co. Ltd. to Hamburg and further with truck to UVR-FIA GmbH in Freiberg. Here it was dried, milled and sieved into fractions < 100 μm , 100-315 μm and 315-500 μm . A lot of additional material not matching these fractions were also produced from the process. most notably is the variant of fraction 100-315 μm including 40 % fines (< 100 μm). The pure 100-315 μm fraction was limited so this one including fines had to be used by SINTEF ER due to the rather high fuel feeding required (> 100 kW_{th}).

The following quantities were finally transported to IFPEN an SINTEF ER:

<u>Size fraction</u>	<u>IFPEN</u>	<u>SINTEF ER</u>
< 100 μm	16.5 kg	100 kg
100 – 315 μm	40 kg	24 kg
315 – 500 μm	4	50
100 – 315 μm incl. 40 % fines < 100 μm)	---	240

The raw petcoke composition is shown in Table 4-1. The moisture content of the raw petcoke was about 13 wt-% which was dried to 1 wt-% at UVR-FIA. The lower heating value LHV of the final dried petcoke was 30 MJ/kg.

Table 4-1: Petcoke composition (wt-% dry) and lower heating value.

C	H	O	N	S	LHV (MJ/kg)
91.6	3.97	1.39	1.68	0.84	~ 30

In Figure 4-1 is shown a picture of the final pre-processed petcoke in size fraction 315–500 μm . The visual similarity with the ilmenite OC material should be noted. Care should be taken in labelling drums and buckets so fuel and OC are not mixed up during tests.



Figure 4-1: Petcoke, here shown size fraction 315 – 500 μm .

4.2 Biomass

The tests at SINTEF ER comprised also biomass as fuel. Biomass will be used in the demo unit and is relevant to test at pilot scale. Biomass is the solid fuel for which SINTEF ER have most experience and is therefore a good starting point before testing petcoke. The biomass fuel used is wood pellets delivered by Arbaflame. This is a steam-exploded wood pellet giving a brown colour and a more water-repellent and less sticky biomass than standard white wood. The biomass fuel was tested in three different variants: As whole pellets having a diameter of 8 mm and typical length 15 – 35 mm; milled and sieved to size $> 800 \mu\text{m}$; and milled without sieving, i.e. with fines included.



Figure 4-2: Arbaflame wood pellets. Whole (left), milled and sieved $> 800 \mu\text{m}$ (mid), milled and un-sieved (right).

Table 4-2: Biomass composition (wt-%) and lower heating value. All values based on fuel as received (a.r.)

C	H	O	N	S	H ₂ O	Ash	LHV (MJ/kg)
50.7	5.8	38.1	< 0.1	< 0.01	4.9	0.5	19.3

5 RESULTS WITH FIRST OXYGEN CARRIER – ILMENITE T1

5.1 SINTEF ER

5.1.1 Overview of tests

Table 5-1 sums up the tests performed with Ilmenite T1, being the basis for the results presented next. The long time between the two first tests were due to the installation of the new fuel screw feeder. With this in place the main test program was done during the last half of 2019.

Table 5-1: Overview of tests at SINTEF ER with ilmenite T1 as oxygen carrier.

21.09.2018	Whole wood pellets	Successful
07.06.2019	Milled and sieved wood pellets	Successful
07.06.2019	Mix 50/50 milled and sieved wood pellets / petcoke 315 – 500 µm	Successful
07.06.2019	Petcoke 315 – 500 µm	Successful
13.06.2019	Mix 75/25 milled and sieved wood pellets / petcoke 315 – 500 µm	Successful
13.06.2019	Milled and sieved wood pellets	Successful
22.10.2019	Petcoke 100 – 315 µm incl. 40 % fines	Un-successful - bed lost to AR downcomer
23.10.2019	Petcoke 100 – 315 µm incl. 40 % fines	Un-successful - bed lost to AR downcomer
24.10.2019	Petcoke 100 – 315 µm incl. 40 % fines	Un-successful – plugging of fuel injection pipe
12.11.2019	H ₂ , C ₃ H ₈ , CH ₄ "stress testing" for oxygen carrier agglomeration	Successful
13.11.2019	H ₂ , C ₃ H ₈ "stress testing" for oxygen carrier agglomeration	Successful
05.12.2019	Milled un-sieved wood pellets	Successful
05.12.2019	Mix 50/50 of milled un-sieved wood pellets / petcoke 100 – 315 µm incl. 40 % fines	Successful – short due to plugging of fuel injection pipe
06.12.2019	Milled un-sieved wood pellets	Successful
06.12.2019	Milled wood pellets, fines fraction after sieving	Un-successful – bed lost to AR downcomer

5.1.2 Summary of main test results

Table 5-2 shows main results and data from the experiments with Ilmenite T1, using biomass, petcoke and mixtures between the two as fuels. The conditions vary quite a bit between the experiments, especially the fuel reactor inventory. In the reactor system, most of the particle mass is found in the loop seals and downcomer pipes as the bed density of these bubbling or moving beds are higher than in the turbulent beds in the reactors, and the volume of these parts is relatively high (made of inside diameter 104 mm pipes). In fact, the downcomer pipes can hold the total particle inventory if it fills up, which has been observed when there has been a blockage in the bottom of the AR downcomer. Depending on the pressure distribution in

the system, the downcomer bed levels will vary, and hence strongly influence the inventory in the air and fuel reactors. The lifter fluidisation is another factor affecting the FR inventory very much.

Table 5-2: Summary of main operating conditions and performance results, SINTEF ER with ilmenite T1.

Test No.	Type of fuel	FR gas conv. efficiency (%)	CO ₂ capture rate (%)	AR riser mass flow (*) (kg/s)	AR top / bottom temp. (°C)	FR bottom temp. (°C)	Fuel power (kW)	FR inventory (kg)	Specific FR inventory (kg/MW)
T1-1	Biomass pellet	81.9	88.3	7.4	1019 / 1011	996	108.6	27.5	253.2
T1-2	Biomass milled/ sieved 1	80.2	92.3	3.4	1010 / 1000	976	99.7	12.2	122.4
T1-3	Biomass milled/ sieved 2	78.3	91.1	3.8	998 / 989	961	113.0	10.0	88.8
T1-4	Biomass milled/ un-sieved	79.4	93.5	2.9	991 / 983	954	120.3	15.4	127.8
T1-5	Mix b/p 75/25	89.1	64.8	4.7	998 / 989	973	80.5	20.0	248.6
T1-6	Mix b/p 50/50	90.9	47.5	4.8	1001 / 990	974	93.1	22.6	242.8
T1-7	Petcoke 315–500	95.7	33.2	3.9	1041 / 1015	1011	126.6	23.5	185.6
T1-8	Mix b/p 50/50 w/fines	85.5	57.6	4.8	999 / 991	966	109.4	28.7	262.3

(*) Analytically calculated theoretical riser mass flow as described in Ch. **Error! Reference source not found.**

5.1.3 FR gas conversion efficiency and capture rate

Figure 5-1 and Figure 5-2 show the CO₂ capture rate and FR gas conversion efficiency for the tests summarised in Table 5-2. The highest capture rate was obtained for biomass. The un-sieved biomass containing a large share of fines has above 93 %, the sieved biomass having larger particles have 91 – 92 % and whole pellets has 88 %. The lowest capture rate was obtained for petcoke in size fraction 315 – 500 µm with just above 30% capture rate. It is obvious that a large part of the petcoke is not gasified in the fuel reactor but follows the oxygen carrier particles to the air reactor, where it is combusted to CO₂ by the hot air. The FR gas conversion efficiency on the other hand, is highest for petcoke, which may seem contradictory to the low reactivity of petcoke. This is because the calculated fuel reactor gas conversion only takes the gaseous species into account. The conversion from solid to gas is not covered by this number. When large part of the petcoke is not converted, less gas is produced, and the oxidation of this smaller amount goes more quickly and

complete towards CO₂ and H₂O. The FR gas conversion efficiency is about 80 % for all the biomass tested. Slightly higher for the whole pellets than for the others, most likely due to the increased residence time in the bottom of the FR.

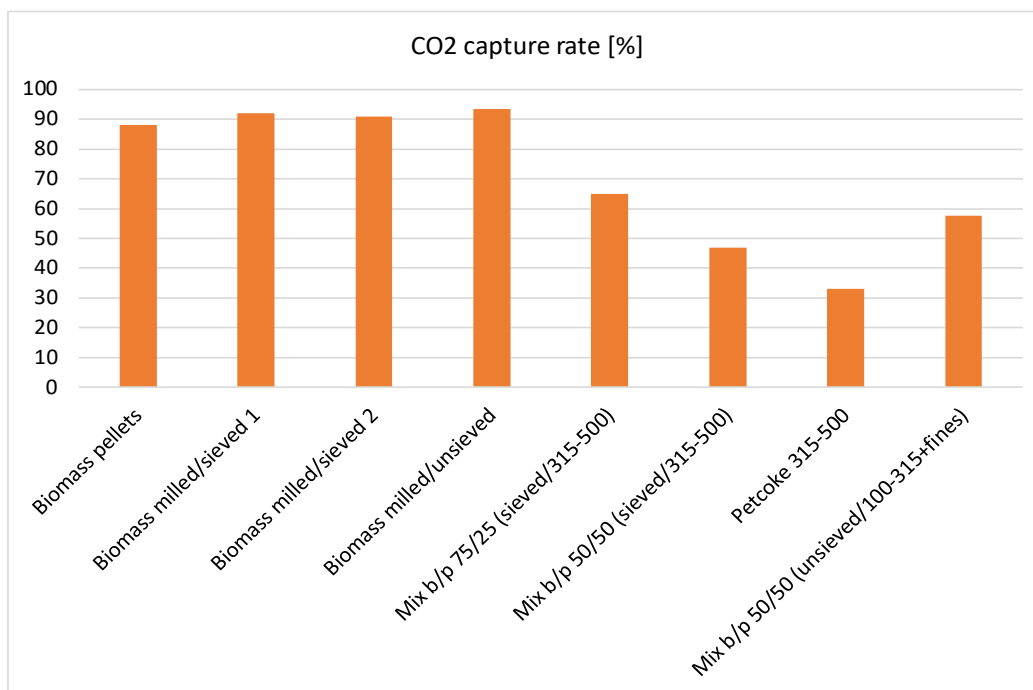


Figure 5-1: CO₂ capture rate.

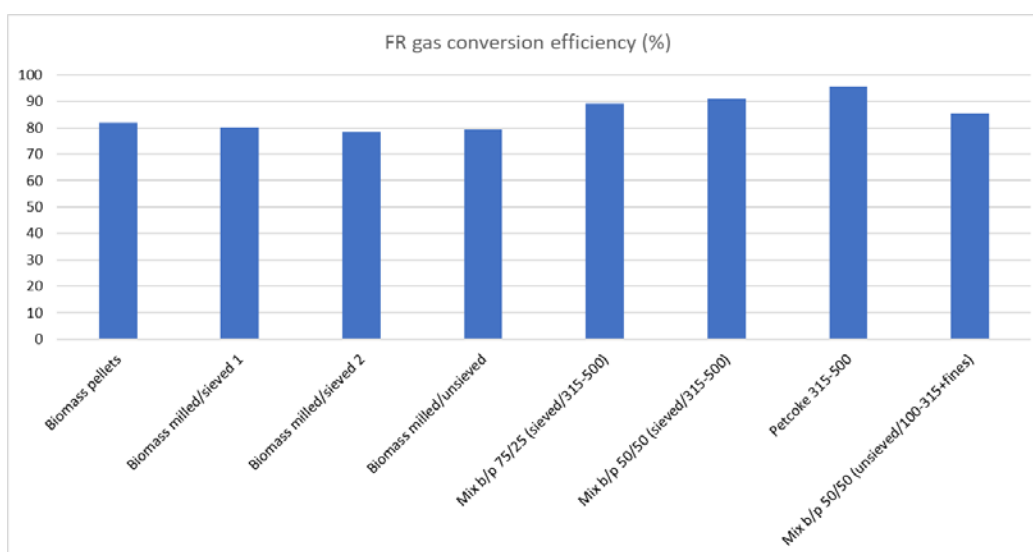


Figure 5-2: Fuel reactor gas conversion efficiency.

The results at the very right in the figures are from using a 50/50 mixture of the un-sieved crushed wood pellets with the fines, and the petcoke 100–315 μm including 40 wt-% fines (<100 μm). For the other tests with fuel mix, the biomass fines are sieved away and the petcoke is the 315–500 μm fraction. Thus, compared

to the other 50/50 mixture, both the biomass and petcoke is in this case of smaller particle size. The CO₂ capture rate becomes higher (57.6 % vs 47.5 %), and the gas conversion efficiency is somewhat lower (85.5 % vs 90.9 %). The smaller petcoke size is clearly increasing the fraction of fuel being gasified in the FR, thereby reducing the char losses to the AR, however, a somewhat smaller share of the gases from gasification is fully converted in the FR.

Figure 5-3 - Figure 5-8 show main temperature data from whole day experiments on September 21st 2018, and June 7th 2019. The tests cover whole biomass pellets, milled and sieved pellets as well as petcoke in 50/50 mix with milled pellets plus petcoke alone. Also shown are some short time series of measured gas concentrations. Even though there are some variations in the way the reactor is operated (variations in the amount of N₂ for loop seal and lifter fluidisation, amount of steam for FR fluidisation, temperatures, fuel power and OC inventory), some general observations can be made. The first thing is that the experiments with pure biomass has much lower CO₂ concentration from the air reactor. This is probably both a result of the high volatile content of biomass, and that the char from biomass is more reactive than the petcoke char. In this way, much less carbon is transferred to the air reactor as the volatiles released in the fuel reactor follows the gas flow upwards in the reactor and is partly converted by the oxygen carrier to CO₂ and H₂O. The biomass char will also react more rapidly. However, because of much higher gasification rates with biomass, the concentrations of CO, CH₄ and H₂ out of the fuel reactor is also much higher. The CO concentration is around 6 vol% when using biomass only, which can be considered very high when comparing to ordinary combustion. The high concentration of these components is a result of low gas residence time and the limited reactivity of the ilmenite. In a full-scale reactor, increased height and thus residence time would lead to a much better conversion of these species.

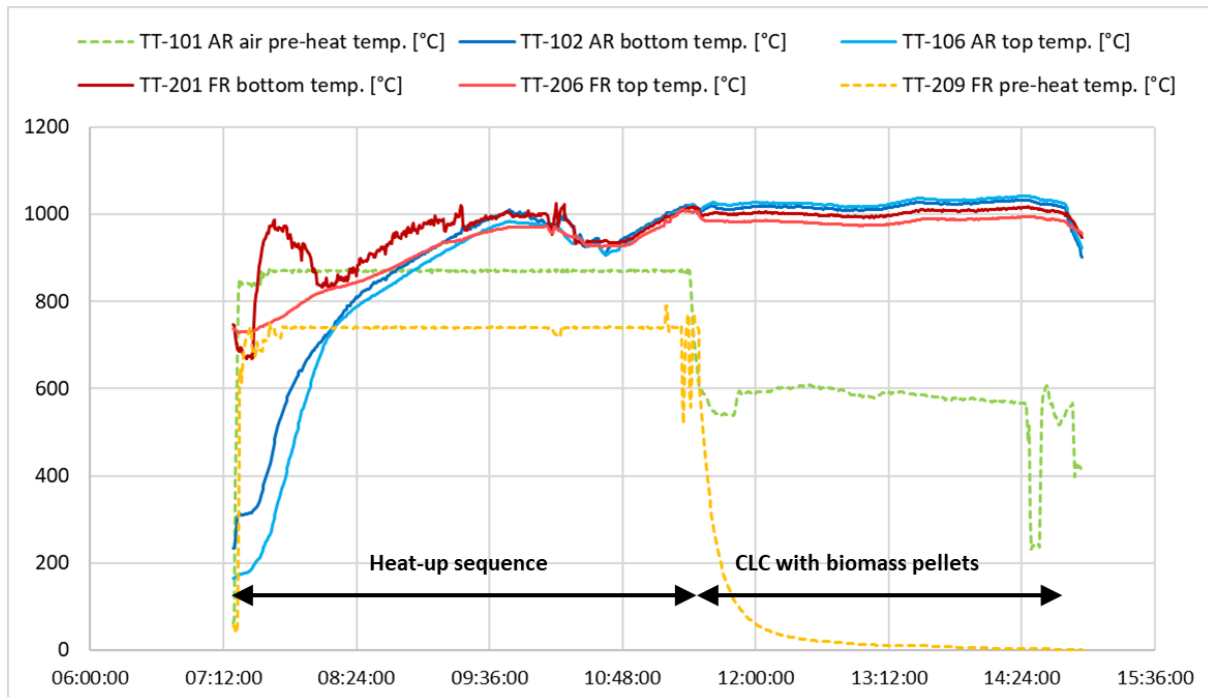


Figure 5-3: Reactor temperatures, test with biomass pellets (September 21st, 2018).

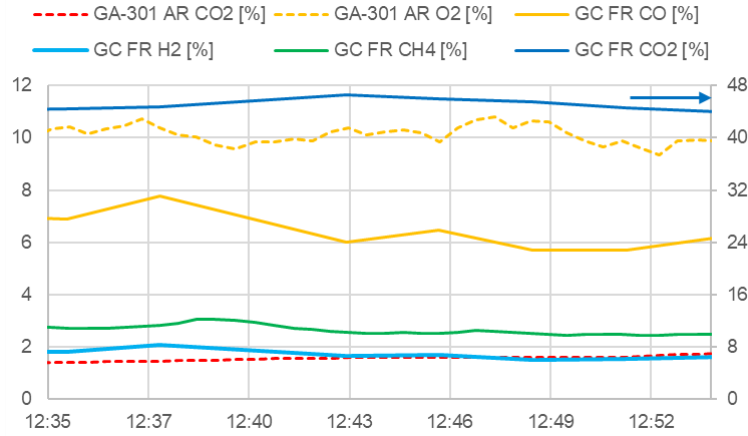


Figure 5-4: Exhaust gas composition from FR and AR, test with biomass pellets (September 21st, 2018).

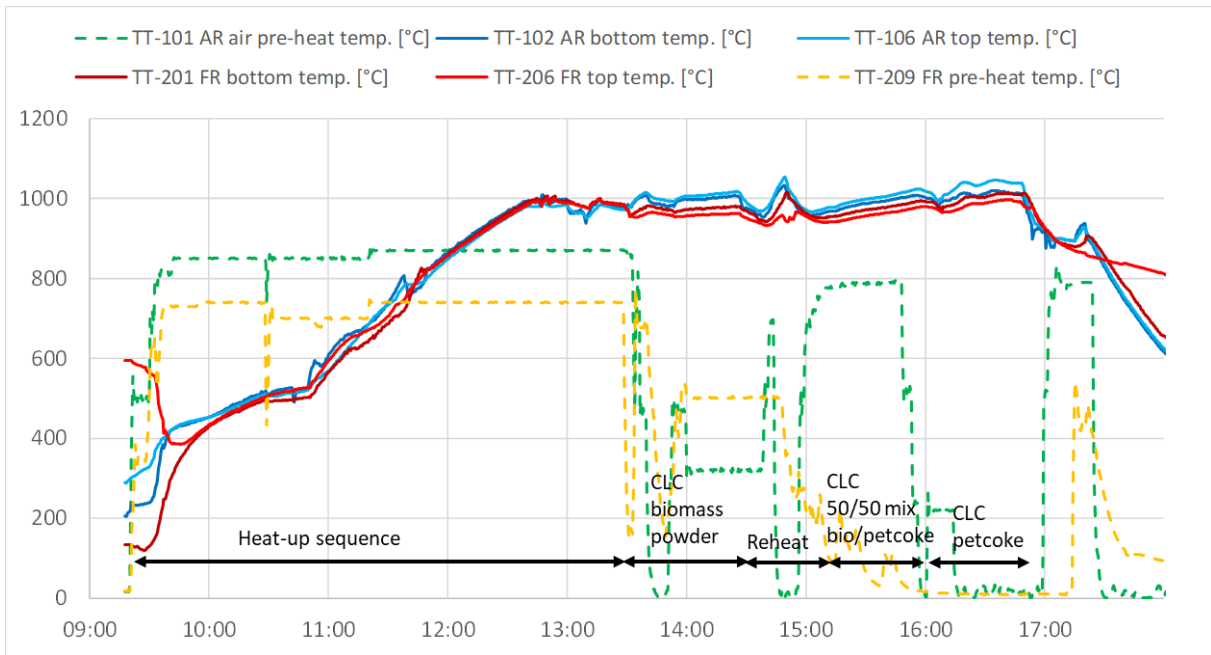


Figure 5-5: Reactor temperatures, test with biomass powder (milled and sieved pellets), mix 50/50 biomass powder/petcoke 315-500 μm, and only petcoke 315 – 500 μm (June 7th, 2019).

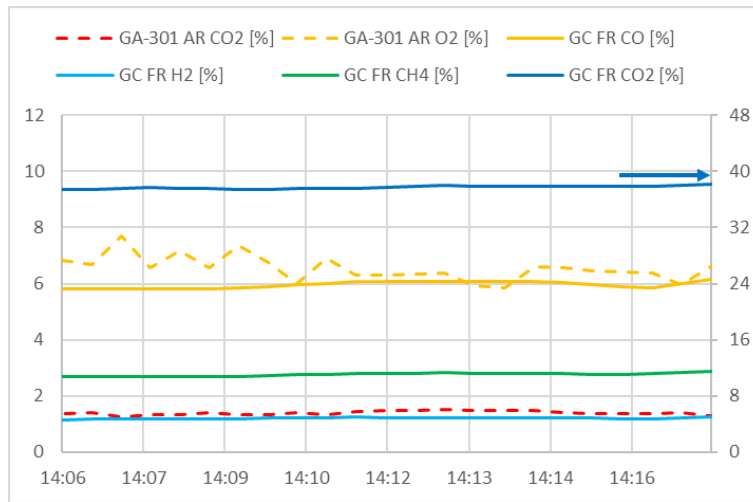


Figure 5-6: Exhaust gas composition, biomass powder (June 7th, 2019)

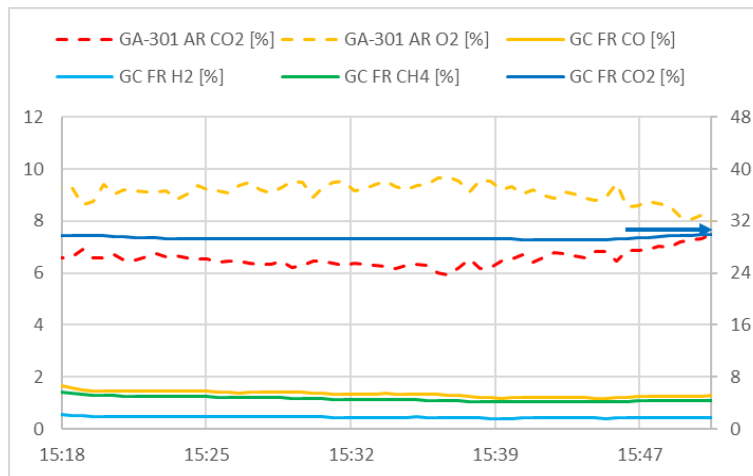


Figure 5-7: Exhaust gas composition, mix 50/50 biomass powder/petcoke (June 7th, 2019)

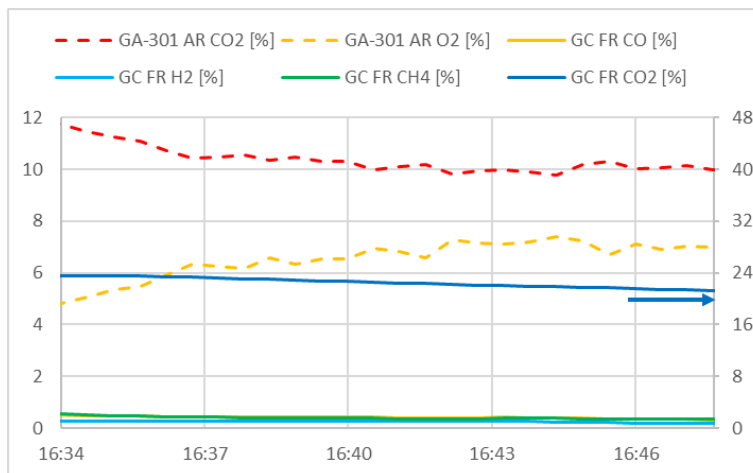


Figure 5-8: Exhaust gas composition, only petcoke (June 7th, 2019)

5.1.4 Solid circulation and oxygen carrier conversion

The theoretical riser mass flow in Table 5-2 is calculated from the pressure gradient in the top part of the AR, the superficial gas velocity, and the terminal velocity of the particles. This is not the true particle circulation between the reactors, because an unknown amount of the particles is moving downwards along the walls of the reactor. Since the unit has no direct measuring of the circulation rate, we can use CFD calculations as an alternative way of assessing this. The whole reactor system was simulated with CFD as reported in the internal deliverable D3.4b (not public). For an earlier case operating with biomass pellets, the time-averaged mass-flow rate of solids leaving the reactors from the top outlets were calculated and compared to the theoretically calculated value. The values are summarised in Table 5-3. As can be seen, the CFD mass flow rate out of the AR is only 28 % of the calculated theoretical riser mass flow rate in the top part of the AR. However, this figure is very well comparable to results obtained by Markstöm et al. ([3], [4]) where it was reported to be about 29 % in one case and as low as 8 % in another case. They point out that this fraction is expected to be different for different reactor designs, superficial velocity, and concentration.

Table 5-3: Evaluation of oxygen carrier mass flow rates.

	AR	FR	Lifter (by difference)
CFD oxygen carrier mass flow rate leaving reactor top outlet	2,25 kg/s	0,55 kg/s	1,7 kg/s
Theoretically calculated riser mass flow for same case	8,1 kg/s		
CFD mass flow rate / theoretical riser mass flow rate	28 %		

The CFD data indicates that the FR circulates only about one-fourth of the total circulation rate, i.e. 0,55 kg/s vs totally 2,25 kg/s. The FR operates like a dense turbulent bed and most of the oxygen carrier enters the AR through the lifter. The AR behaves more like a circulating fluidised bed. This difference in the reactor fluidisation regime is also seen from the experimental pressure profiles shown in Figure 5-9.

The case used in Table 5-3 has almost identical operating conditions as the first case in Table 5-2 on whole biomass pellets. Assuming that the total circulation rate will be 28 % of the theoretical riser mass flow, the total circulation rate for the first case in Table 5-2 will be 2,07 kg/s or 7450 kg/h of oxygen carrier. With a maximum oxygen capacity of ilmenite (R_0) of 4.9 %, this is equivalent to a maximum oxygen transfer of 365 kg/h. This is enough to completely convert about 255 kg/h wood pellets (or about 132 kg/h petcoke). In the present case the biomass pellet feed was 20,2 kg/h and the oxygen carrier conversion factor (ΔX) would then be about 0,08 for full conversion of this fuel feed. In addition, 12 % of the fuel is lost to the AR which indicates a conversion factor (ΔX) of 0,07. This gives a $R_0\Delta X$ value of 0,34%. And in fact, it is likely slightly lower since not all fuel in FR is fully converted. I.e., the present reactor system is characterised by high solid circulation and low exploitation of the oxygen capacity of the oxygen carrier. This is also indicated by the temperature difference between the reactors, which is usually below 35 °C (cf. Table 5-2).

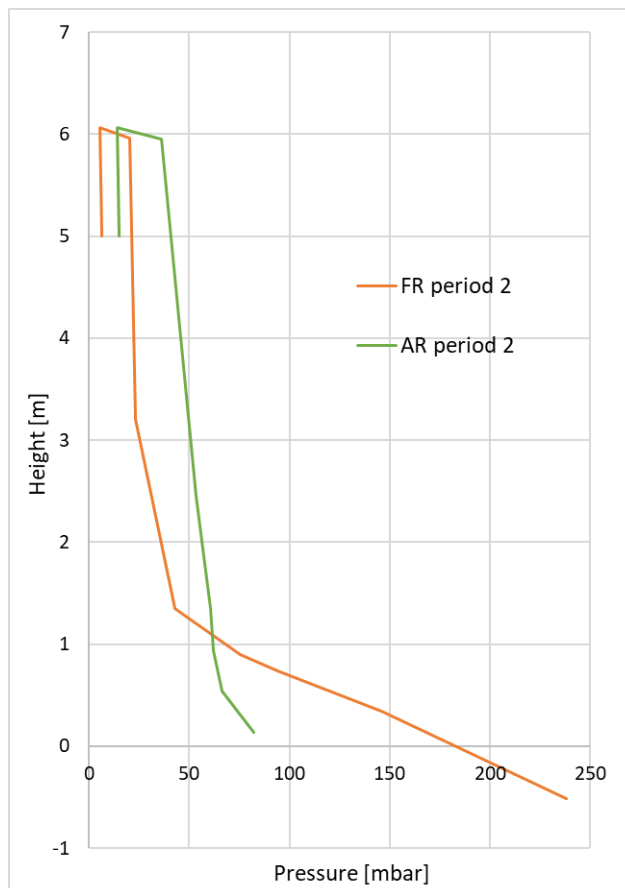


Figure 5-9: Pressure profile up along reactor height from experiment

From the analysis above it can be concluded that the oxygen carrier particles will not be very "stressed" in the present system and will likely be far from fully reduced. From the initial lab testing of the ilmenite, it has been shown that highly reduced material is more prone to agglomeration. Such a condition will be more likely in the demo unit with much larger residence times and less overall oxygen surplus. The design of the IFPEN pilot unit is more equal to the demo unit in that respect.

5.1.5 Oxygen carrier characterisation

As mentioned in chapter 2.1, the possibilities for oxygen carrier sampling during operation is limited to the material lost from cyclones. Since the cyclones do not separate very sharply, the samples taken downstream the cyclones are still relevant to evaluate the particle porosity, elemental composition, and possible element segregation. Especially the iron-titanium segregation is of interest since iron diffusing to the surface is a main cause of agglomeration of ilmenite.

During operation, the bucket and the larger low-velocity chamber (cf. section 2.1) of each reactor are emptied regularly to keep track on total OC inventory. Since the cyclones do not separate efficiently enough, the loss of useful OC would be too large if it were just disposed of. Therefore, a large share of the OC collected after the cyclones are fed back through the OC feeding screw. Especially the OC from the buckets since the particles here are generally larger in size than those from the low-velocity chamber. With this OC re-use, the average operational time for each particle within the reactor system increases.

Figure 5-10 shows a SEM and an EDS picture of a fresh ilmenite sample. NOTE! This is taken from a sample of larger particle size than used in the present tests, however, the microstructure of the particles will be the same. As can be seen, the particles consist mostly of a well-mixed Fe-Ti oxide being violet in the Fe-Ti EDS map. Some areas with Ti enrichment are also seen.

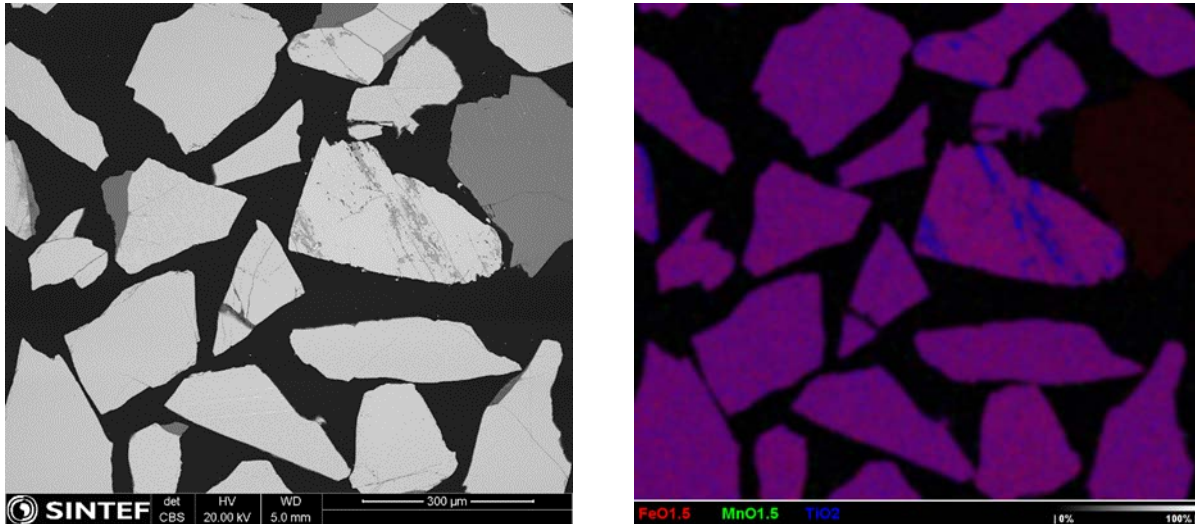


Figure 5-10: Fresh ilmenite T1. SEM atomic mass contrast (left) and EDS Fe, Mn, Ti oxides (right). Analysed in May 2018. NOTE! This is from a larger size fraction than used in the present tests.

In Figure 5-11 to Figure 5-14 are shown SEM and EDS pictures for samples taken the last day of the tests, on December 6th (cf. Table 5-1). The samples will therefore represent a mix of particles that have spent long time within the reactors, and some particles that could be rather fresh since we had to start refilling with fresh particles we had from earlier. Figure 5-11 and Figure 5-12 show pictures from FR bucket and FR chamber. Compared to the fresh ilmenite, we see that the particles range from well-mixed Fe-Ti oxide (as the fresh ones) to marked porous Ti-core with a Fe-shell. Logically, the average particle size of the chamber sample is smaller than for the bucket sample. The particles being well-mixed Fe-Ti oxide with little porosity seem to be the larger ones. This is strange with respect to cyclone efficiency and is a good indication it does not separate well enough.

Figure 5-13 and Figure 5-14 show SEM and EDS pictures from the AR bucket and chamber. The trend is the same for the FR samples with respect to elemental segregation and porosity. Two clear differences from the FR samples are:

- The average particle size of the chamber sample is just slightly smaller than the bucket sample. The difference was larger for the FR samples.
- It seems that the particle losses through the AR cyclone in general have a larger average particle size than the losses from the FR.

The last point is also clearly seen from the optical images in Figure 5-15.

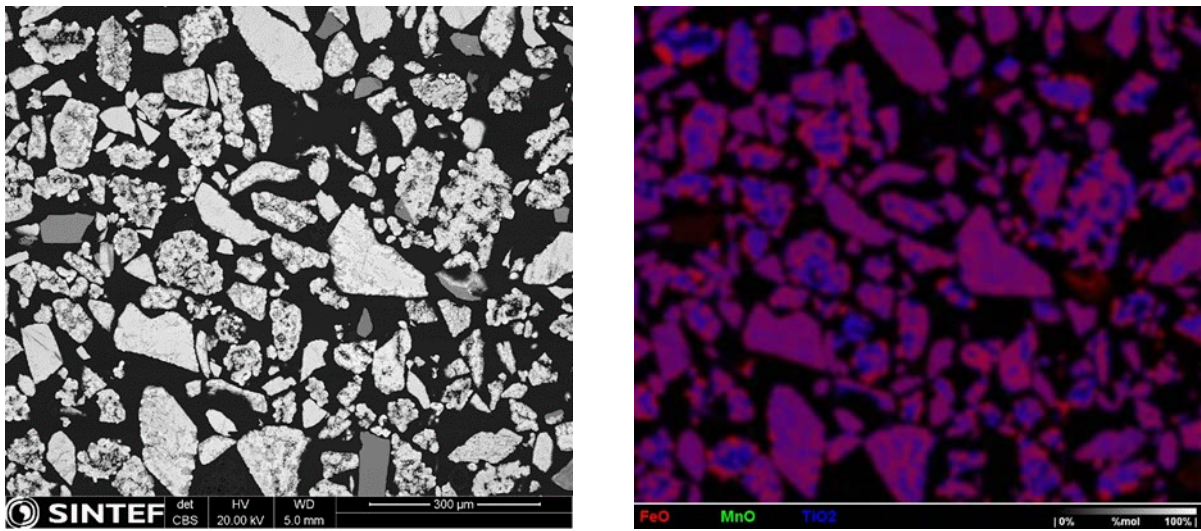


Figure 5-11: Sample from FR bucket. SEM atomic mass contrast (left) and EDS Fe, Mn, Ti oxides (right)

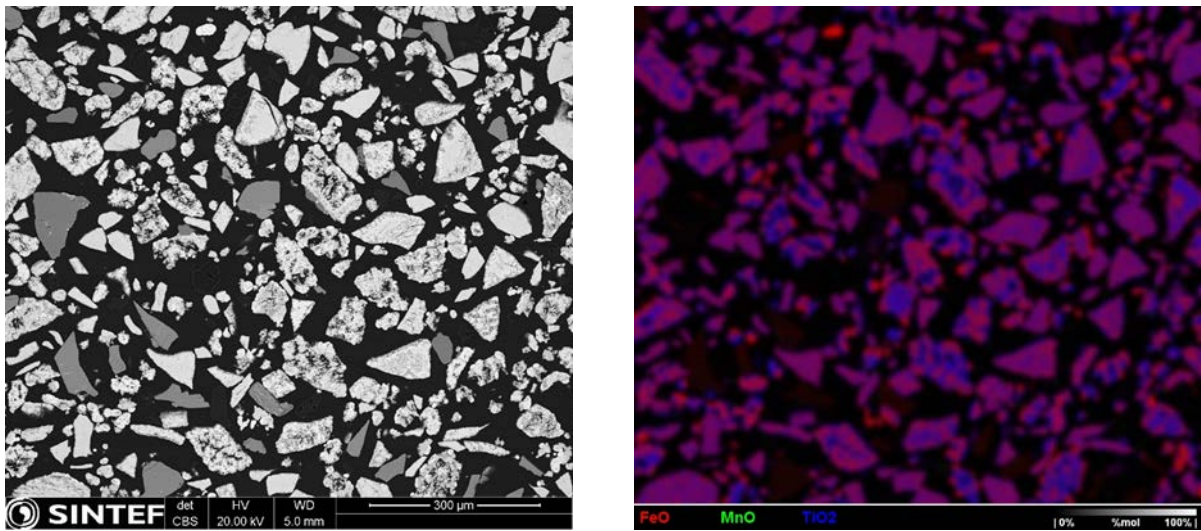


Figure 5-12: Sample from FR chamber. SEM atomic mass contrast (left) and EDS Fe, Mn, Ti oxides (right)

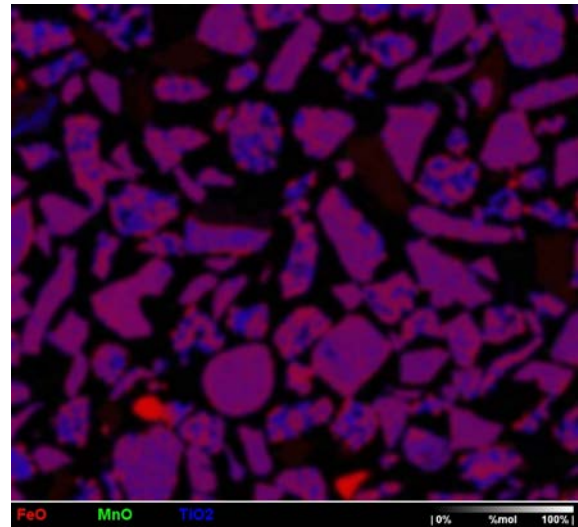
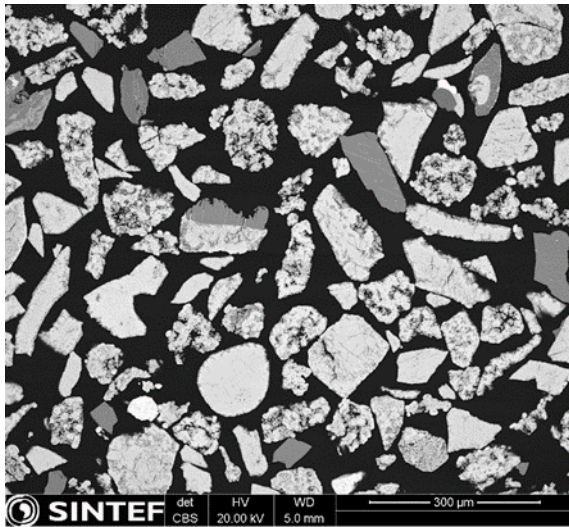


Figure 5-13: Sample from AR bucket. SEM atomic mass contrast (left) and EDS Fe, Mn, Ti oxides (right)

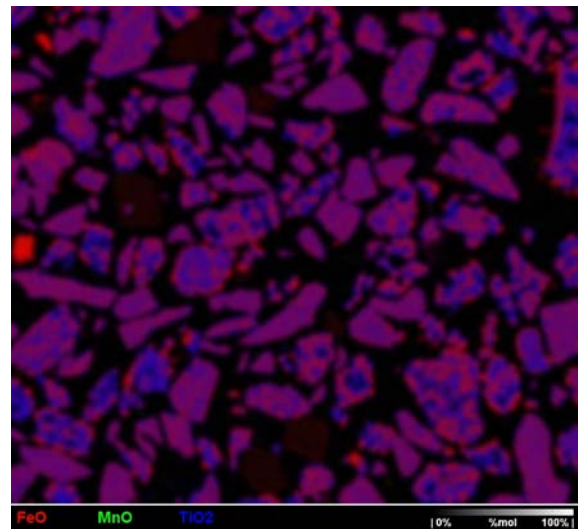
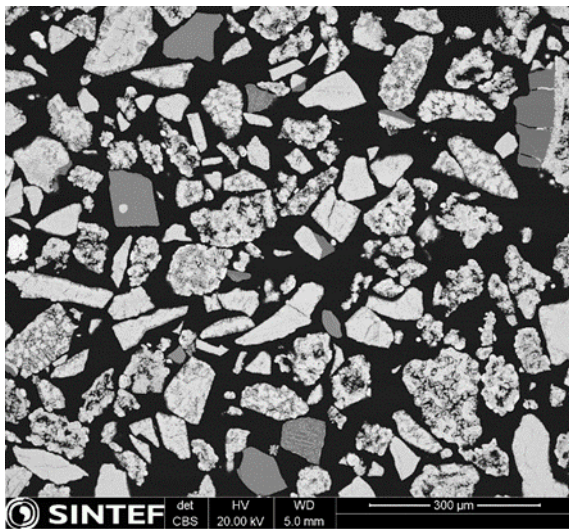


Figure 5-14: Sample from AR chamber. SEM atomic mass contrast (left) and EDS Fe, Mn, Ti oxides (right)

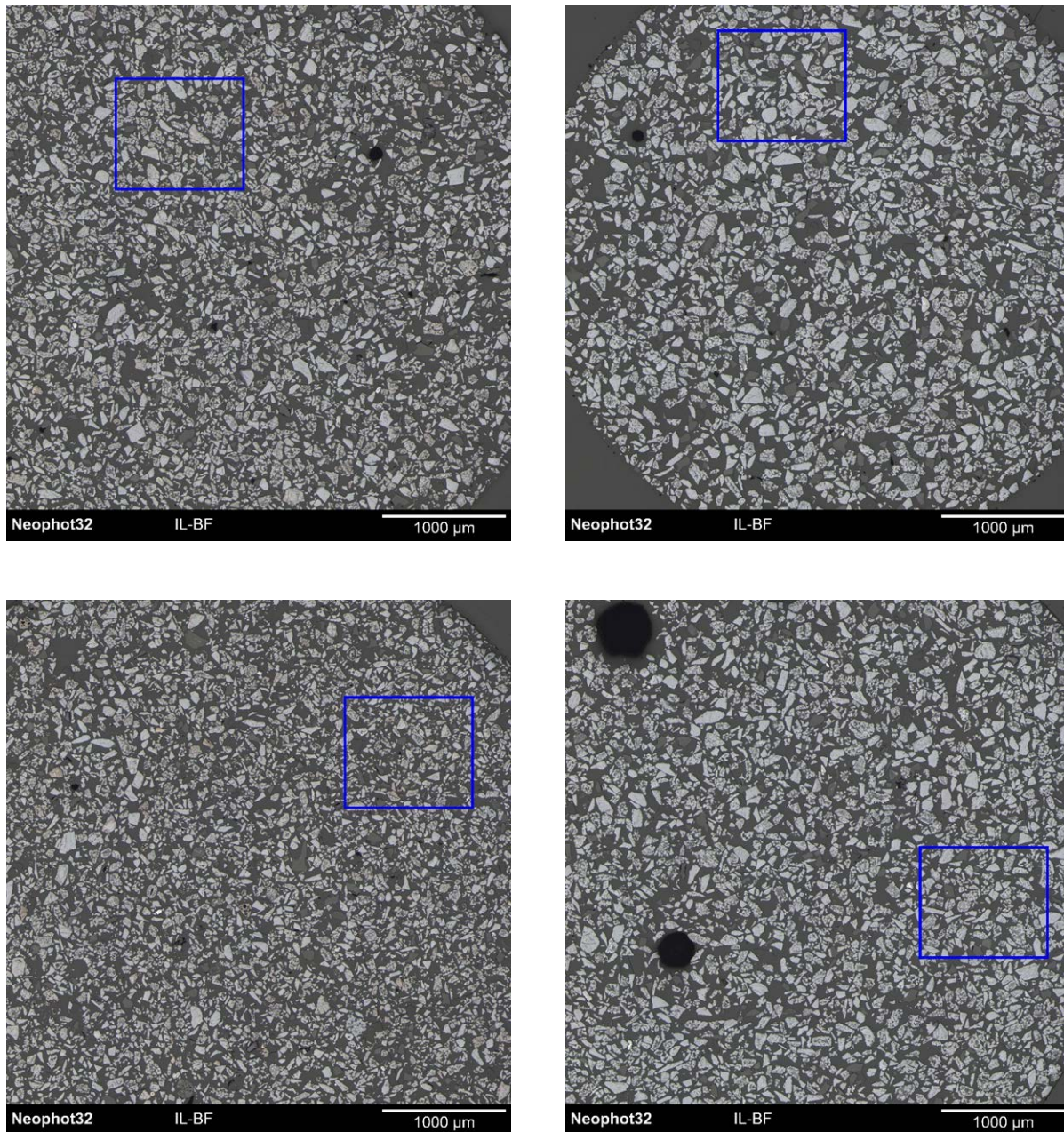


Figure 5-15: Optical images, bright field. FR bucket (upper left), FR chamber (bottom left), AR bucket (upper right), AR chamber (lower right).

From the SEM and EDS pictures it can be concluded that the oxygen carrier particles are somewhat more porous and segregated than the fresh one. Some of them show a clear Fe shell that may cause agglomeration issues, but as pointed out in section 5.1.4, the particles are not very "stressed" and should have a lot of remaining lifetime. No fully degraded particles with only Ti-oxide core were observed.

5.1.6 Agglomeration tests

Very strong agglomerations of ilmenite particles have been observed both in the batch unit and in the continuous pilot unit of IFPEN. As this could potentially be a large problem for the demo unit, it was decided to study this further. A main concern has been that the ilmenite particles could strongly agglomerate if the fluidisation gas is lost when the reactor is at high temperature, leading to an almost impossible task of removing agglomerated or sintered ilmenite in the whole reactor system. In the SINTEF pilot, only weak agglomerations have been observed, which seems to crush by very little force. It was decided to do tests in the SINTEF rig that should really facilitate agglomeration, to stop fluidisation at high temperature and let the particle beds stay to agglomerate. NOTE! These tests were done in November (cf. Table 5-1) and the particle samples did not have as long time in operation as the samples shown earlier, taken after end of tests.

The first test day, the reactor was heated by combustion of propane, methane and hydrogen with air in both reactors. Temperature time series are shown in Figure 5-16.

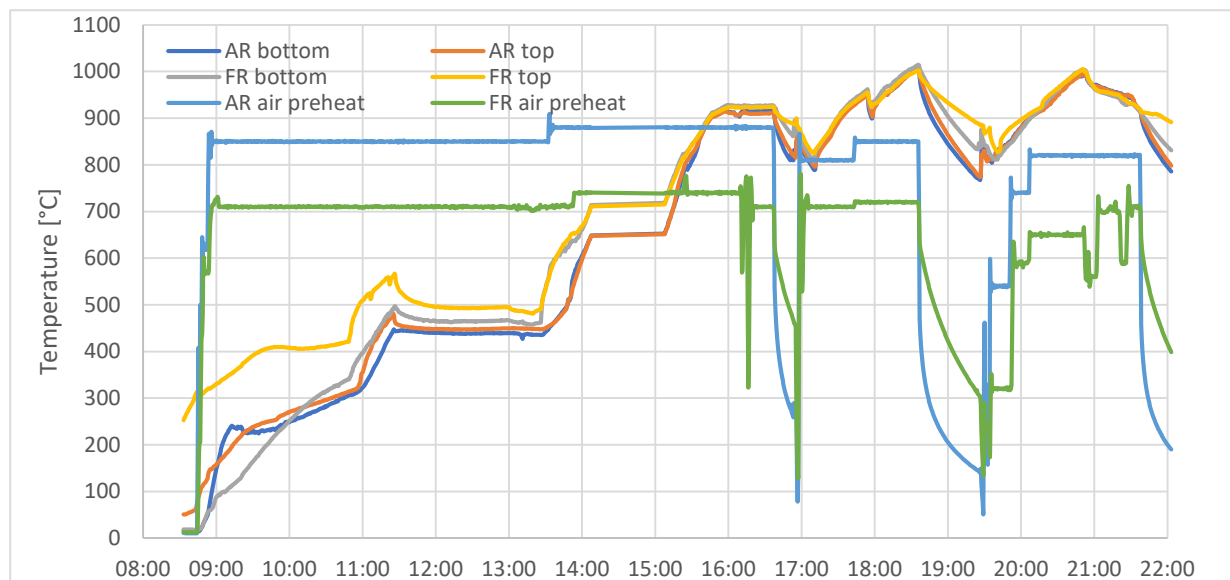


Figure 5-16: Reactor temperatures during agglomeration test, day 1

Following the temperature development in the reactor, the temperature was above 900°C at around 16 o'clock. Then all fluidisation was shut down by pushing the emergency shut down bottom at around 16:40. The reactor was left without fluidisation for about 15 minutes before air was introduced, and at around 17:05 the flow of fluidisation gas was the same as before the shutdown. There were no signs of de-fluidisation or plugging. The heating was then continued by combustion in both reactors until the temperature reached 1000°C at around 18:35. Then a new emergency shutdown was performed, and the reactor was left without fluidisation for 50 minutes before starting fluidisation. No signs of agglomeration were observed after this test either, and heating was continued until the temperature was back to 1000°C at 20:55. Then a transition to CLC operation was attempted, because agglomeration tendency will be stronger when the particles are in reduced state. The fuel to the fuel reactor was methane, and full CLC mode was not obtained as the temperature gradually decreased and the fuel conversion was poor (which is a general issue with methane and ilmenite). At around 21:30, the fluidisation was therefore abruptly stopped, and the reactor was left for the next day.

No problems with fluidisation were observed when starting at day 2 either, except that some of the pressure transducer tubes were blocked and had to be flushed. The aim for this experiment was to run full CLC before abrupt shutdown, and to achieve as reduced particles as possible in the fuel reactor. Figure 5-17 shows the temperature development during the experiment.

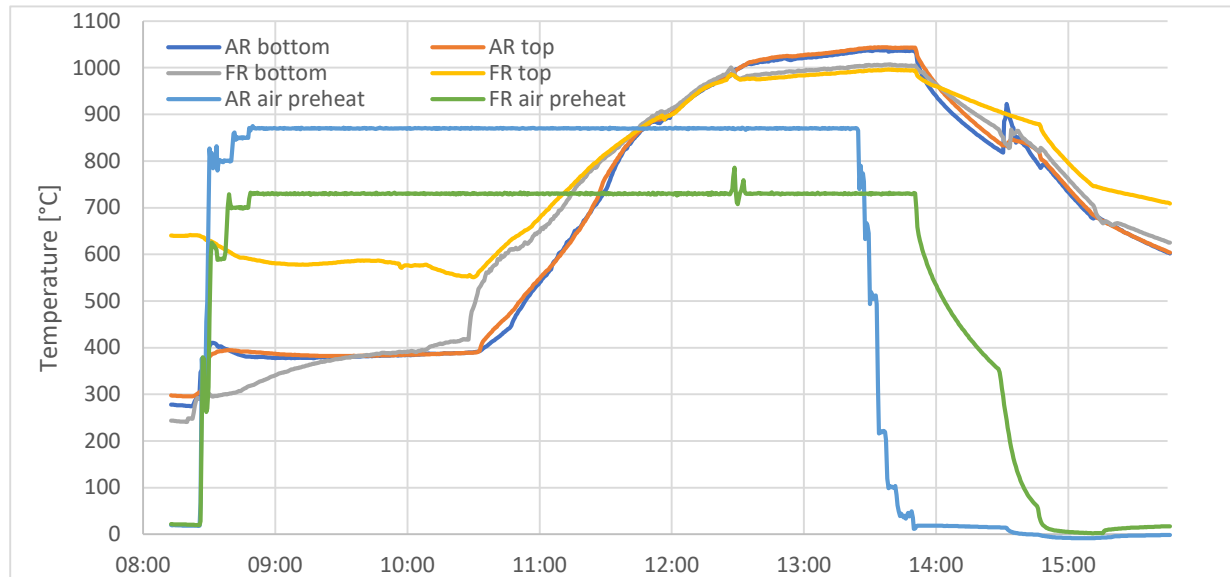


Figure 5-17: Reactor temperatures during agglomeration test, day 2

The transition to CLC operation took place at about 12:30, and full CLC was obtained at 13:00. The fuel reactor was then fuelled with about 63 kW hydrogen and 52 kW propane. A full gas analysis was not performed during this experiment, but the O₂ was measured from the AR and the CO was measured from the FR. During the CLC period, the O₂ level from the AR was 3 – 4 vol% dry, and the CO level was 4 – 5 vol% dry, which means the oxygen carrier should be in a rather reduced stage. At 13:50, an emergency stop button was pushed so fluidisation was abruptly stopped. The temperature was then about 1040°C in the AR and 1000°C in the FR. The fluidisation was started again at 14:30. Again, no indications of agglomeration was observed, and particle circulation could be restored without problems. However, several pressure transducer tubes were blocked.

The tests suggest that ilmenite is not particularly prone to serious agglomeration in case of loss of fluidisation, at least not in the present system. As described in chapter 5.1.4, the system is not stressing the oxygen carrier very much with respect to oxidation and reduction degree. Unfortunately, no particle samples could be obtained from within the reactors just before it was stopped, and it is therefore not possible to establish exactly to what degree the particles were reduced. However, particle samples were taken from the reactors after the test was finished but then they had been subject to a short fluidisation to check it could start again. There were found some small agglomerates in the samples taken out, such as shown in Figure 5-18. The agglomerates could be easily broken and crushed with the fingers, as shown in the picture.

SEM and EDS pictures of the agglomerates are shown in Figure 5-19 and Figure 5-20. There are only a few contact points between the particles in the agglomerate. The higher magnification shows clearly that the contact points are enriched in Fe.

One notable difference between these agglomerates and the samples presented in Ch. 5.1.5, is that the agglomerates seem to contain a much higher content of well-mixed Fe-Ti oxide and are less porous and

degraded. This is likely due to the shorter time in operation for the OCs in this test compared to the tests in Ch. 5.1.5.



Figure 5-18: Small agglomerates taken out from reactors after agglomeration test day 2. Easily broken and crushed with the fingers.

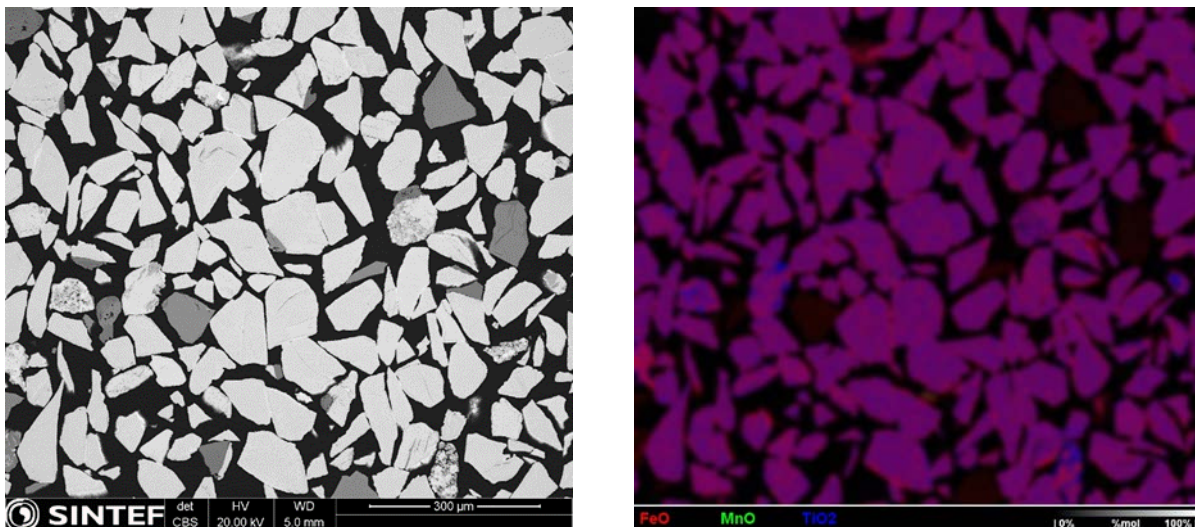


Figure 5-19: SEM (left) and EDS (right) of agglomerates

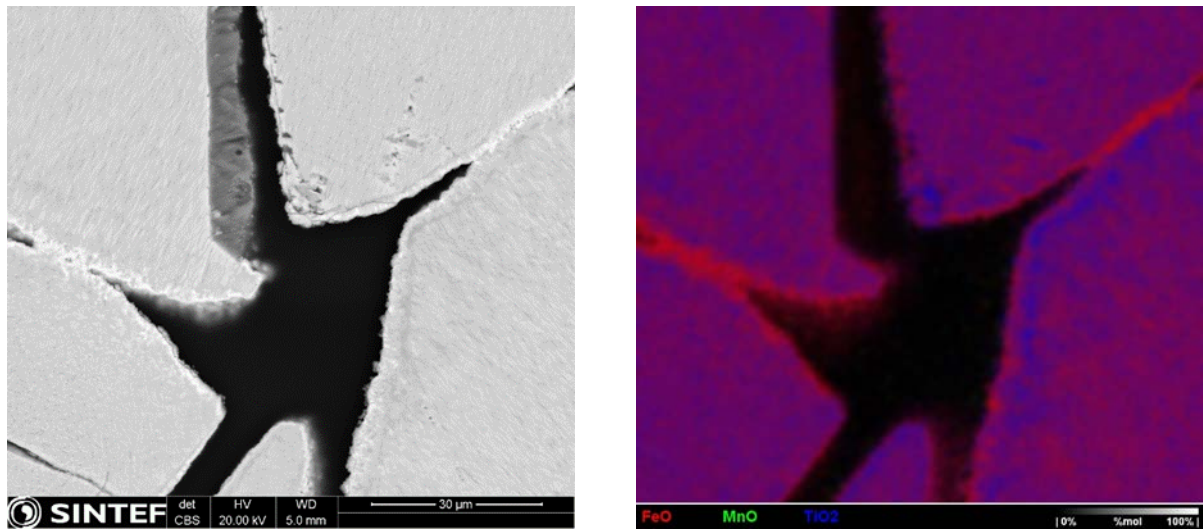


Figure 5-20: SEM (left) and EDS (right) of agglomerates, higher magnification.

5.2 IFPEN

IFPEN's tests were performed using the same ilmenite ore as that used by SINTEF ER, except the OC particles were selected in the 180-300 μm size range as required by the IFPEN pilot design.

Red-ox cycles with methane was used to activate the particles before starting the petcoke tests.

5.2.1 Operating conditions

The performance of the CLC process depends on the selected operating conditions, among which:

- Reactors' temperature:

The temperature of the reactors is controlled on the pilot unit with heating wire. The fuel reactor (FR) temperature can be modified for each test. In these campaigns, it was varied between 900 and 950 °C with a value of 900 °C for most of the tests. Since petcoke requires a high temperature to reach good conversion, lower temperatures were not studied.

The target temperature of both air reactors was set at 850 °C for each test. In the second air reactor, where reaction exothermicity is lower (most of the OC re-oxidation is performed in the first air reactor), the heating power is sometimes insufficient for achieving 850°C but this has no impact on the process since the OC is fully oxidized at that stage.

- Reactors gas flow rates:

The reactors inlet gas flow is composed of steam and nitrogen (+ methane in gas combustion mode) for the FR and air for the air reactors (AR1 and AR2).

Experimental measurements have been performed with ilmenite in order to determine its minimal fluidization velocity. Fluidization begins at a gas velocity of 5.8 cm/s at 19°C. The value of the total inlet gas flow rate in the FR has been chosen to operate between 2 and 3 times the minimal fluidization velocity of the OC to ensure proper fluidization regime.

The inlet gas flow rates of the air reactors are adjusted to obtain a high oxidation level of the material in both reactors in order to ensure a fully oxidized state of the material at the inlet of the fuel reactor. The total gas flow rate used in these reactors is generally around 2 Nm³/h which corresponds to a superficial velocity around 5 times the minimal fluidization velocity.

In the tests at varying temperatures, the total gas flow rate has been adjusted in order to maintain the required gas velocity in the fuel reactor.

- Methane concentration:

During OC activation, the operating conditions have been adjusted progressively to reach a $R_0\Delta X$ value of 2%: the methane concentration at fuel reactor inlet was varied from 2 to 10 mol% which corresponds to a variation of power from 0.4 to 2 kW.

- Solid flow rate:

The solid flow rate can be controlled in this unit thanks to the use of L-valves. When leaving a reactor, the OC proceeds through a L-valve which is used to regulate the solid flow rate injected in the subsequent lift. At the outlet of the lift the solid passes through the carbon stripper (when leaving the FR) or a cyclone (when leaving AR1 or AR2) before entering the next reactor. With this device, the solid flow rate is controlled by the gas flow rate injected in the L-valve. The pressure drop in the lift is directly linked to the solid flow rate and a correlation between the solid flow rate and the lift pressure drop has been established for ilmenite before

the campaign and at the end of the campaign (Figure 5-21). For comparison, the results obtained with a copper-based material and a perovskite during the FP7 - SUCCESS project are presented.

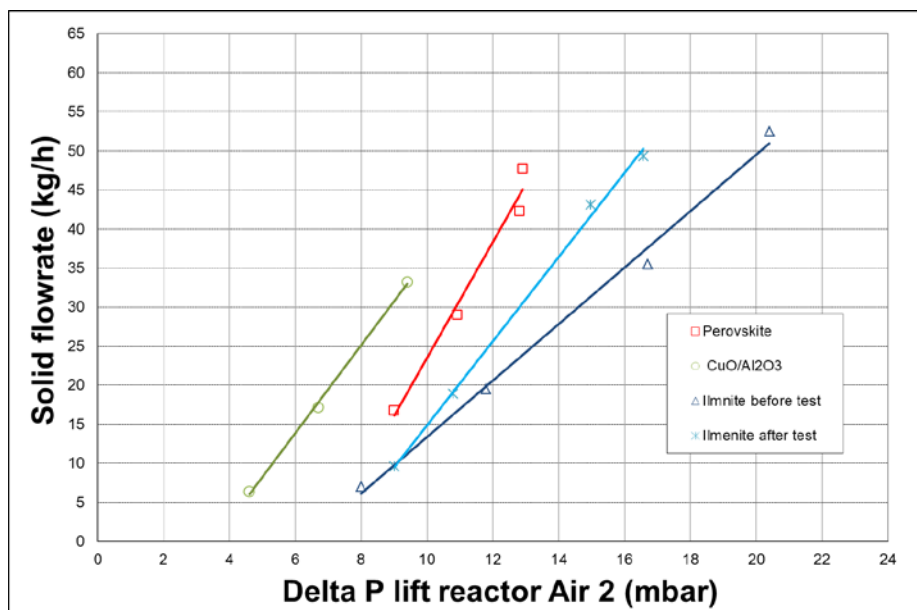


Figure 5-21: Relation between solid flow rate and lift pressure drop for Ilmenite before and after the campaign, perovskite, and copper-based material.

From Figure 5-21, the ilmenite flow rate with lift pressure drop has evolved during the campaign. This is due to a change in ilmenite's properties upon ageing, which changes this material's fluidization properties. The range of solid flow rates used in this campaign is between 10 and 20 kg/h. Within this range, the solid flow rate correlation with the lift pressure drop stays unchanged.

- Solid inventory in each reactor:

The impact on process performance of the solid inventory in the fuel reactor has been studied. The solid flow rates between each reactor are adjusted with L-valves, which allows to have a total control of the solid levels in the unit. The tests have been performed at constant levels of solid in the fuel reactor. The solid levels in both air reactors are dependent on the total inventory of solid in the unit. The solid levels of the air reactors are adjusted in order to remain similar to each other whatever the total solid inventory. As a consequence, the solid level in the fuel reactor being constant, when the total solid inventory decreases the solid level in the air reactors decreases. Tests have been performed with two different levels of material in the FR.

The experimental campaign performed has been divided in two parts in order to correctly characterize the impact of operating conditions on the oxygen carrier performances. First, ageing of the OC and characterization of its reactivity and morphology variations over time under gaseous fuel (CH₄) have been performed. Then, the influence of the following parameters on petcoke gasification rate were studied:

- the fuel reactor (FR) temperature,
- the oxygen carrier flow rate,
- the petcoke flow rate,
- the solid level in the FR,
- the steam concentration

5.2.2 Ilmenite agglomeration

At the very beginning of the test campaign, the L-valve of the fuel reactor, and later the loop-seal, have been plugged by ilmenite while heating up the pilot unit and circulating the OC with air at the air reactors and 7% O₂ in nitrogen at the fuel reactor. Particles circulation failed when the temperature reached ~700°C in the fuel reactor. The unit had to be stopped, and very strong agglomerates (difficult to break) were found in all dead zones of the fuel reactor as shown in Figure 5-22. If a small part of these agglomerates goes through an L-valve or a loop seal, it will plug it and stop the solid circulation. The campaign was interrupted several times due to such agglomeration problems.



(a)



(b)

Figure 5-22: (a) reconstitution of an agglomerate retrieved on the distribution plate of the fuel reactor and (b) agglomerates remaining in the fuel reactor at the end of the campaign.

XRD analysis of the particles after the first agglomeration incident showed that pseudobrookite was not formed at 700°C, only hematite (Fe_2O_3) and rutile (TiO_2) were detected, as well as the aluminosilicates contained in the fresh ore (phases with structures close to those of albite ($\text{Na}(\text{Si}_3\text{Al})\text{O}_8$) and glauconite ($(\text{K},\text{Na})(\text{Fe},\text{Al},\text{Mg})_2(\text{Si},\text{Al})_4\text{O}_{10}(\text{OH})_2$)).

After unclogging the pipes, the same particles could be fully oxidized at 850°C in the FR and 700°C in the air reactors, and a sample of the oxidized OC showed the expected presence of pseudobrookite (Fe_2TiO_5), along with still a large amount of hematite and rutile present (see §5.2.5).

Similar to SINTEF's observations, SEM analysis of the FR agglomerate (Figure 5-23) shows that the particles are tied together through a layer of hematite that has formed on the surface of the particles upon oxidation. Such an oxide layer was also observed on the particles that had not agglomerated.

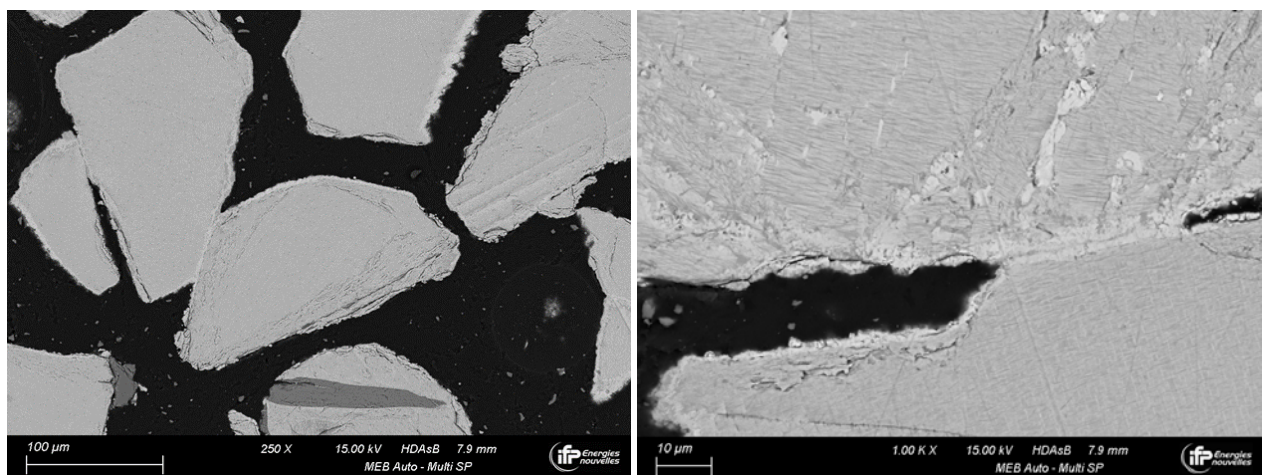


Figure 5-23: SEM cross-cut section of the FR agglomerate formed during the first oxidation of the OC.

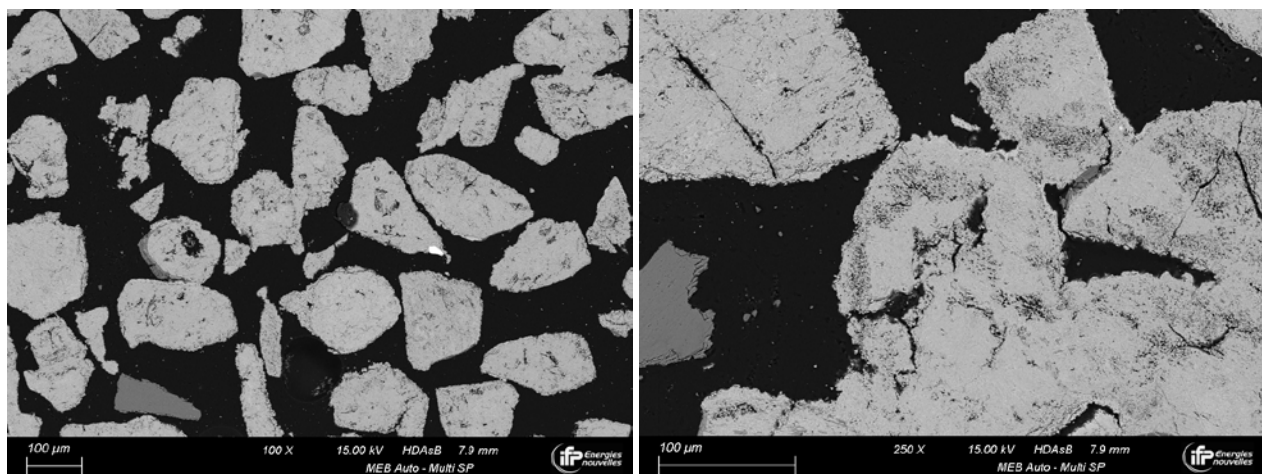


Figure 5-24: SEM cross-cut section of the FR agglomerate recovered after the complete test.

After the test was complete, the particles were fully oxidized and the cooling down of the unit was performed with 7% oxygen injection in the fuel reactor. A similar agglomerate to that formed during the start-up procedure was recovered at the bottom of the fuel reactor. Interestingly, despite probably being formed at the early stages of the test campaign, and hence despite being in a reduced form almost throughout said

campaign (it is likely the agglomerate formed during start-up from the oxidized particles, was then reduced during the campaign, and re-oxidized at the end of the campaign), the morphology of the particles trapped in the agglomerate has evolved, as shown in Figure 5-24, with the appearance of a few cracks and holes as well as some iron oxide scale on the surface.

5.2.3 Ilmenite activation

During the first days of the campaign and after the ilmenite was eventually fully oxidized, the fuel reactor operating conditions were progressively adjusted to increase the oxygen carrier reduction degree. The aim of this procedure was to activate the oxygen carrier and stabilize its reactivity while avoiding too deep a reduction, which may occur by directly using highly reducing operating conditions.

The pilot plant was initially filled with ~30 kg of the material distributed among the three reactors. Due to fluidization, part of the solid was continuously leaving the pilot plant at the gas outlet of the carbon stripper and at the cyclones. The accumulated OC was collected periodically. A small part of this powder was kept as sample for analysis and the rest was sieved. Particles with a diameter higher than 100 μm were reintroduced in the pilot plant while the remaining particles (under 100 μm) were discarded. In order to avoid variations of gas and solid residence time in the fuel reactor, the operating conditions have been chosen to maintain a constant solid level in the fuel reactor (~9.5 kg of OC) during the entire experiment's duration (Table 5-4).

At the beginning of the campaign, both air reactors were filled at their maximum capacity. The solid level in the air reactors (AR1 and AR2) decreased over time since samples were kept for analysis and some solid was lost with the fines produced by attrition, but the solid level of AR1 was kept equal to that of AR2.

Table 5-4: Operating conditions of the first 60 hours of activation period.

Balance	Time under CH ₄	CH ₄ fraction	Temperature	OC flowrate	Gaz flowrate
-	h	%	°C	kg/h	NL/h
1	11.35	2.0	898	20.6	2040
2	28.35	2.4	900	20.6	2050
3	31.92	2.4	902	20.6	2050
4	34.35	3.8	897	20.6	2080
5	36.35	4.8	901	20.7	2100
6	53.35	4.8	900	20.6	2100
7	55.35	7.5	901	20.7	2000
8	59.35	7.5	900	20.7	2000
9	61.43	7.5	903	20.4	2000

The initial evolution of methane conversion and oxygen carrier conversion (ΔX) as a function of time and of oxygen carrier number of reduction/oxidation cycles are presented in Figure 5-25 and Figure 5-26 respectively. As shown in Figure 5-25, at each injected methane flow rate, methane conversion increases slowly with time on stream, which indicates a slow increase in OC reactivity. Each time the operating conditions are modified to reach a deeper oxygen carrier reduction (increase of methane flow rate, decrease of OC flow rate), the methane conversion decreases as well. Due to this competition between oxygen carrier activation and methane flow rate increase, the mean methane conversion increase is quite low (gain of 16%) in comparison to the evolution of $R_0\Delta X$ (increase of 230%) (Figure 5-26). Over this period of time, no carbon monoxide was observed at the fuel reactor outlet. This indicates that methane conversion is the limiting reaction and carbon monoxide and hydrogen reoxidation are very fast, as observed in previous experiments performed in IFPEN's batch unit. Since petcoke gasification produces hydrogen and carbon monoxide, ilmenite reactivity may be high enough for this application.

After an average of 60 reduction/oxidation cycles (corresponding to ~70h methane combustion), ilmenite reactivity was more or less stabilised (more than three days of operation), after 30 more hours of combustion (and 30 additional reduction/oxidation cycles) the unit had to be stopped again due to agglomeration troubles in the fuel reactor L-valve and instabilities at the cyclone. The cyclone instabilities were solved easily by a pressure adjustment, but the plugging of the L-valve required to cool the unit down and clean it manually.

After unblocking the L-valve, 15kg of fresh ilmenite were added, and a second methane activation was performed for a further 81 hours.

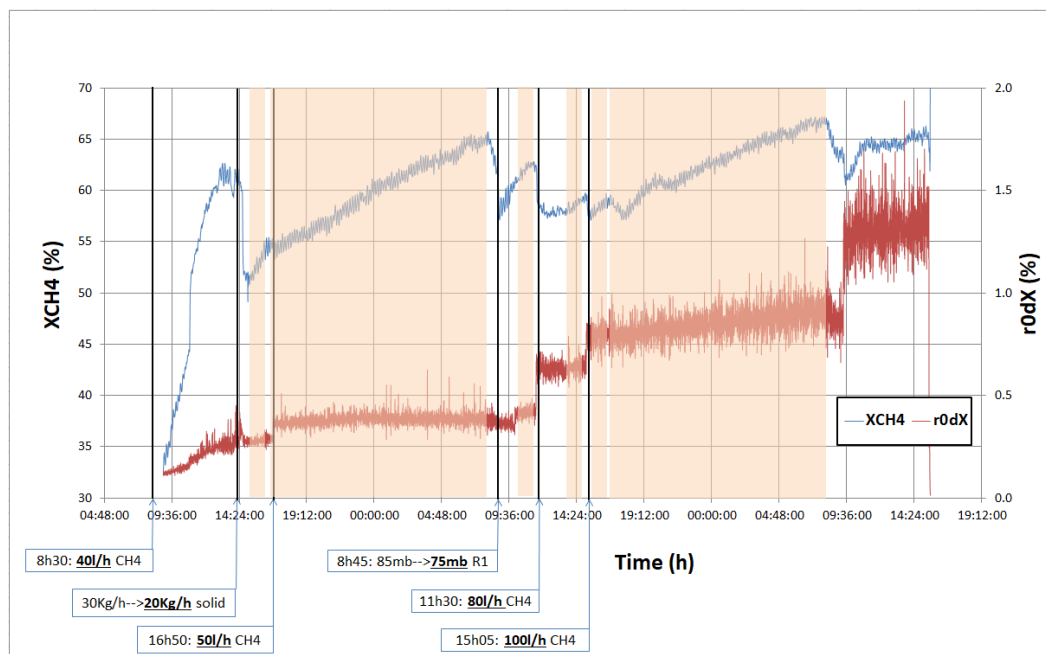


Figure 5-25: Methane conversion and $R_0\Delta X$ as a function of time and methane flow rate.

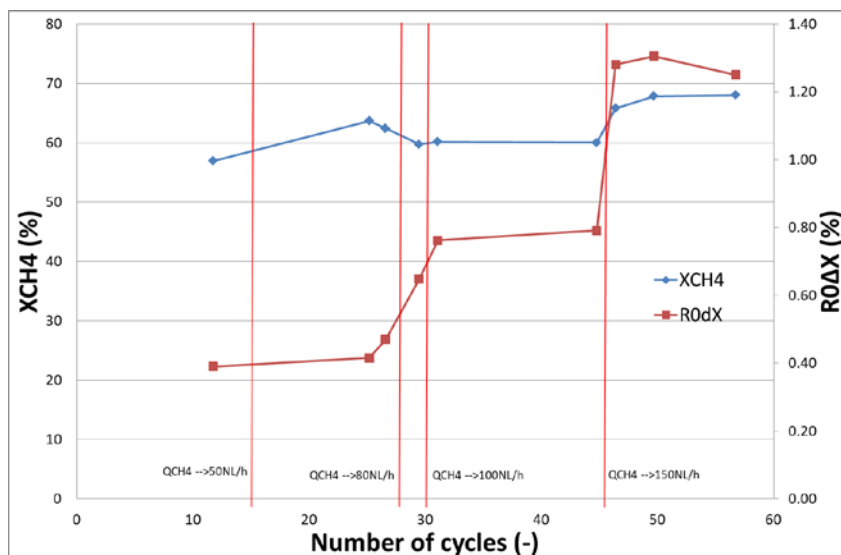


Figure 5-26: Methane conversion and $R_0\Delta X$ as a function of number of cycles.

5.2.4 Petcoke reactivity tests

Reference test conditions were set for petcoke combustion characterization, and each selected operating condition was varied independently of the others. The reference conditions used are presented in Table 5-5, and Table 5-6 summarizes the range of variation of the operating conditions in this campaign.

Table 5-5: Reference operating conditions for Ilmenite.

Material	-	Ilmenite
Temperature in FR	°C	930
OC mass in FR	Kg	9.6
Petcoke flowrate	g h^{-1}	120
Total FR inlet gas flow rate	$\text{Nm}^3 \text{h}^{-1}$	2
GHSV ^(*) in FR	h^{-1}	1289
OC flow rate	Kg h^{-1}	20
OC residence time	Min	28.8
Steam content	Mol%	50

(*) Gas hourly space velocity, i.e. ratio of gas flow rate to the volume of the bed.

Table 5-6: Range of variation of operating conditions.

Operating conditions	Unit	range
Temperature in FR	°C	898-904-930
OC mass in FR	kg	9.6-12
Steam concentration	mol%	31-50
OC flow rate	kg h ⁻¹	10-20
Petcoke flow rate	g h ⁻¹	120-260

For each operating condition, the gas phase leaving the reactors was analyzed and samples were taken at FR, CS and AR1 outlets. Mass balances were performed in order to characterize the combustion efficiency of the process. The mass balance on carbon was evaluated by integrating the concentration profiles of CO, CO₂ and CH₄ at the outlet of the fuel reactor and the concentration of CO₂ and CO at the outlet of the air reactors. Solid samples were taken at the carbon stripper and at the reactors outlets to measure the amount of solid petcoke lost. The water produced in the fuel reactor was collected in a condenser and weighed. The integration of the gaseous components at the outlet of the fuel and air reactors and the quantity of water produced allowed to check the oxygen mass balance. Hydrogen mass balance was also checked.

The operating conditions of the tests performed with petcoke are presented in Table 5-7, and Table 5-8 presents the experimental results obtained.

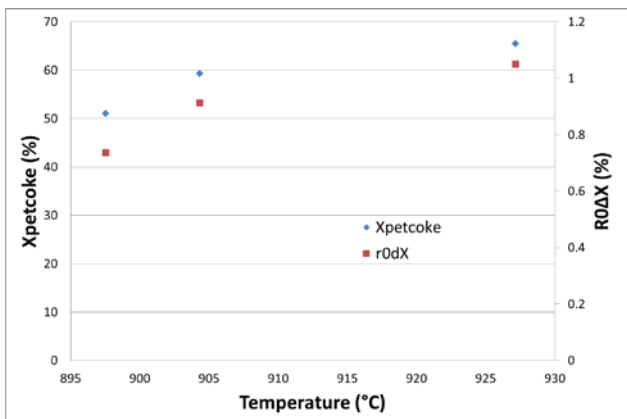
Table 5-7: Operating conditions of tests performed with petcoke.

Balance		Steam content	Petcoke flowrate	Temperature	OC flowrate	Bed height
-		%	g/h	°C	kg/h	cm
ref		49	117	927	20	53
T		50	110	904	21	55
QP		50	258	928	21	51
Hbed		50	114	929	22	66
T		50	120	894	21	52
xH ₂ O		31	115	929	21	51
QOC		50	119	922	10	51

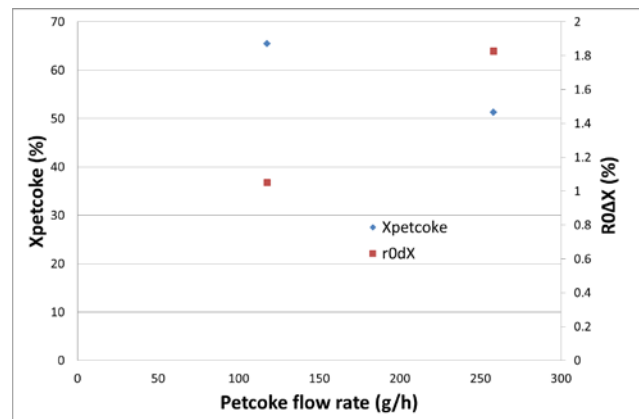
Table 5-8: Petcoke tests experimental results.

Balance	Steam content	Petcoke flowrate	Temperature in FR	OC flowrate	H _{bed}	R _{0dX}	Carbon stripper efficiency	FR losses	X _{petcoke}
-	%	g/h	°C	kg/h	cm	%	%	%	%
ref	49	118	927	20	53	1.05	29	6	65
T	50	110	904	21	55	0.91	25	10	59
T	50	120	898	21	51	0.74	22	12	51
QP	50	258	928	21	51	1.83	29	29	51
Hbed	50	114	929	22	66	0.90	28	15	64
xH2O	31	115	929	21	52	0.49	23	16	53
QOC	50	119	922	10	51	2.31	41	6	73

Figure 5-27 presents graphical representations of the observed tendencies. A stable oxygen carrier circulation and operation with petcoke has been reached.



(a)



(b)

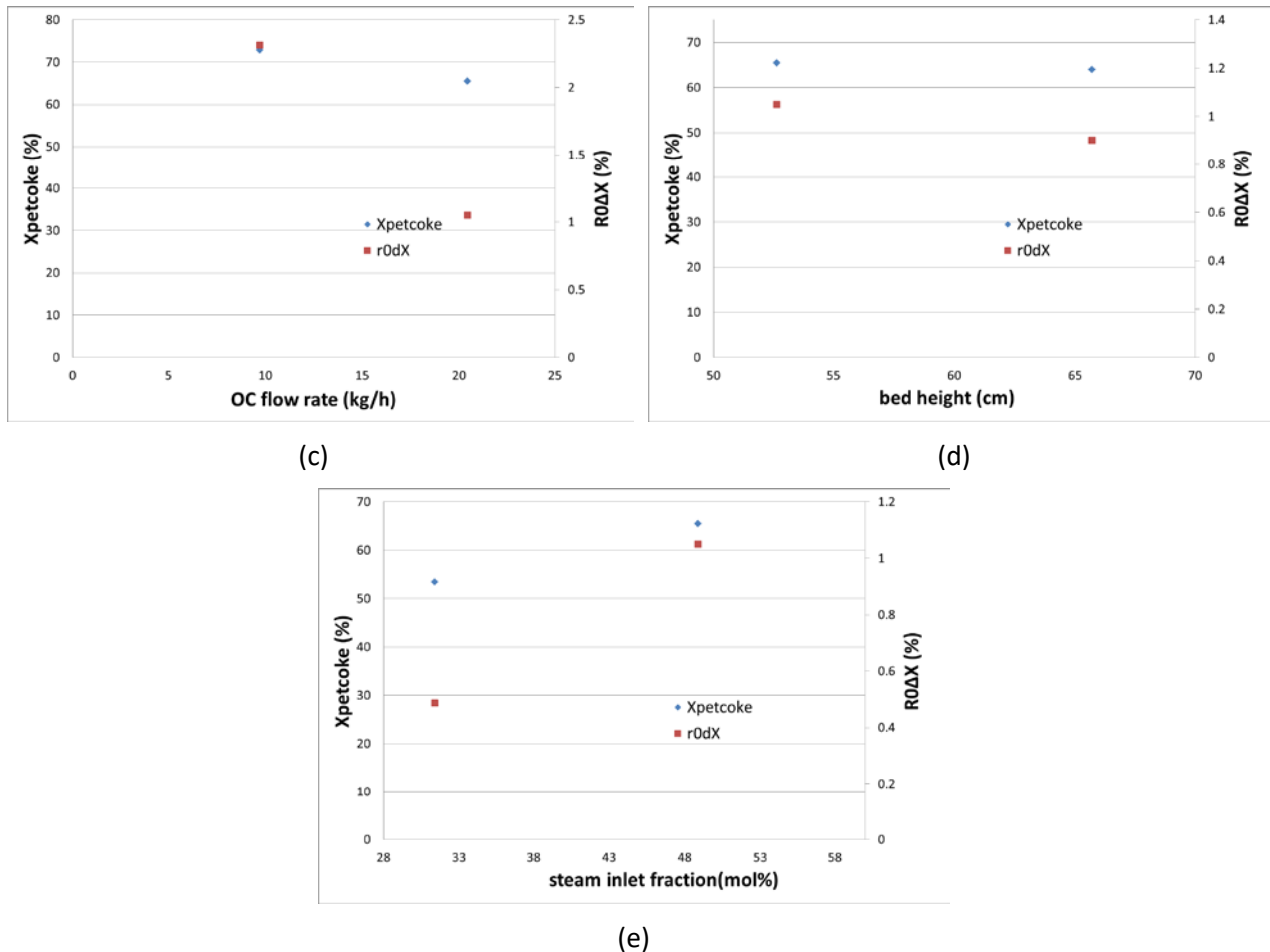


Figure 5-27: Evolution of petcoke conversion and oxygen carrier $R_0\Delta X$ at different (a) temperature, (b) petcoke flowrate, (c) oxygen carrier flow rate, (d) bed height and (e) steam inlet fraction.

The following observations can be made:

- As it was expected, when temperature or steam fraction increases, the petcoke conversion and the oxygen carrier $R_0\Delta X$ values increase (Figure 5-27(a) and (e)).
- If petcoke and oxygen carrier residence times were independent, the impact of oxygen carrier flow rate on petcoke conversion should be negligible and petcoke conversion should be greatly impacted by petcoke flow rate. Actually:
 - o When petcoke flowrate increases, its conversion is slightly decreased and the oxygen carrier $R_0\Delta X$ increases (Figure 5-27 (b)). Indeed, more petcoke is sent to the fuel reactor, so the oxygen carrier needs to provide more oxygen to oxidize the petcoke gasification products. Furthermore, only a slight reduction of petcoke conversion is observed, which can be explained by the fact that petcoke is continuously being dragged away to the carbon stripper with the oxygen carrier. In that case, petcoke residence time is imposed by oxygen carrier residence time.
 - o Petcoke conversion is greatly impacted by oxygen carrier residence time (see Figure 5-27 (c)). When the oxygen carrier flow rate increases, its residence time decreases, as well as that of petcoke, hence petcoke conversion decreases as well.

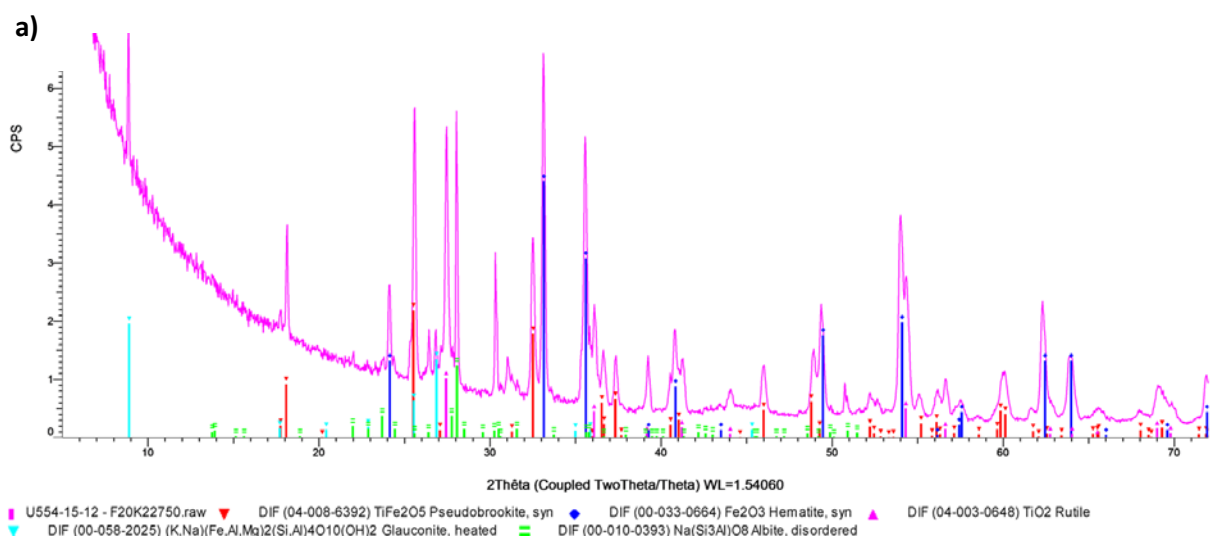
- Surprisingly, bed height does not impact petcoke conversion and oxygen carrier $R_0\Delta X$ value. This is explained by a higher loss of petcoke dragged away with the fuel reactor gases (Figure 5-27 (d)).
- Since a lot of problems of agglomeration have occurred during this campaign, it was not possible to adjust the carbon stripper operating conditions to reach a good separation. The mean efficiency observed was around 30 wt% of petcoke retrieved.

All the results obtained in this 10 kW continuous fluidized bed unit are in the line with the results obtained in a batch fluidized bed reactor used in WP3. A kinetic model is being developed in WP5 and its calibration and validation will be performed using the experimental results obtained in batch and fluidized bed reactors.

5.2.5 OC characterization

During the first 108 hours of methane activation, the solid levels in the air reactors were high enough, and no fresh material was added in the unit. Thus, during this period of time, the total OC mass in the pilot plant decreased over time but the solid was homogeneous in terms of chemical and mechanical evolution. The crystallographic evolution of the particles extracted from AR2 (i.e. fully oxidized particles) was followed by XRD analysis. As mentioned in §5.2.2, ilmenite oxidized at 850°C consists mainly of pseudo-brookite, hematite and titanium. Figure 5-28 and Table 5-9 show that the amount of pseudo-brookite increases between 0 and 34 hours activation, while hematite and rutile signals decrease, implying that maybe ilmenite oxidation to pseudo-brookite occurs through the intermediate formation of hematite and rutile. Little crystallographic evolution of the particles is observed thereafter, between 34h activation and the end of the experimental campaign, even after the fuel was changed to petcoke. The nature of the fuel does not seem to have affected the behavior of the OC particles, but petcoke combustion was performed during a total of 23 hours only, after a total of 190h of methane exposition, several clogging's and a period of 31 days of OC circulation. Unidentified peaks in the $31^\circ 2\theta$ region are also observed, which are not always at the exact same position.

Furthermore, glauconite was surprisingly not detected in the final sample (recovered after cooling down of the particles under oxidizing conditions both in fuel and air reactors).



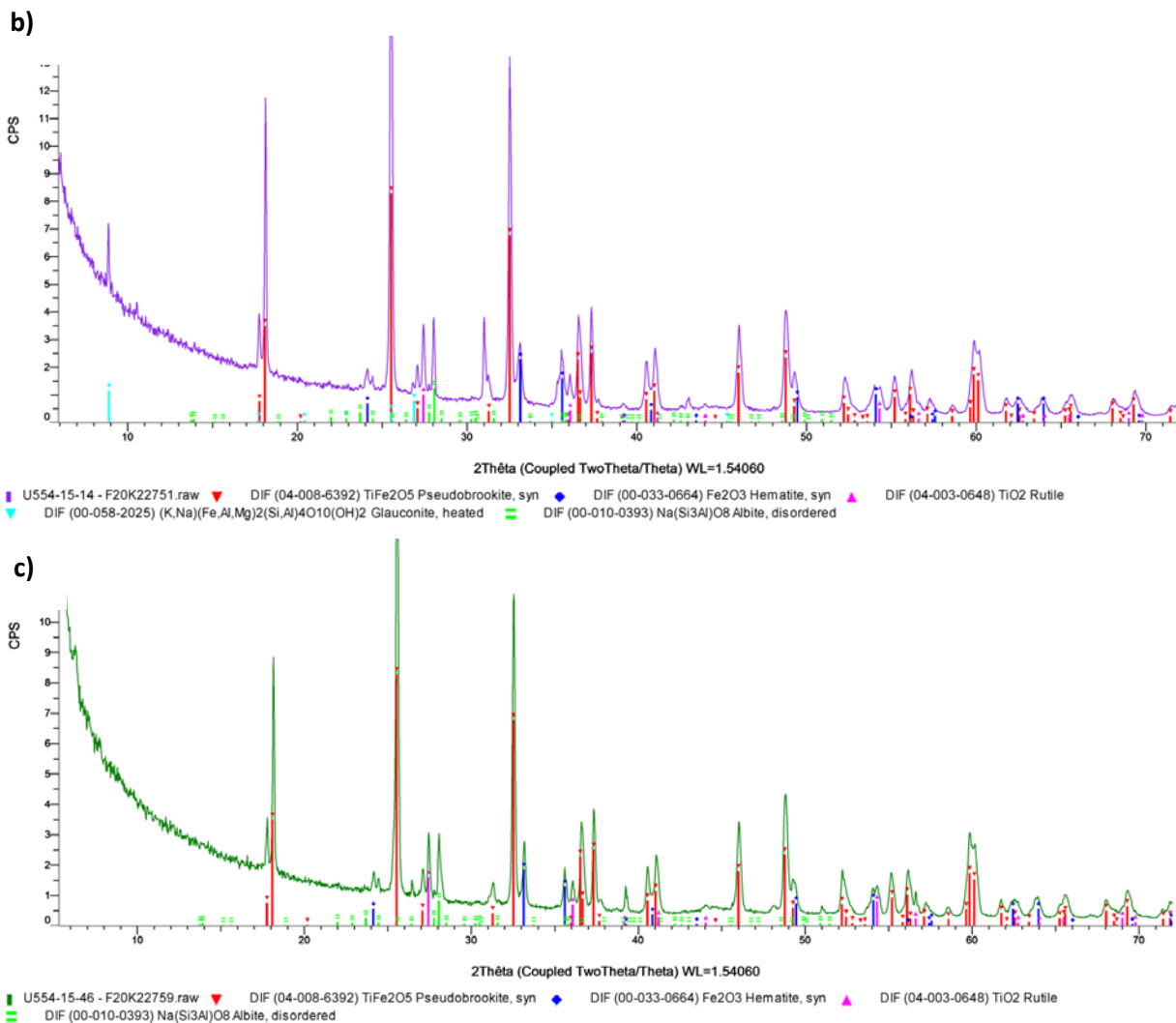


Figure 5-28: X-ray diffractograms of OC samples extracted from AR2 : a) oxidized at 800°C; b) after 23h methane activation; c) after petcoke tests, recovered oxidized powder.

Table 5-9: Crystallographic phases detected by XRD during methane activation and petcoke combustion.

Sample \ Detected phase	Pseudo brookite TiFe2O5	Hématite Fe2O3	Rutile TiO2	Albite	Glauconite	Unidentified peaks (°2θ)
Oxidized - before methane activation	+	++	++	++	++	-
~34h activation	++	+	+	+	++	31° / 43°
~53h activation	++	+	+	+	+	29.6°
~59h activation	++	+	+	?	+	31°

~89h activation	++	+	+	+	+	-
~108h activation	+	++	+	+	++	29.6°/31°
4h Petcoke combustion	+	+	+	?	+	31.5°
17h Petcoke combustion	+	+	+	+	0	26.7°

It should be noticed that a large amount of ilmenite had to be added halfway through methane activation and during the petcoke tests, to make up for particles losses (fines lost at filter candles + particles lost during manipulation/recovery, sampling, etc...). Figure 5-29 shows the amount of fine particles recovered in the cyclones and filter candles as a function of circulation time, as well as the amounts and times of fresh ilmenite addition throughout the campaign. No fines were collected after the start-up procedure (the candles were not cleaned, and no particles below 100µm were collected from the cyclones), which implies that fresh particles are mechanically strong and well suited for fluidization. However, after methane activation has started, the amount of collected fines increases somehow linearly with the particles' circulation time, and the change to petcoke combustion reduced slightly the fines' formation rate. The mean value of inventory loss calculated under methane exposure is 0,13%/h, leading to a particle lifetime of 770h. When petcoke is used as fuel, the inventory loss is around 0.07%/h, which corresponds to a particle lifetime of 1430h. This difference in fines production rate can be explained by the difference of mean $R_0\Delta X$ value (0.85% against 0.6%) observed during methane and petcoke tests. Such a high inventory loss can be explained by the fact that the activation process has led to the formation of large cracks in the particles, as shown in Figure 5-30. The estimated lifetimes are in line with the ones reported by Linderholm et al. [5].

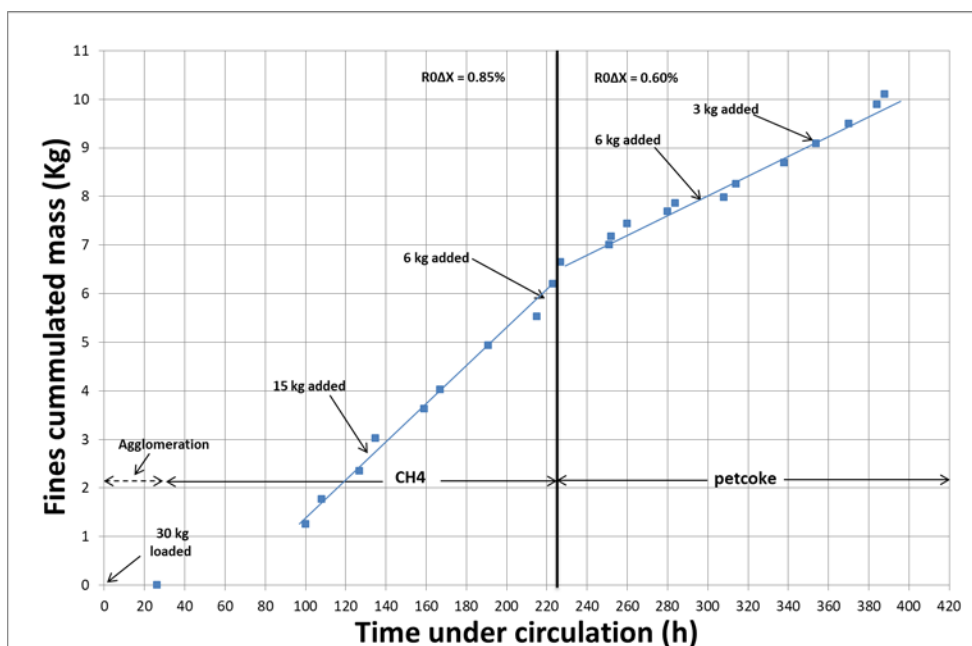


Figure 5-29: Mass of fines recovered as a function of circulation time. Petcoke combustion was not performed on a continuous basis.

Cross-cut section SEM analysis of the particles over the activation period (Figure 5-30) also shows that a layer of hematite is formed on the surface of the particles during the oxidation/heating up of the particles, which remains present all along the methane activation period. An evolution of the particles' morphology very similar to that observed by SINTEF in terms of iron and titanium separation is also seen, albeit with much more pronounced cracks formation after 108h activation.

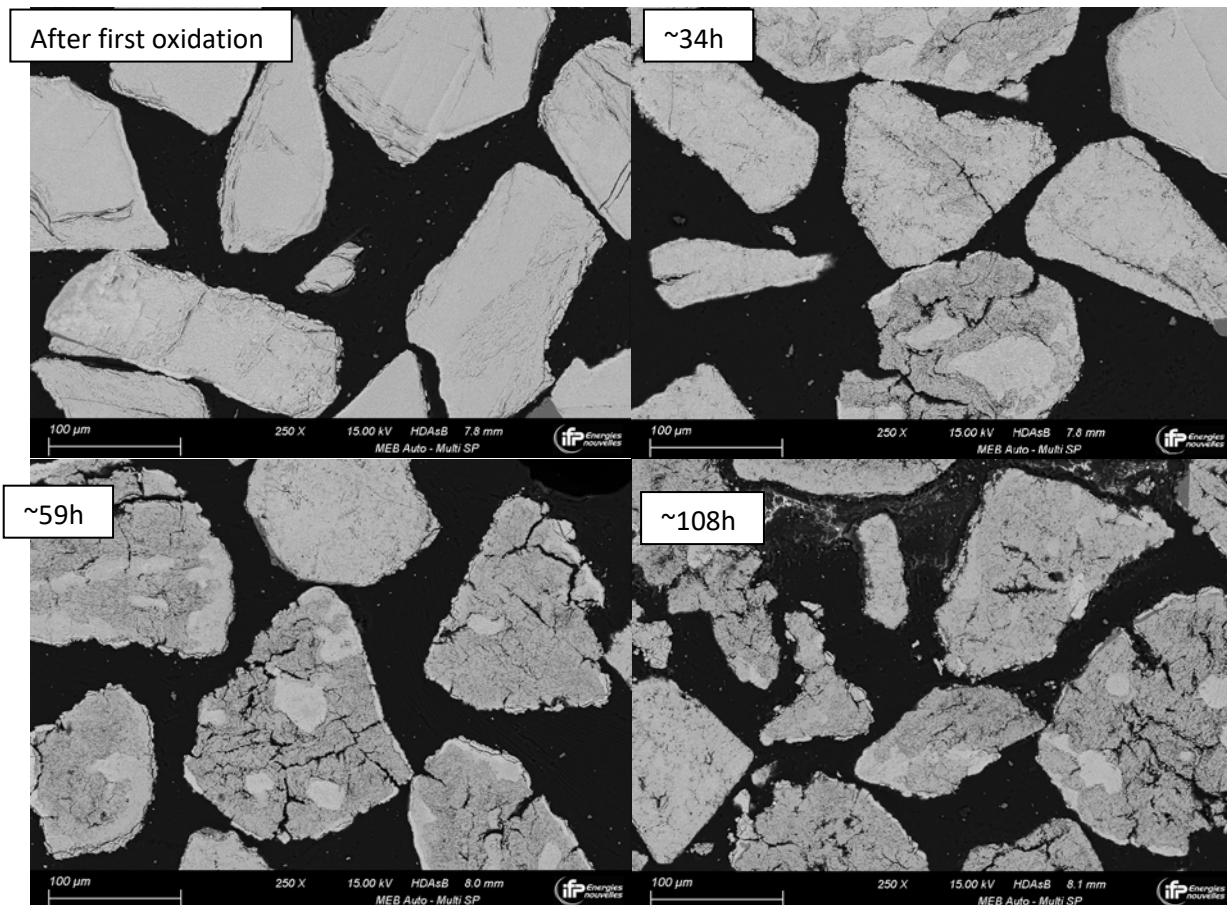


Figure 5-30: SEM cross-section analysis of OC during methane activation.

After their first oxidation, the OC particles are still completely non-porous, and the appearance of large cracks with methane activation is further evidenced by mercury porosimetry (Figure 5-31). The size of the cracks after 34h activation is between 100 nm and 1 µm, and it increases with activation time. The porous volume also increases, but it remains fairly low (0.05 ml/g after 108 h activation). It then decreases slightly (not shown) due to fresh ilmenite addition before and during the petcoke tests.

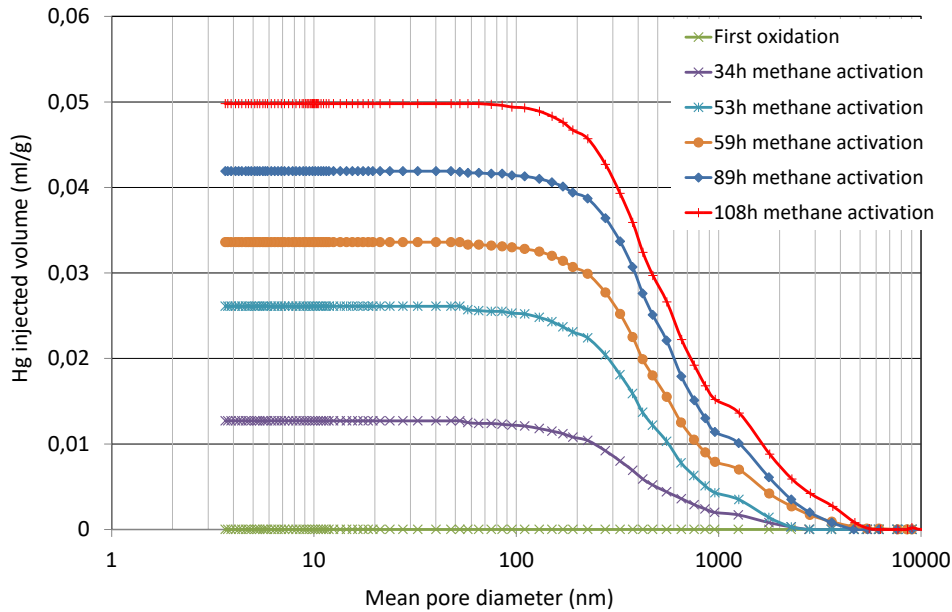


Figure 5-31: Evolution of particles porosity during methane activation measured by mercury porosimetry.

SEM analysis of the OC after the campaign (Figure 5-32) shows some particles that were activated as well as others for which the reacting time was much lower, hence their less cracked appearance.

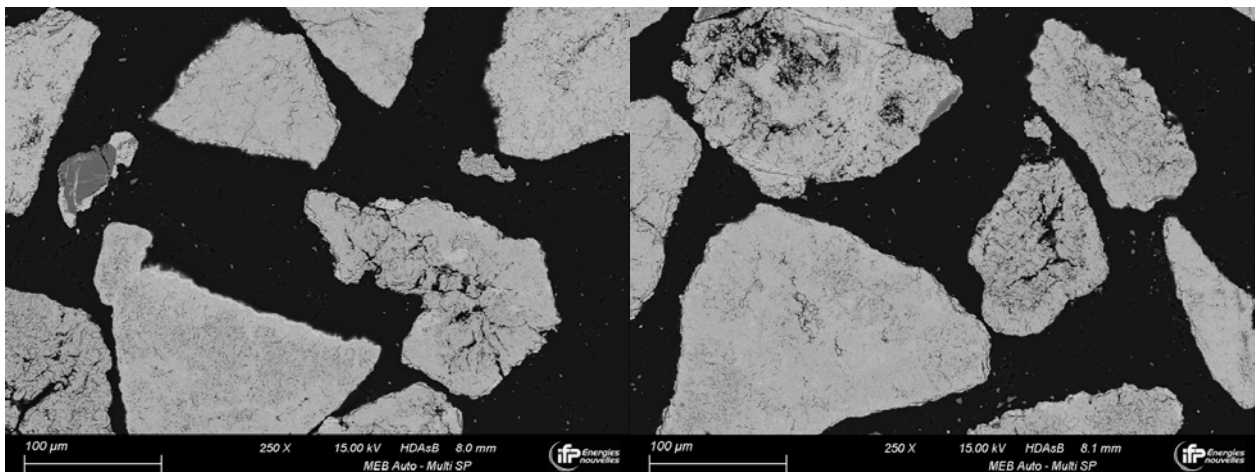


Figure 5-32: SEM cross-section analysis of OC after petcoke tests

The particle size distribution of the OC (not shown) remains relatively constant throughout the test, with a D_{v50} around 205µm. This implies that the generated fines have been evacuated, both at the cyclones and at the filter candles. SEM analysis of the fines collected at the filter candles (Figure 5-33) shows that these fines are made of fragmented particles as well as flakes of the hematite layer formed upon oxidation of the particles. Figure 5-33 shows that larger particles have also been carried to the filter candles by the fluidizing gases. It may be due to the high gas velocity used to fluidize the bed. Indeed, for fresh ilmenite a high velocity is required, but when time increases, ilmenite density decreases considerably which favour the loss of particles dragged away with the gas.

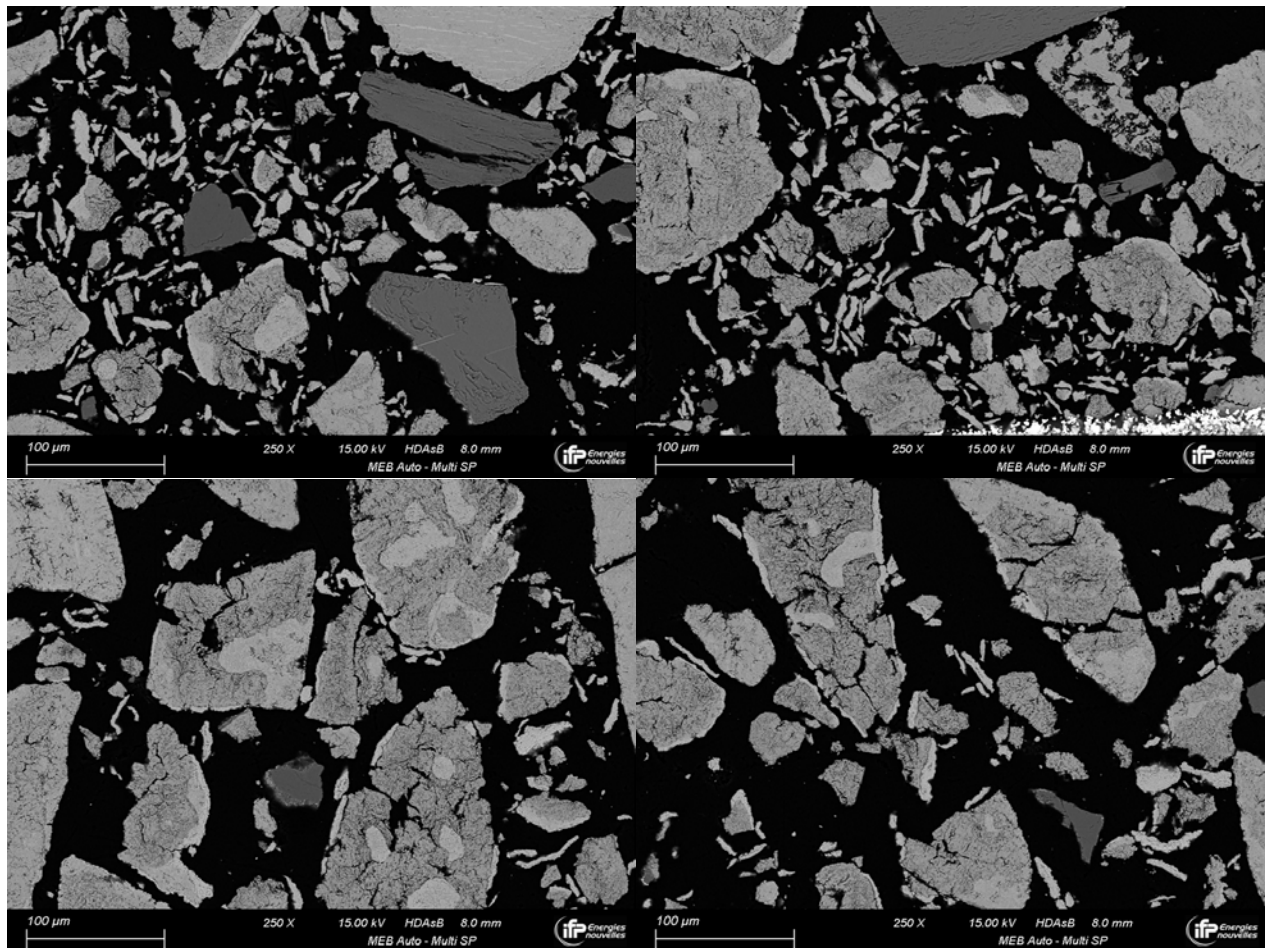


Figure 5-33: SEM cross-section analysis of particles collected at filter candles – top:AR2, bottom: FR.

5.2.6 Lessons learned from unit operation

According to IFPEN experience, ilmenite will agglomerate in dead zones or in fuel reactor L-valves where ilmenite flow is low. Agglomeration caused a lot of problems in IFPEN’s 10kW unit due to the small L-valves internal diameter. In a bigger scale unit, since the L-valves diameter will be higher, less problems are expected. Nevertheless, special care should be taken to ensure the particles are constantly being fluidized during start-up and ilmenite oxidation, with as few dead zones as possible to avoid agglomeration. When the oxygen carrier is circulating, a slow increase of the temperature to at least 850°C should allow full oxidation of the oxygen carrier and avoid any agglomeration issue. If the circulation were to stop during this process, it is highly likely that the partly oxidized oxygen carrier would agglomerate.

Clogging of L-valve pipes has been mainly encountered after the fuel reactor, where the solid flow rate is low, and the oxygen carrier is reduced to some degree. This is possibly due to the iron oxide flakes that form during oxidation of ilmenite via iron oxide migration, which seems difficult to avoid. In a larger scale unit, the higher diameter of the lines should reduce such agglomeration probability.

As mentioned in deliverable D3.1.b, ilmenite as an oxygen carrier must be activated for it to be operational. About 70 redox cycles with methane as fuel were required to achieve stable fuel conversion.

During the start-up of the CHEERS demonstration unit, when the reactors temperature reaches 400 °C, it is recommended to fill the reactor with oxygen carrier and start the oxygen carrier circulation before heating the unit further. From this point onwards, the circulation must never be stopped until the start-up is finished. The air and fuel reactors must be fluidized with air or steam during the whole start-up step. When the solid circulation is stable, heating the unit further from 400 °C to the operating temperature is done progressively. Hot points must be avoided, and circulation must not be stopped until a temperature higher than 900 °C is reached. At this temperature, oxidized ilmenite has reached a more stable state which reduces its agglomeration tendency.

If the unit operation and OC circulation must be stopped, it should be done by firstly stopping the fuel injection while the solid (OC) circulation is maintained until the oxygen carrier is fully oxidized. In the same time, the temperature of the unit should be decreased to around 700°C. Indeed, ilmenite shows more agglomeration at high temperature in reduced state.

5.3 Discussion and conclusions of Ilmenite T1

Ilmenite's reactivity is high enough to convert the gases produced by petcoke gasification. In IFPEN's 10 kW pilot unit with high solid residence time, a petcoke conversion up to 73% was observed without any recycle of unburnt petcoke. A parametric study has confirmed the tendencies observed in IFPEN's batch unit and it has been shown that petcoke residence time is imposed by the oxygen carrier residence time.

The ilmenite structure is stressed a lot by redox cycling, and cracks are observed in the activated particles. The mean inventory loss in the tests at IFPEN is between 0.07 and 0.13%/h for a $R_0\Delta X$ value of 0.6 % and 0.85%, respectively, which corresponds to a bed lifetime of between 770 and 1430h.

The pilot unit at SINTEF ER was operated with both petcoke and biomass, as well as different mixtures of those, and with different fuel particle size. For biomass, the FR fuel conversion was about 80% for all cases ranging from whole pellets, milled and sieved particles > 800 μm as well as the fines after sieving. The capture rate was about 90 %. Increasing the share of petcoke in the fuel decreases rapidly the CO_2 capture rate whereas the FR fuel conversion is slightly increasing. For a pure petcoke with size 315 – 500 μm the capture rate is only 33% and the FR fuel conversion is nearly 96%. These differences clearly show that the design of this unit is not well suited for a very low-reactive fuel as petcoke. Longer residence time and a carbon stripper is needed. However, for more reactive fuels as biomass it works much better.

The tests at SINTEF ER covered high temperatures as is intended in the demo unit. AR temperatures were in the range 990 – 1040 °C and FR temperatures in the range of 950 – 1000 °C. These temperatures did not impose problems to the operation of the ilmenite. It should be noted that the unit operates at close to auto-thermal conditions since the only effective additional heating during operation is the pre-heated air.

The pilot unit at SINTEF ER is characterized by large solid circulation and thereby lower utilization of the OC. A $R_0\Delta X$ value of 0,34 % or slightly lower, was estimated from the results. The redox cycling is more "gentle" in this case than in the IFPEN unit. This results in less cracking of the particles and the Fe segregation and the Fe shell that can cause agglomeration, is less pronounced. This is probably why there is limited problems with agglomeration in this unit. However, for the demo unit the $R_0\Delta X$ value should be larger than 1%. The redox cycling will be more stressing to the ilmenite structure, as described above from the IFPEN tests.

To conclude, the ilmenite seems to have enough reactivity to operate with petcoke. Stable operation is possible. Even though agglomeration issues have been observed, it may be avoided in bigger scale unit. The limitation of this material lies in its low lifetime, which implies a high make up quantity to be expected.

These conclusions were transferred from WP3 to WP2 and included in the pre-FEED study as procedures for how to avoid agglomeration during start-up, normal operation, and shutdown of the demo unit. Most importantly is to keep the whole system fluidised and in circulation. Dead zones in the fuel reactor and carbon stripper should be avoided. Special procedures should be followed during start-up, shut-down and in case of emergency shut-down, to ensure necessary fluidisation and circulation always when the system is at high temperature and fuel are injected.

6 RESULTS WITH SECOND OXYGEN CARRIER – MN ORE LY

6.1 IFPEN

Two batches of LY Mn ore have been tested in batch unit and have shown different trends regarding ageing under methane (probably due to different pre-treatments). To avoid confusion, the following paragraphs will focus on the second batch received in October 2020 (tested in both batch and continuous unit at IFPEN).

The experimental campaign performed has been divided in two parts in order to correctly characterize the impact of operating conditions on the oxygen carrier performances. First, ageing of the OC and characterization of its reactivity and morphology variations over time under gaseous fuel (CH_4) have been performed in the batch unit. Then, the influence of the selected operating parameters on petcoke gasification rate were studied in conditions of continuous circulation in the 10 kWth pilot unit.

The main results of LY Mn ore performance tests in batch and continuous pilot unit are assessed below.

6.1.1 Performance tests in batch unit

6.1.1.1 Methane ageing test results

Figure 6-1 shows the methane conversion (%) at 900 °C as a function of the number of cycles, as well as $R_{O\Delta X}$, for LY Mn China Ore. The comparison is done with two other OC already tested: Perovskite CMTF 8431 and ilmenite T2 (provided by SINTEF with well adapted PSD).

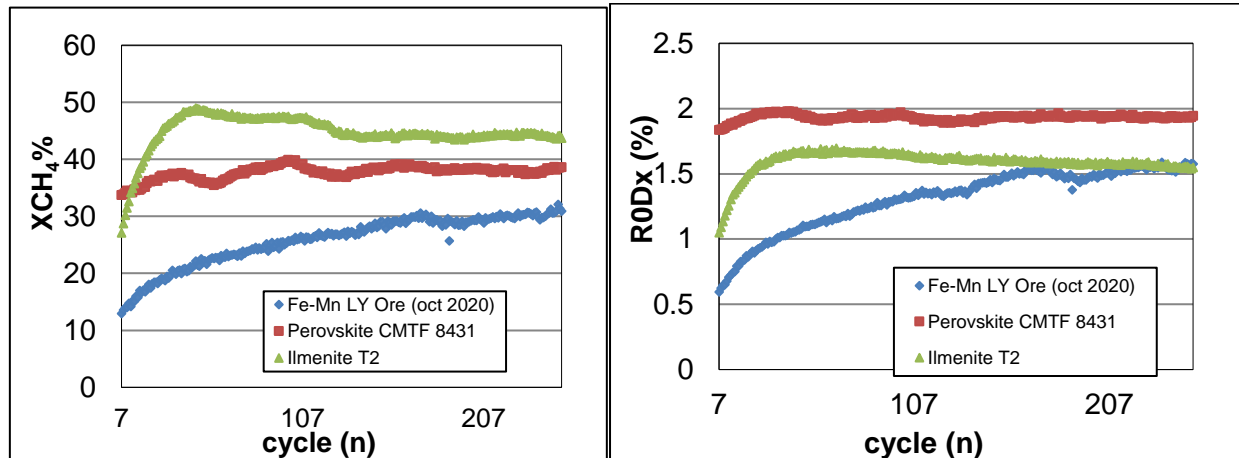


Figure 6-1: Methane conversion rate and oxygen mobilization for different materials tested in the CHEERS project

As can be seen, methane conversion begins at 14 % under our operating conditions, before continuously increasing to reach around 30 % at cycle number 250. The same trend is observed with the oxygen consumption provided by the material ($R_{O\Delta X}$) (from 0.6 to 1.6)

When the reactor was unloaded, some agglomeration of the particles was observed, representing about 15 wt% of the initial inventory. The agglomerates were however rather friable (see Figure 6-2).

The amount of fines generated is 6 wt%. The mean particle size (D_v^{50}) thus decreases slightly from 257 μm to 228 μm .



Figure 6-2: Photo of the agglomerates recovered at the end of the ageing test.

Although not easily visible on direct powder observation, a strong change of structure of the particles occurred upon methane ageing (Figure 6-3), with a large increase in porosity of many particles, and the disappearance of the crystalline precipitates and the dendrites that were initially observed (see § 3.2). A very large number of fines can also be seen both in direct observation of the powder and in polished cross-cut section.

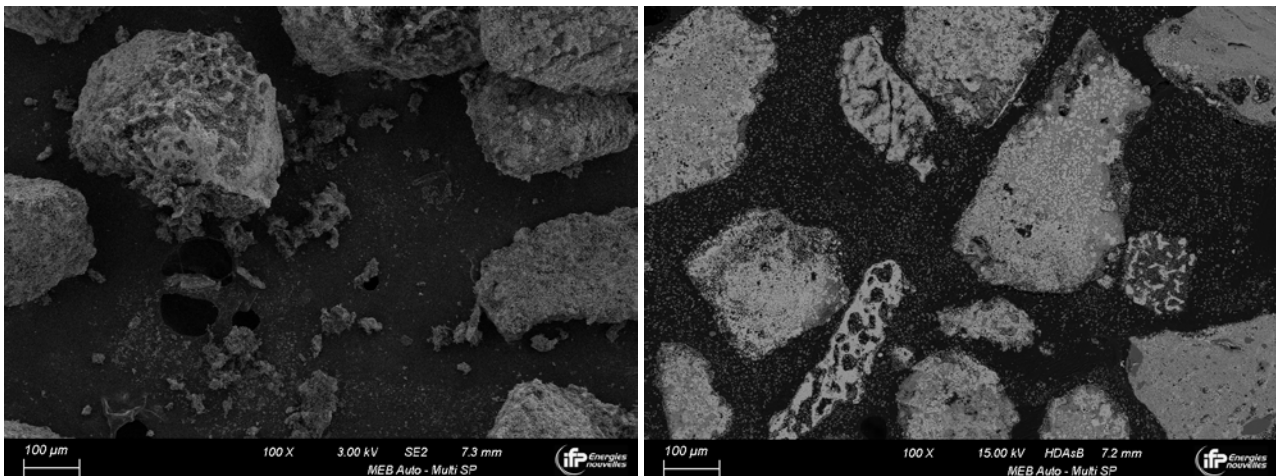


Figure 6-3: SEM pictures of LY-Mn ore particles after 250 redox cycles (left: direct observation; right: polished cross-section)

XRD analysis of the aged particles shows that the initial major phases (tephroite $\text{Mn}_2(\text{SiO}_4)$ and pyrolusite MnO_2 , see § 3.2) phases have given way to a mix of braunite ($\text{Mn}_7\text{SiO}_{16}$), rhodonite (MnSiO_3) and hausmanite (Mn_3O_4), along with large amounts of Fe_2O_3 and/or Mn_2O_3 , while surprisingly, no more quartz is present.

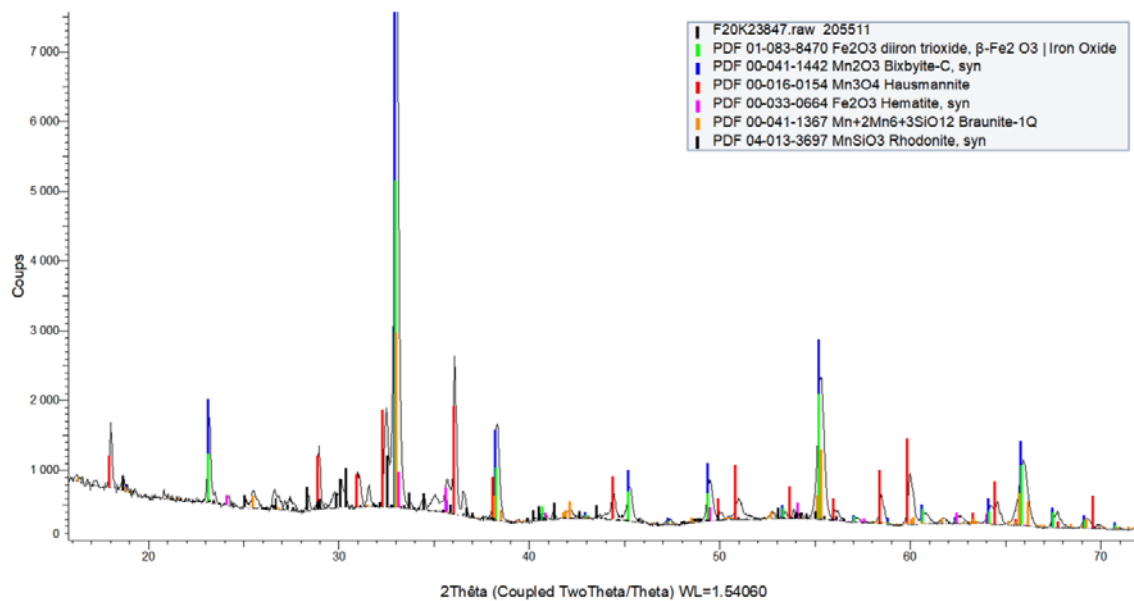


Figure 6-4: X-ray diffractogram of LY Mn ore after methane ageing in batch unit

6.1.2 Performance tests in 10 kW continuous pilot unit with LY Mn ore

The final step in oxygen carrier characterization are performance tests in continuous pilot unit, to consider the circulation effects on mineral behaviour. Given the promising results in batch tests of Ly Mn ore, it was decided to proceed with testing in IFPEN's 10 kW pilot unit to obtain comparison with ilmenite T1.

In the proceeding sections, the specific conditions of operation with LY Mn ore as well as experimental results of operation with LY Mn ore will be provided and compared to Ilmenite T1 performances.

6.1.2.1 LY Mn ore loading and circulation stage

The beginning stages of performance tests include unit loading, through R3 (2nd air reactor), fluidization and circulation between the reactors to reach the desired constant fluidized bed levels at desired pressure and temperature of the system. In the case of LY Mn ore operation, typical operating conditions are provided in Table 6-1.

Table 6-1: Typical operating conditions during unit circulation start-up with LY Mn ore

H_{FR} , cm	H_{AR} , cm	T_{FR} , °C	T_{AR} , °C	P , mb
42	45	900	800	1050

Fluidization in the reactors is controlled by N₂ flowrate to the reactors, while circulation is achieved by imposing desired pressure drops on L-valves between reactors (by adjusting N₂ flowrate to lifts). As with ilmenite, a linear correlation between oxygen carrier flowrate and pressure drop in the lift between R3 and R1 (2nd air and fuel reactor) was measured. This correlation was used to choose a value of set point for the lift pressure drop in automatic regulation mode, so as to ensure constant oxygen carrier flowrate condition (see Figure 6-5).

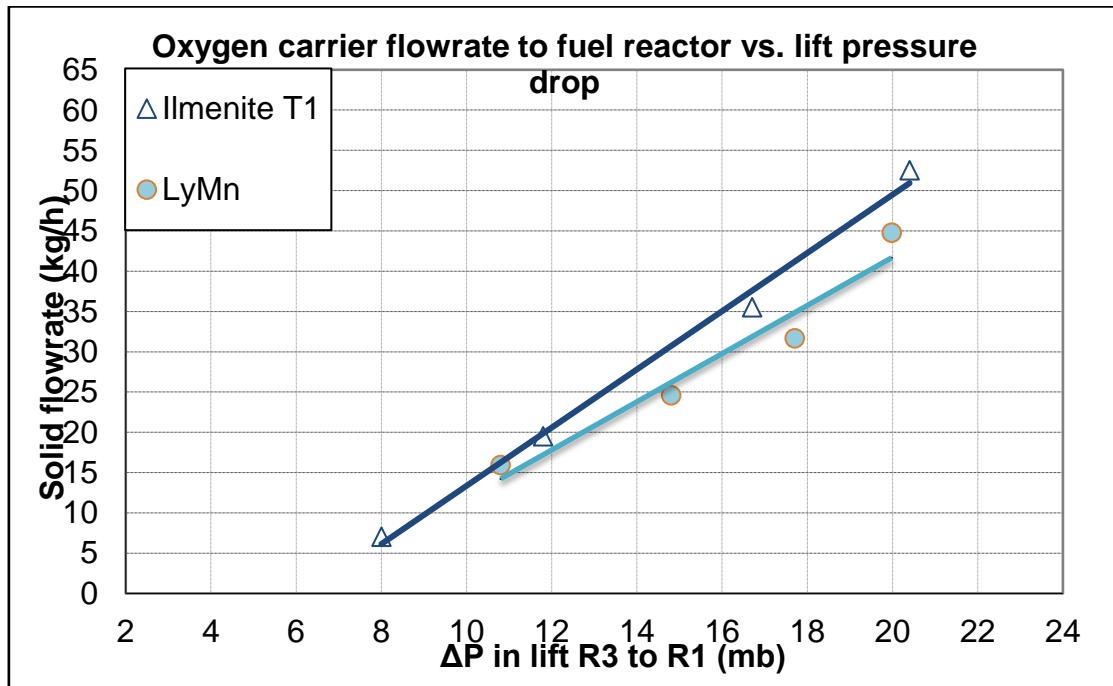


Figure 6-5: Correlation between oxygen carrier flowrate and pressure drop in lift leading to fuel reactor

During the unit start-up procedure, no significant circulation incidents occurred. In fact, when compared with ilmenite T1, the operation with LY Mn ore was more straightforward and allowed for a stable overnight circulation.

6.1.2.2 LY Mn ore activation stage

Operating conditions during activation stage of LY Mn ore were kept as close as possible to the ones established for ilmenite T1 operation. Due to similarity of mechanical characteristics of the two minerals, it was supposed that similar operating conditions and reduction severity could be imposed for activation of LY Mn ore (see section 5.2.3).

Table 6-2: Operating conditions in 10 kW pilot unit over LY Mn ore activation period

H_{FR} (cm)	CH_4 fraction (%)	Temperature FR ($^{\circ}C$)	OC flowrate (kg/h)	Inlet gas flowrate (NI/h)
42	10	900	20	2000

In the initial stages of methane injection, some agglomeration and blockage in the lift to the fuel reactor occurred. However, stable operation with methane combustion was achieved and tests were performed without major incidents with reference to oxygen carrier circulation.

To calculate the characteristic parameters of oxygen carrier performances ($R0\Delta X, X_{petcoke}$), mass balances were performed during a certain period of time when the system was stable. During these periods, methane was continuously converted into CO, CO₂, H₂O and H₂ at the outlet of FR. The measuring devices of CO, CO₂ and H₂ concentrations have already been described in section 2.2.1. Water was collected in a condenser at

the outlet of the FR. The main operating conditions used during the activation with methane are given in Table 6-3, as well as the methane conversion, mean $R_0\Delta X$ and CO/CO₂ ratio for each mass balance. The tests have been performed at constant levels of solid in the fuel reactor (except for mass balance 10), where the effect of increasing the height of bed level was tested.

Table 6-3: Operating conditions and performance for all the mass balances during the activation with methane.

Balance	FR T (°C)	AR1 T (°C)	AR2 T (°C)	H _{R1} (cm)	OC flow rate (kg/h)	CH ₄ in (%v)	R ₀ ΔX (%)	CH ₄ conversion (%)	CO/CO ₂ (/)
1	892	731	759	43.2	19.3	5	0.48	39.8	0.028
2	895	804	759	41.4	20.1	10	0.8	31.4	0.033
3	893	799	769	41.3	21.2	10	0.66	26.6	0.038
4	899	750	770	41.4	23.2	5	0.41	34.1	0.038
5	901	755	773	41.1	22.2	5	0.45	32.5	0.036
6	899	739	770	43.1	19.1	2.5	0.29	39.5	0.036
7	902	798	818	42.0	20.7	2.5	0.35	49.7	0.12
8	903	852	834	40.1	21.8	2.5	0.18	29.2	0.012
9	900	823	830	41.3	20.3	10	0.9	37.3	0.027
10	901	807	818	53	20.3	10	1.0	39.3	0.023
11	899	851	835	41.2	20.2	10	0.85	35	0.028
12	901	776	780	41.2	18.7	10	0.99	35.6	0.022
13	900	799	782	42.2	18.6	10	0.99	35.5	0.022

Figure 6-6 and Figure 6-7 show the evolution of methane conversion and $R_0\Delta X$ with increasing number of cycles (with the same initial fraction of methane -10 vol%- in the FR inlet gas to be comparative). The activation is visible even if this not marked. 52 hours of methane activation are needed to stabilize the activity of the OC. $R_0\Delta X$ and methane conversion reach respectively a value of 1 and 35 % (Table 6-3). Mass balance n°10 is not representative of the activation of the OC since the FR bed level was higher than the bed levels in the other mass balances. However, this shows that the FR bed level (and in this case the gas residence time in the FR) impacts the methane conversion and $R_0\Delta X$. The carbon capture efficiency (η_{CC}), which is calculated with the formula below, is near 99 % for all the tests under methane.

$$\eta_{CC} = \frac{F_{CO_2,FR}^{out} + F_{CO,FR}^{out} + F_{CH_4,FR}^{out} - F_{CO_2,FR}^{in}}{F_{CO_2,FR}^{out} + F_{CO,FR}^{out} + F_{CH_4,FR}^{out} + F_{CO_2,AR1}^{out} + F_{CO_2,AR2}^{out} - F_{CO_2,FR}^{in}}$$

Experimental results of LY Mn ore activation with respect to methane conversion evolution and value of $R_{o\Delta X}$ are provided in graphical representations below, in comparison to Ilmenite T1 behaviour.

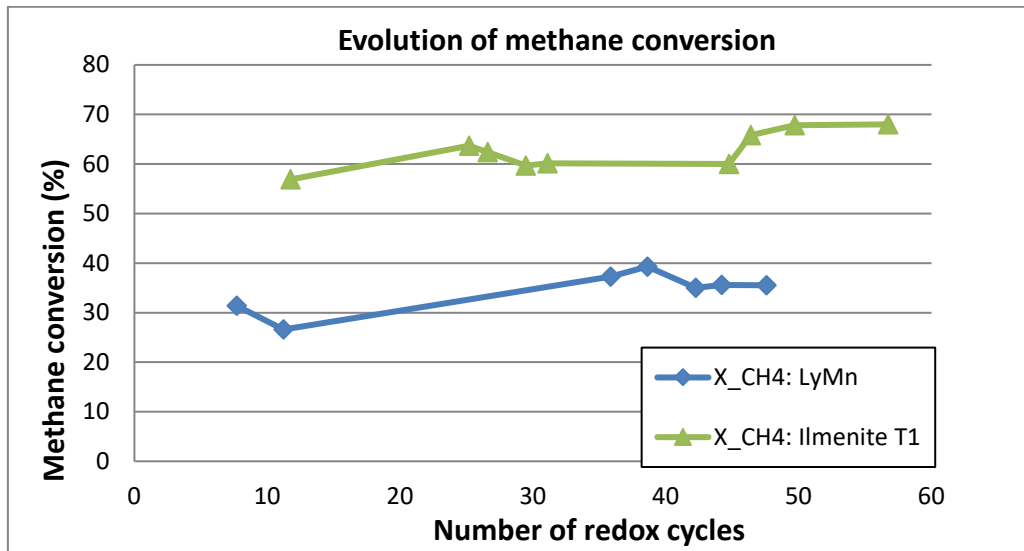


Figure 6-6: Evolution of methane conversion during LY Mn ore activation cycles in comparison to Ilmenite T1 behaviour

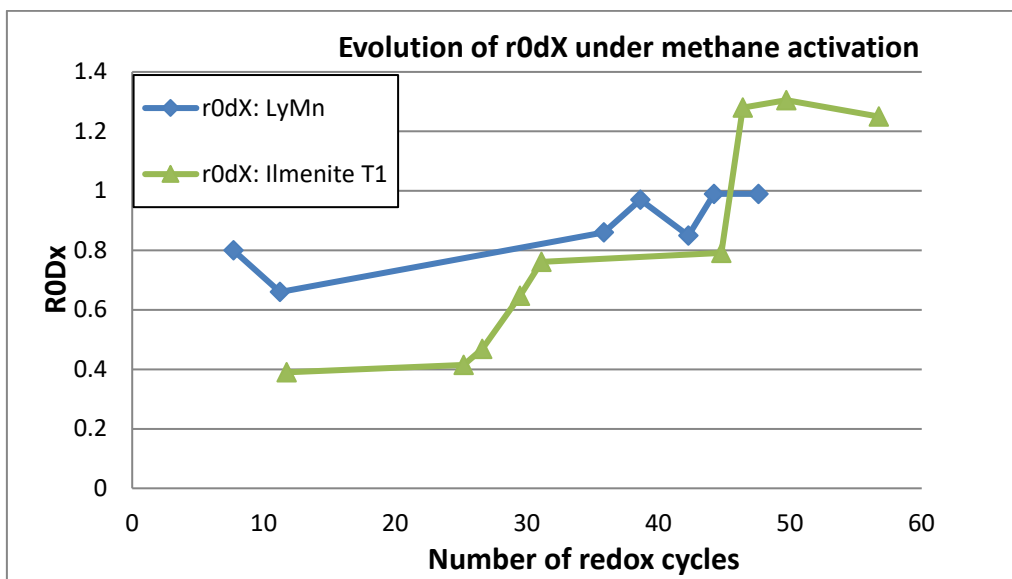


Figure 6-7: Evolution of $R_{o\Delta X}$ during LY Mn ore activation cycles in comparison to Ilmenite T1.

It could be observed from methane conversion evolution that LY Mn ore achieves lower conversion of the methane in comparison to ilmenite T1. Where the oxygen carrier conversion capacity is concerned, the

activation period for LY Mn ore is shorter, since the initial value of $R_{o\Delta X}$ for LY Mn ore is higher. Limited increase in methane conversion values of LY Mn ore is consistent with changes in $R_{o\Delta X}$, since both trends indicate an overall lower degree of changes in the material, with respect to Ilmenite T1, that required significant activation of reduction potential.

6.1.2.3 Petcoke reactivity tests with LY Mn ore

Final stage of tests in continuous pilot unit comprises petcoke combustion characterization. Similar to performance tests with ilmenite T1, the most important operating parameters were tested and compared to reference test results. Since the same reference test conditions were used (see Table 6-4), in the following section only an overview of experimental results is provided in Table 6-4.

Table 6-4: An overview of petcoke combustion performance test results with LY Mn ore

<i>Balance</i>	<i>Steam content</i>	<i>Petcoke flowrate</i>	<i>Temperature FR</i>	<i>OC flowrate</i>	<i>Hbed</i>	<i>R_{ODx_red}</i>	<i>X_{petcoke}</i>
-	%	g/h	°C	kg/h	cm	%	%
<i>Reference</i>	50	121	934	20	43	1.06	83
<i>Temperature</i>	50	121	904	20	55	0.49	75
<i>Petcoke flowrate</i>	50	244	930	20	51	2.08	82
<i>Steam content</i>	30	121	932	19.9	52	1.06	79
<i>Oxygen carrier flowrate</i>	50	121	920	30	51	0.76	89

Graphical representation of key parameter effects on petcoke conversion and oxygen carrier reduction potential in fuel reactor will be provided below.

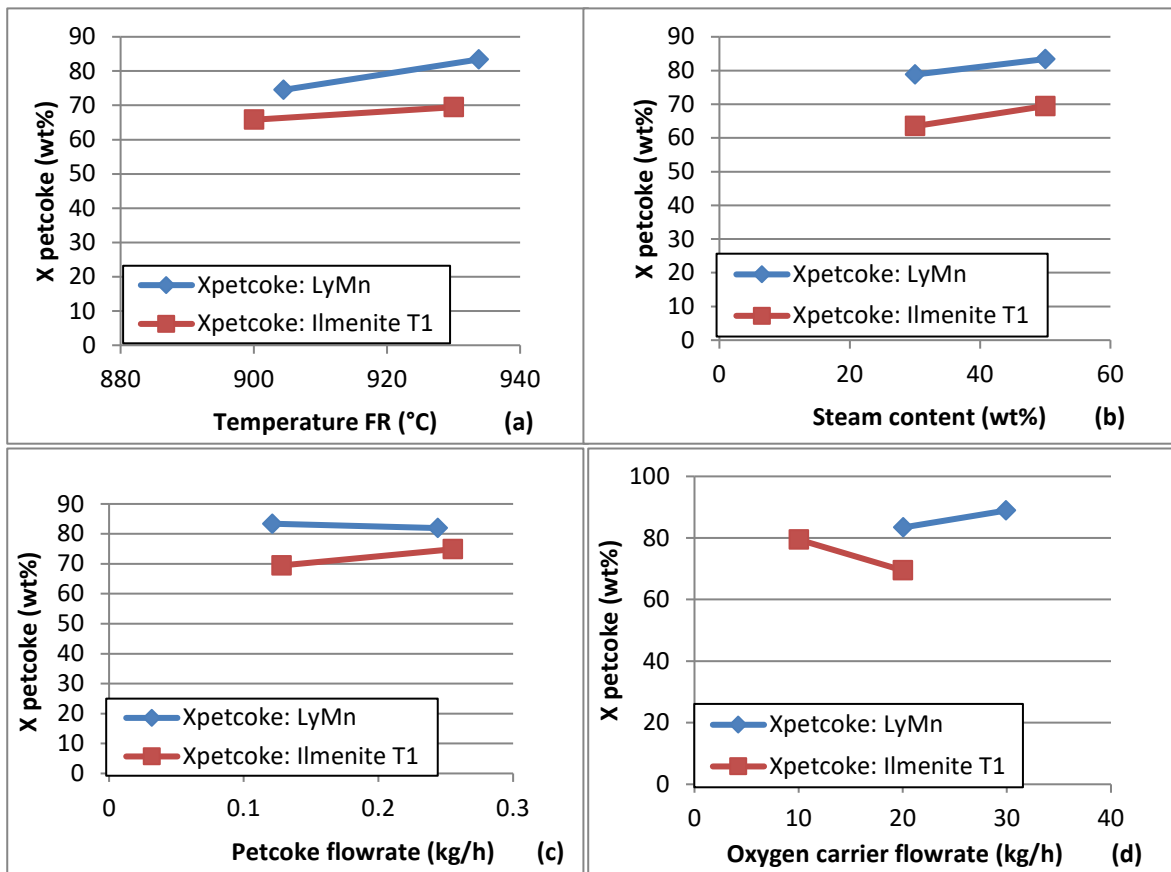


Figure 6-8: Effects of (a) Temperature in fuel reactor, (b) steam content in inlet gas to fuel reactor, (c) petcoke flowrate and (d) oxygen carrier flowrate on petcoke conversion in petcoke tests with LY Mn ore

Key parameters effects on petcoke conversion in fuel reactor could be summarized in following points:

1. **Temperature effect:** Temperature increase has a positive effect on petcoke conversion, as it would be expected according to previous batch results and established kinetic mechanism.
2. **Steam content:** An increase in water content helps petcoke gasification and expectedly has a positive effect on petcoke conversion.
3. **Petcoke flowrate:** With LY Mn ore as an oxygen carrier, the effect of petcoke flowrate increase is negligible.
- **Oxygen carrier flowrate:** In the case of LY Mn ore test with an increased oxygen carrier flowrate, an increase in fuel conversion is observed. Fluidization gas flowrate and bed level in fuel reactor remain the same, thus petcoke residence time in the fuel reactor is unchanged. This explains the observed increase in conversion, since more oxygen is available for petcoke combustion.

Note that the target temperature of the fuel reactor temperature of the last test of Table 6-4 was initially 930 °C but was not achieved during operation. Then, the influence of the oxygen carrier flowrate should have been more accentuated than showed by Figure 6-8 (d).

Overall, conversions achieved with LY Mn ore as an oxygen carrier are higher ($X_{petcoke} \approx 85\%$) with respect to ones obtained with Ilmenite T1 ($X_{petcoke} \approx 70\%$) in the previous campaign in continuous pilot unit.

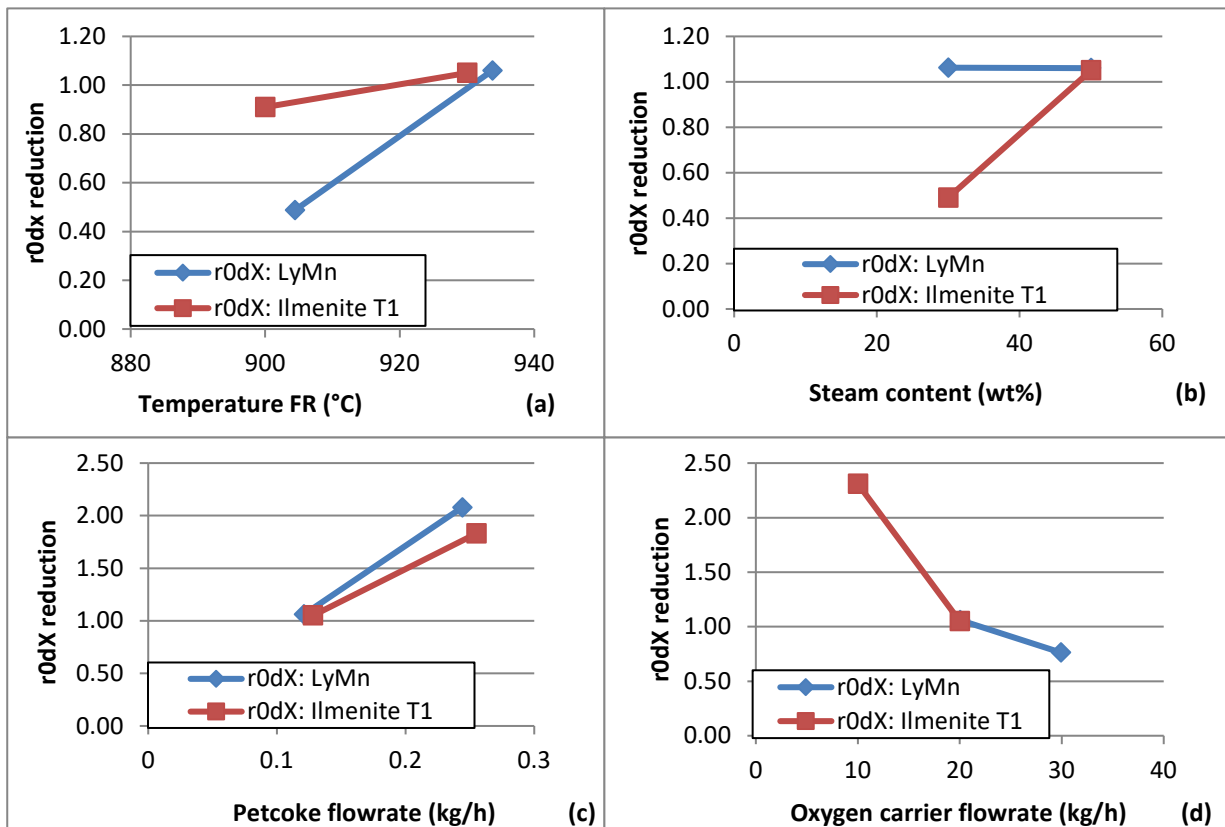


Figure 6-9: Effects of (a) Temperature in fuel reactor, (b) steam content in inlet gas to fuel reactor, (c) petcoke flowrate and (d) oxygen carrier flowrate on R_{0dX} value in petcoke combustion tests with LY Mn ore

Key parameters effects on R_{0dX} reduction value in fuel reactor could be summarized in following points:

1. **Temperature effect:** Temperature increase has a positive and more pronounced effect on reduction capabilities of LY Mn ore, with respect to Ilmenite T1.
2. **Steam content:** In the case of LY Mn ore, steam content is not a significant parameter for oxygen carrier conversion, contrary to ilmenite T1, which is highly sensitive to steam content in inlet gas to fuel reactor. This could be explained by looking more closely into experimental test conditions. Since CO/CO₂ ratio at outlet of FR was a bit higher in the reference test case than at lower steam content, this means that by increasing H₂O content a bit more CO is produced in steam gasification reaction, but not converted into CO₂, so the consumption of oxygen carrier remains the same.
- **Petcoke flowrate:** With LY Mn ore as an oxygen carrier, the effect of petcoke flowrate increase causes a strong positive gradient of oxygen carrier conversion, like Ilmenite T1 behaviour. Indeed, more petcoke is sent to the fuel reactor, so the oxygen carrier needs to provide more oxygen to oxidize the petcoke gasification products, while at the same oxygen carrier flowrate the petcoke conversion reduces. This proves potential to operate at high R_{0dX} values at large scale.
3. **Oxygen carrier flowrate:** An increase in oxygen carrier flowrate causes lower residence times of the solid in fuel reactor, and expectedly, lower R_{0dX} reduction value. The results for both minerals are completely in accordance.

Performance and kinetic tests show satisfying behavior of LY Mn ore. It could be concluded that this is an oxygen carrier with good oxygen transferability properties and overall high solid fuel conversion. In addition, it is well circulated in the unit and fewer unplanned unit troubles are expected in demonstration unit operation.

6.1.2.1 Structural and morphological evolution of the OC

After methane activation

After methane activation was completed, the pilot unit had to be cooled down and stopped due to Christmas holidays. The cooling down of the unit was performed with air injection in the air reactors, and nitrogen fluidization in the fuel reactor. Therefore, the methane activated sample is representative of fully oxidized particles. XRD analysis shows that most of the Mn and Fe are engaged in either hematite (Fe_2O_3) or bixbyite (MnFeO_3), along with some hausmannite (Mn_3O_4). The quartz initially present is still detected, as well as small amounts of pyroxmanganite ($\text{Mn}_7\text{Si}_7\text{O}_{21}$) and tephroite.

Compared to the particles aged for a larger number of cycles and with higher $R_0\Delta X$ in the batch unit, it looks as if the reaction(s) between Mn and Si oxides to form braunite ($\text{Mn}_7\text{SiO}_{16}$) and rhodonite (MnSiO_3) is underway, suggesting that the particles were not fully activated when methane was stopped.

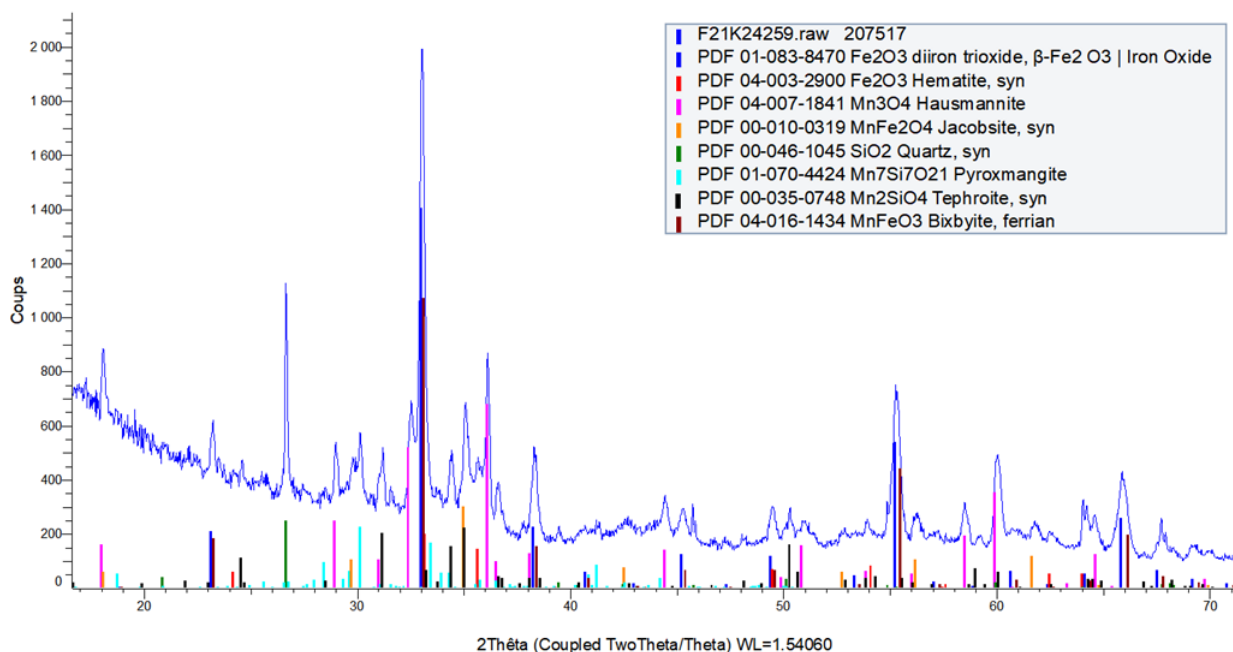


Figure 6-10: X-Ray Diffractogram of LY-Mn ore after methane activation

Direct SEM observation of the sample after activation shows that most of the fine particles present in the sieved ore are effectively removed from the circulating powder (Figure 6-11). It also shows the presence of what looks like an outgrowth of oxide(s), sometimes covering a large part of the surface of the particles, but mostly forming small, smooth looking 'islands' that are a few micrometers thick above the particles' surface. (Sub)micrometer sized particles are also attached to the surface, either through electrostatic forces or via chemical bonding.

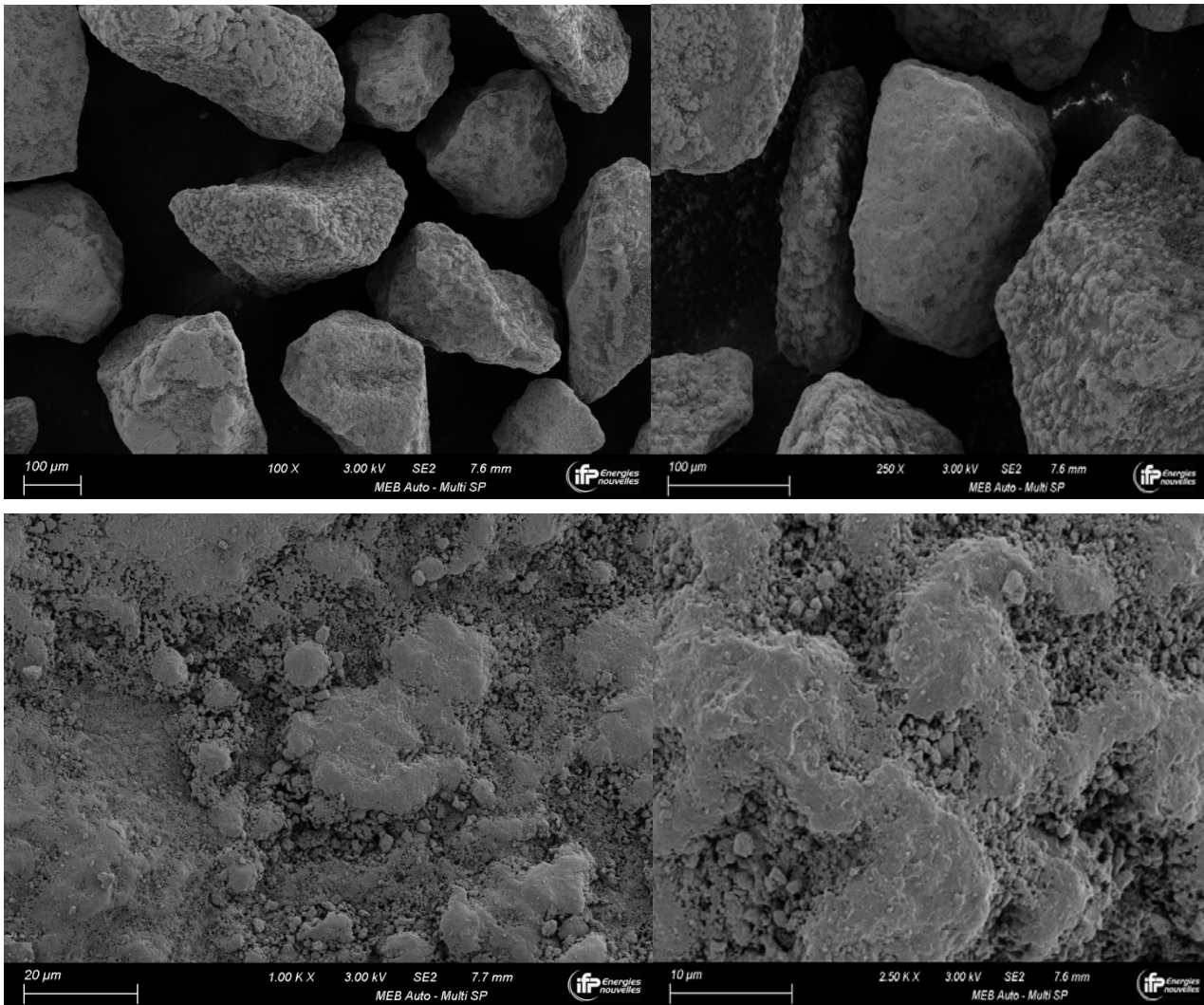


Figure 6-11: SEM pictures of LY-Mn ore powder after methane activation

Cross-section analysis of methane activated particles shows the same crystals and dendrites as the calcined ore, but some porosity can now be observed in some particles (Figure 6-12), which probably accounts for the activation of the ore.

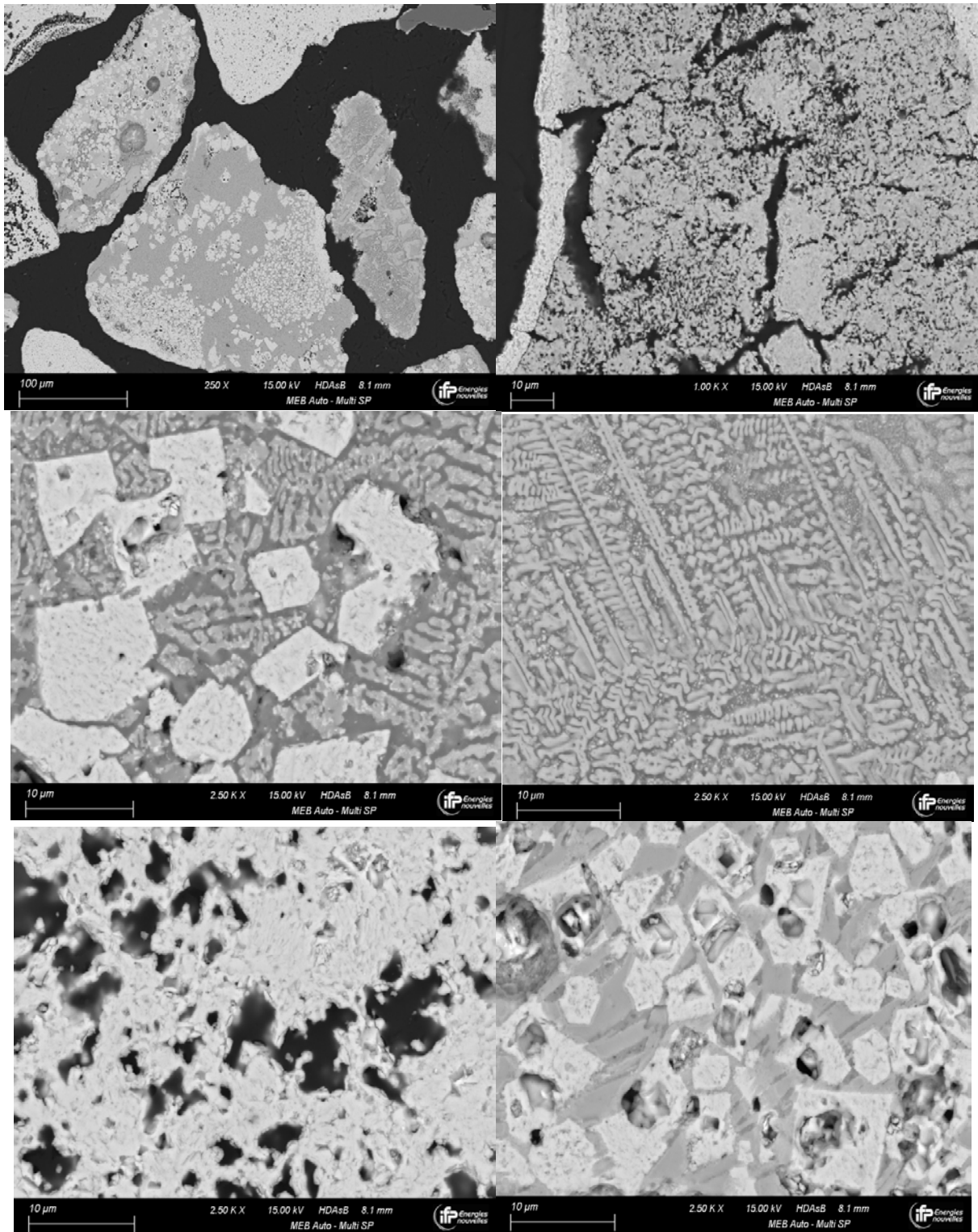


Figure 6-12: Cross-section SEM pictures of LY-Mn ore particles after methane activation

6.1.3 After petcoke injection (end of campaign)

XRD analysis of the particles after the test campaign shows that a mix between MnFeO_3 and Fe_2O_3 is the main phase present, i.e. $\text{Mn}_x\text{Fe}_{1-x}\text{O}_3$. A fair amount of quartz is also still detected (Figure 6-13), while minor amounts of other phases are also present. Very small amounts of hausmannite (Mn_3O_4) are still observed, suggesting that the $\text{Mn}_x\text{Fe}_{1-x}\text{O}_3$ mixed oxide is more stable than the corresponding pure oxides.

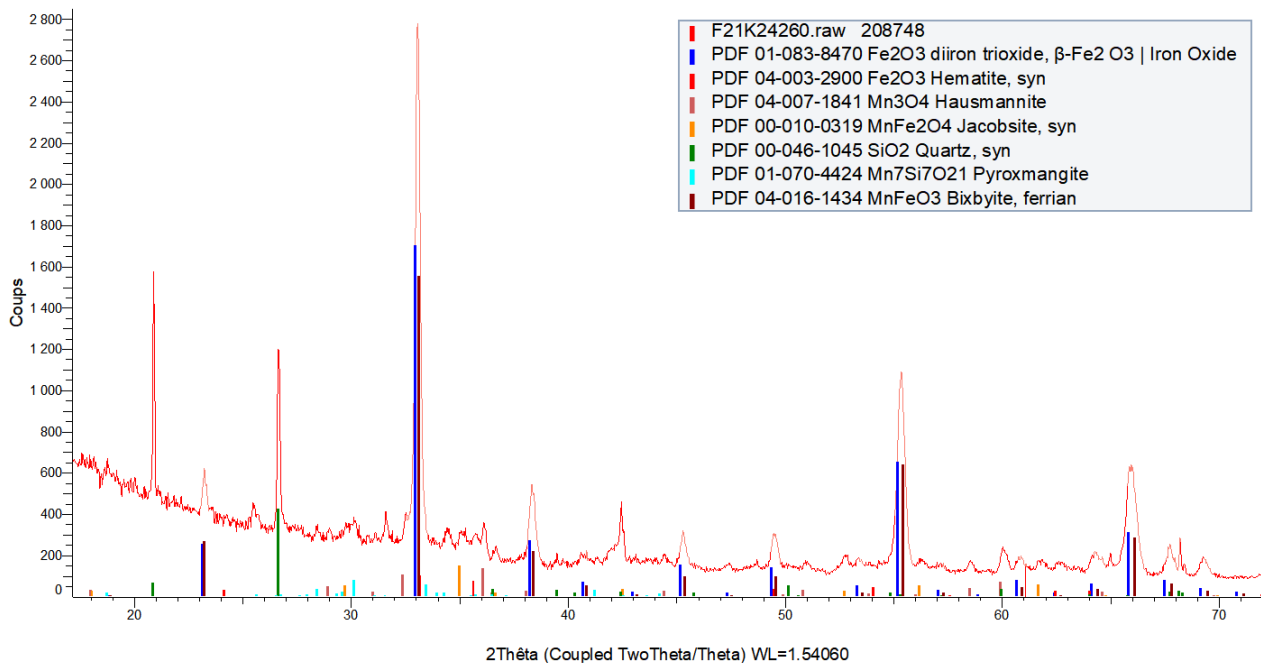


Figure 6-13: X-Ray Diffractogram of LY-Mn ore after test campaign

Upon direct SEM observation of the particles, no difference with methane activated particles can be observed (Figure 6-14). However, when looking at the cross-section SEM analysis after the complete test campaign, it appears that while still present, both the crystallites and the dendrites inside the particles tend to give way to much more porous particles with less well defined contours (Figure 6-15).

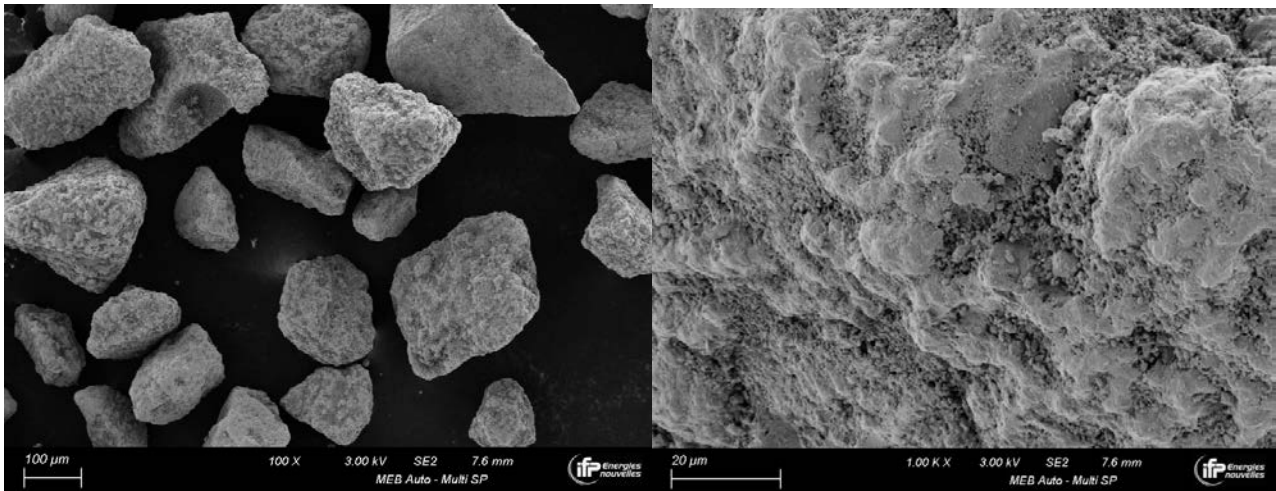


Figure 6-14: SEM pictures of LY-Mn ore powder after the test campaign

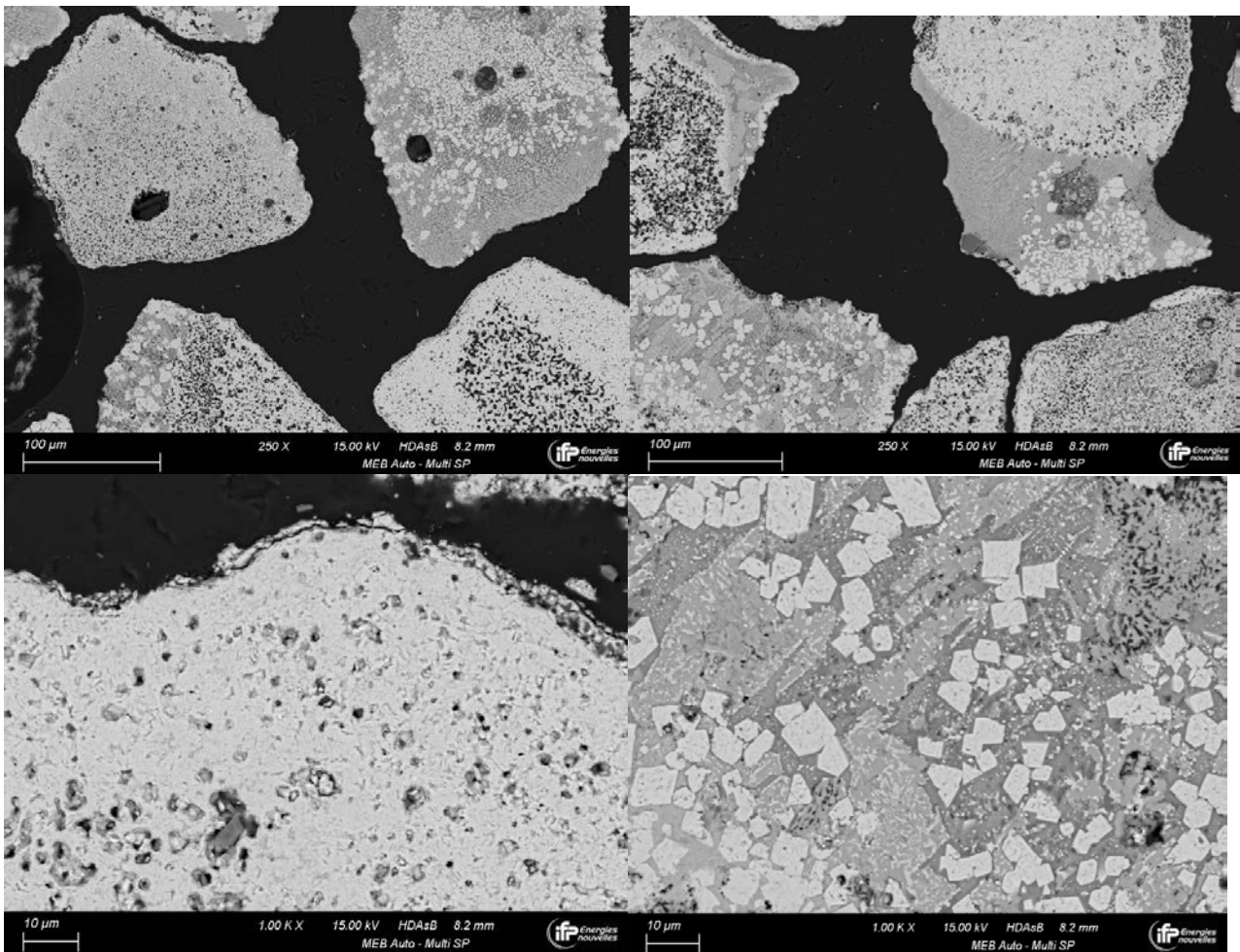


Figure 6-15: Cross-section SEM pictures of LY-Mn ore particles after test campaign

6.1.4 Fines production

The fraction of fines produced is a good indicator of the mechanical resistance of the material. Figure 6-16 shows the cumulated mass of fines recovered during the campaign over the number of hours of circulation (612 h of total circulation and 65 h under combustible conversion). In total, 39 kg of OC were loaded in the unit and 7,3 kg of fines were produced, which represents a fine particles loss of 18.5 %.

The unit was initially filled with 31 kg of fresh OC distributed among the three reactors. Due to fluidization, a part of the solid continuously leaves at the gas outlet of the carbon stripper and at the cyclones. The accumulated OC was collected periodically at every outlet. A small part of this powder was kept as sample for analysis and the rest was sieved. Particles with a diameter higher than 100 µm were reintroduced in the pilot plant while the remaining particles (under 100 µm) were discarded. In order to avoid variations of gas and solid residence time in the fuel reactor, the operating conditions have been chosen to maintain a constant solid level in the fuel reactor during the entire campaign duration.

Passing from gas to solid fuel injection does not drastically change the fines formation, as it could be seen in Figure 6-16, while petcoke combustion with Ilmenite T1 had significant impact on fines formation.

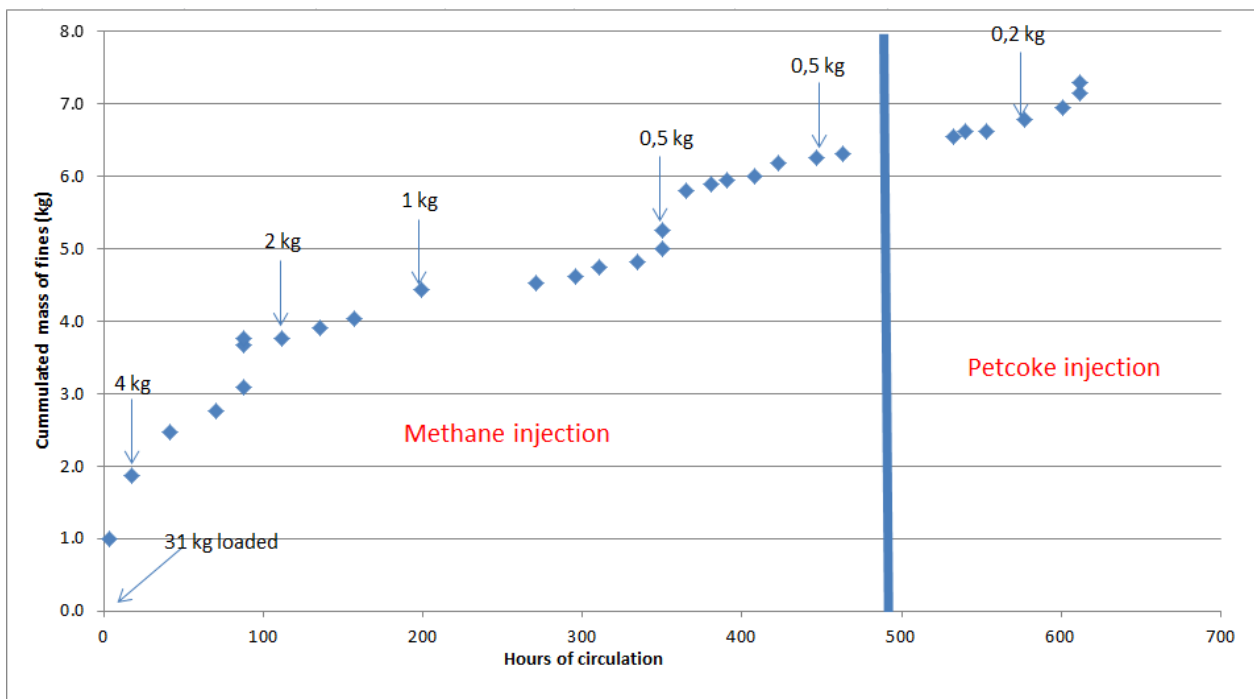


Figure 6-16: Evolution of fines production during the campaign

The mean value of inventory loss under methane exposure is 0.30%/h (or 0.12 kg/h) which leads to a particle lifetime of approximately 331 hours. With petcoke, the inventory loss is around 0.21%/h, leading to a particle lifetime of 482 h. Fragmentation of LY Mn ore seems to be more important with methane as fuel.

As a reminder, the mean value of inventory loss calculated under methane exposure with ilmenite T1 was 0,13%/h, leading to a particle lifetime of 770h. And when petcoke was used as fuel, the inventory loss was around 0.07%, which corresponds to a particle lifetime of 1430h.

The higher amount of fines produced, and the lower lifetime of the Mn-ore LY, is also clearly seen from the hot attrition testing done by SINTEF MK, as shown in section 7.2.1.

This is in line with some previous experiments in the Chalmers 10 kW CLC unit which have shown that manganese ores are more sensitive to attrition than ilmenite, with respective lifetimes of 50-290 hours and 700-800 hours (Linderholm et al. 2014; Linderholm et al. 2016; Linderholm, Lyngfelt et Dueso 2013; Linderholm et al. 2012).

6.1.5 Agglomeration phenomena

Some technical problems occurred during the campaign. Most of those technical problems were due to the formation of agglomerates in several parts of the unit. Figure 6-17 shows some agglomerates formed during the campaign.



Figure 6-17: Left : agglomerates formed in the L-valve of AR2 ; right : agglomerates formed at the outlet of FR (around 5 cm of diameter)

The zones of poor fluidization (typically in the L-valve and far from the holes of the gas distributors in each reactor) favor the agglomeration and should be avoided to limit the technical problems inherent to the solid circulation.

As mentioned previously, at the end of the test campaign, the unit was cooled down with oxidation of the OC in the air reactors, and with nitrogen fluidization in the fuel reactor. One would thus expect the agglomerates at the bottom of the fuel reactor to be reduced. However, XRD analysis shows that the recovered agglomerates are oxidized (Figure 6-18). Indeed, the main detected phases are Fe_2O_3 (and/or MnFeO_3), MnFe_2O_4 and Mn_3O_4 . Quartz (SiO_2) and some tephroite (Mn_2SiO_4) are still present, and pyroxmanganite ($\text{Mn}_7\text{Si}_7\text{O}_{21}$) has formed. The oxidation of the agglomerates during the cooling down procedure probably occurred due to oxygen released by the OC upon switching from air to an oxygen deficient environment (CLOU effect). The emission of oxygen by LY-Mn ore has indeed been observed in the batch unit when switching the fluidizing gas from air to nitrogen.

SEM analysis Figure 6-19 shows that many particles in the agglomerate are surrounded by an oxide scale.

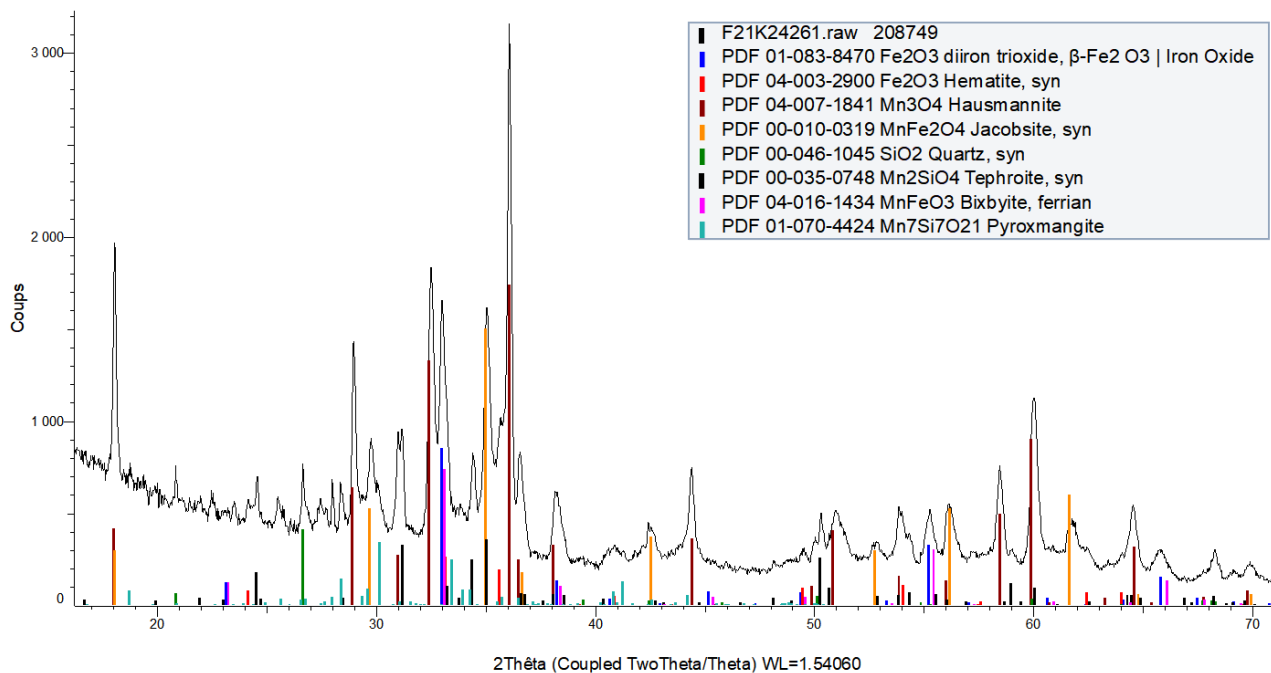


Figure 6-18: X-Ray diffractogram of agglomerates formed at the outlet of FR

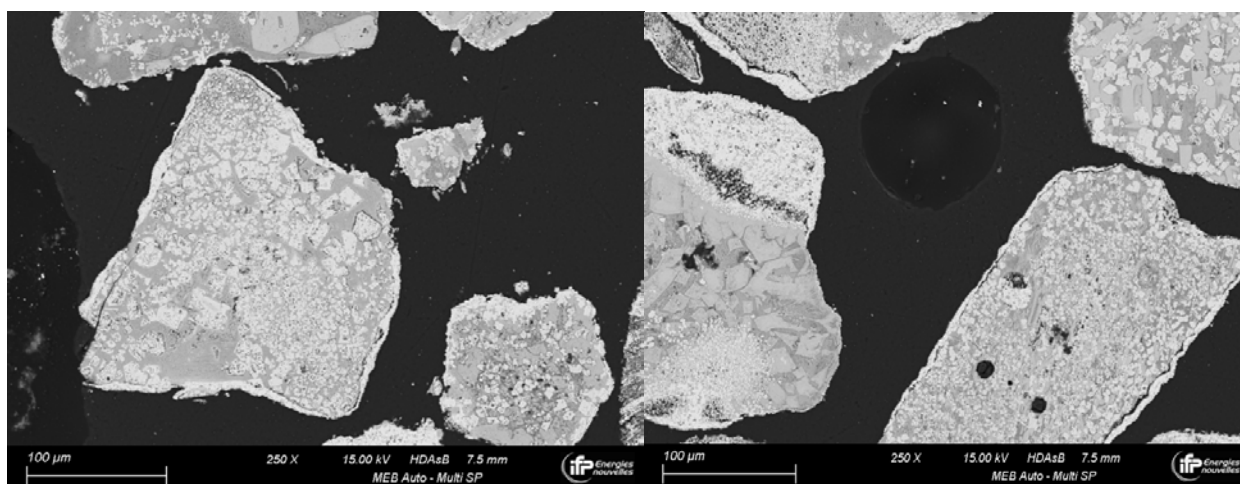


Figure 6-19 : Cross-section SEM pictures of agglomerates formed at the outlet of FR

6.1.6 Lessons learned from unit operation

The reactivity of LY Mn ore is high enough to convert the gases produced by petcoke gasification. In IFPEN’s 10 kW pilot unit with high solid residence time, a petcoke conversion of up to 89% was observed without any recycle of unburnt petcoke. A parametric study has confirmed the tendencies observed in IFPEN’s batch unit. It was observed that LY Mn ore has a high initial $R_0\Delta X$ value ($R_0\Delta X=0.8$), which lead to shorter activation period in comparison to campaign with Ilmenite T1. In the conditions of higher petcoke flowrate it was possible to achieve high values of $R_0\Delta X$ parameter, approximately 1.9, which proves the potential to operate at high oxygen transfer capacities at large scale.

However, some agglomerates were formed during the campaign in areas of poor fluidization. This is a key point to maintain a good circulation in the unit.

The conclusion is that the second selected oxygen carrier (LY Mn ore) achieves slightly better performance than the first selected oxygen carrier (Ilmenite) regarding solid fuel conversion (rate of gasification). However, manganese ores are more sensitive to attrition than ilmenite, as shown in 6.1.4

6.2 SINTEF ER

6.2.1 Main test results

The pilot unit at SINTEF ER is operated on a daily basis and is stopped at nights. During night, the 10-kW heating cable on each reactor is maintaining some temperature level in the reactor system, reducing the time for the heat-up sequence the next day. However, getting the whole reactor system up to operation temperature usually takes around 5 hours, which normally makes it possible to run the reactor for 5 – 6 hours in CLC mode. Table 5-1 sums up the test days with Mn-ore. Some challenges were experienced during the testing with the Mn-ore, but not all can be ascribed to the oxygen carrier itself. One reoccurring problem was plugging of the pipe between the AR cyclone and the AR loop seal. This has also been observed earlier when using ilmenite. The plugging could most of the times be opened by hammering on the top of the cyclone, as the vibrations loosened the agglomeration / bridging. Another problem was associated with the quite large fraction of fines which was not possible to remove during the sieving (cf. Figure 3-6). Much of the fines followed the gas streams out of the cyclones, creating problems with the gas sampling. The high temperature gas sampling filter units were clogged several times, thereby reducing the flow to the gas analysers, and sometimes stopping it completely. A third problem, which cannot be ascribed to the oxygen carrier, was plugging of the fuel inlet pipe and blockage of the feeding screw. With petcoke, it has been observed earlier that the petcoke particles can plug the inlet pipe close to the reactor because it gets sticky at elevated temperatures. However, this time it also happened with the milled wood pellets.

An overview of the different tests with Mn-ore LY is provided in Table 6-5. The first two days were used to activate the OC material. The tests on January 28 provided stable results for biomass operation. Then there were two days in February with some initial problems operating on petcoke. The test March 2nd provided successful results for petcoke operation.

Table 6-5: Overview of tests at SINTEF ER with Mn-ore LY as oxygen carrier.

21.01.2021	Milled un-sieved wood pellets	Successful operation about 2 h. Ends with blockage of fuel pipe (but managed to open up again by feeding air)
26.01.2021	Milled un-sieved wood pellets	Ca 0.5 h CLC operation with some propane to AR to keep temperature. Ends with AR downcomer blockage
28.01.2021	Milled un-sieved wood pellets	Ca 4 h CLC successful operation. N ₂ as fluidisation. Blockage of AR downcomer at end, but manage to open it
09.02.2021	Petcoke 100 – 315 µm (without fines)	Unsuccessful. First lifter blockage because of water in lifter, then blockage of fuel pipe
12.02.2021	Petcoke 100 – 315 µm (without fines)	Unsuccessful. Feeding screw stuck
02.03.2021	Petcoke 100 – 315 µm and petcoke 100-315 µm incl. 40 % fines (< 100 µm)	About 6.5 hours successful CLC operation. Switched to wood pellets at end but got problems with downcomer plugging

Operating conditions and main performance results with Mn-ore LY are shown in Table 6-6 and Table 6-7. The CO₂ capture rate and FR gas conversion efficiency is also shown in Figure 6-20 and Figure 6-21. The FR gas conversion is generally lower than comparable results from using ilmenite T1. The solid circulation was

lower in the Mn-ore cases to increase residence time and reduce amount of carbon transported to AR. For the biomass cases we have a high capture rate of about 96 – 97 % whereas FR gas conversion is about 65 – 67 %. For ilmenite T1 and biomass it was about 90 % capture rate and 80 % FR gas conversion efficiency. It may be that solid circulation became too low in the Mn-ore cases, and that some higher solid circulation could have helped on the FR gas conversion without sacrificing too much the capture rate.

For the biomass cases, the carbon balance is not 100 % as indicated with red fonts. More carbon is leaving FR and AR as gaseous components than total carbon fed with the fuel. This is most likely a consequence of one or more of the uncertainties discussed in chapter 2.1.4. Biomass test periods with carbon balance less than about 10 – 12 % deviation has been retained as relevant test results.

For the cases using petcoke with fines, the capture rate is higher than ilmenite T1 and petcoke, about 50 % vs 33 %. As mentioned, the lower solid circulation can be one reason. In addition, petcoke with fines have diameter 100 – 315 μm plus 40 % fines being less than 100 μm . The only pure petcoke case with ilmenite T1 was for a petcoke with size 315 – 500 μm . This can more easily go towards FR bottom and to AR via the lifter.

The FR gas conversion efficiency is lower for the Mn-ore LY petcoke cases than petcoke cases using ilmenite T1. This follows the same trend as mentioned for biomass above. It was assumed that the Mn-ore should be more reactive and give some CLOU effect, giving higher FR gas conversion than the ilmenite. However, here it is only in the range 63 – 72 %. The higher values in this range can be attributed to the higher solid circulation, and slightly higher FR temperature and inventory. And the higher circulation does not impact the capture rate negatively, indicating that increased circulation could have been to the better, and that the performance is not only related to the OC itself.

Table 6-6: Main operating conditions, SINTEF ER with Mn-ore LY.

Test No.	Type of fuel	Fuel feed rate (kg/h)	Fuel power (kW)	AR top / bottom temp. (°C)	FR top / bottom temp. (°C)	AR riser mass flow (*) (kg/s)	FR inventory (kg)	Specific FR inventory (kg/MW)
MnLY-1	Bio milled unsieved	22.0	115.9	1008 / 1006	954 / 967	2.1	15.1	130
MnLY-2	Bio milled unsieved	22.0	115.9	1015 / 1013	960 / 973	1.9	17.0	147
MnLY-3	Petcoke w/o fines	10.0	83.3	1038 / 1025	956 / 975	1.3	15.4	185
MnLY-4	Petcoke with fines	12.0	100.3	1002 / 998	939 / 945	1.4	16.3	163
MnLY-5	Petcoke with fines	12.0	100.3	1021 / 1018	945 / 958	1.4	16.3	162
MnLY-6	Petcoke with fines	12.0	100.4	1013 / 1011	945 / 957	1.6	18.7	186
MnLY-7	Petcoke with fines	12.0	100.2	1012 / 1009	955 / 970	2.1	20.5	204

(*) Analytically calculated theoretical riser mass flow as described in Ch.2.1.3.

The capture rate of the case MnLY-3 with petcoke without fines (i.e., size 100 – 315 μm only) is very low, only 18.3 %. For this case, the carbon balance indicates that all carbon fed with fuel is leaving FR and AR as gaseous components, with a deviation of only 1.6 %. Only 19.9 % of the fuel carbon is being converted to gas in the FR. All the remaining 80 % of carbon with fuel can be found as CO_2 from the AR outlet gas. Even though this petcoke is smaller than the petcoke used with T1 (which was 315 – 500 μm), it still seems to follow the OC easier from FR to AR. And it contains no fines that will flow more easily upwards the FR, that would have compensated somewhat. For the case MnLY-3, the fuel power is very low, and it may be too low to produce enough gasification and combustion products to support upwards particle entrainment. The FR pressure profile clearly indicate very little particles and gas flow in the upper part of FR. For cases MnLY-4 to 7, the fuel power is higher but still not as high as for T1 and petcoke. Increased FR fluidisation would also help.

The cases MnLY-4 to 7 have about the same fuel carbon conversion as MnLY-3 (~ 20 %). However, in this case, the remaining 80 % carbon is not only going to the AR. Nearly 30 % of the total carbon feed is leaving the FR in particulate form.

Table 6-7: Main performance results, SINTEF ER with Mn-ore LY.

Test No.	Type of fuel	Fuel carbon conversion X_{fuel-C} (*) (% of total fuel carbon)	Carbon leaving AR (as CO_2) (% of total fuel carbon)	Carbon out as FR and AR gas components (% of total fuel carbon)	Carbon balance = carbon out FR as particles (% of total fuel carbon)	FR gas conv. efficiency (%)	CO_2 capture rate (%)
MnLY-1	Bio milled unsieved	109.0	3.7	112.6	-12.6	64.8	96.3
MnLY-2	Bio milled unsieved	108.9	3.2	112.1	-12.1	67.1	96.8
MnLY-3	Petcoke w/o fines	19.9	81.7	101.6	-1.6	70.5	18.3
MnLY-4	Petcoke with fines	21.2	50.9	72.2	27.8	63.6	49.1
MnLY-5	Petcoke with fines	18.8	52.1	70.9	29.1	63.8	47.9
MnLY-6	Petcoke with fines	20.5	51.0	71.5	28.5	68.2	49.0
MnLY-7	Petcoke with fines	21.8	48.0	69.9	30.1	72.8	52.0

(*) Fuel carbon conversion is equivalent to amount of fuel carbon leaving FR as gas components.

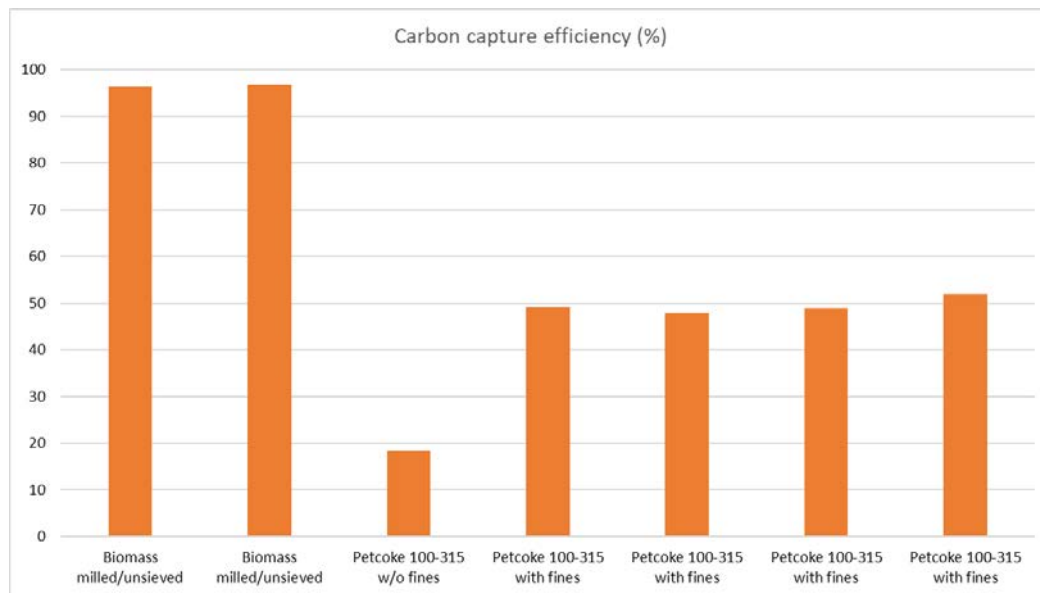


Figure 6-20: CO₂ capture rate, SINTEF-ER with Mn-ore LY as OC.

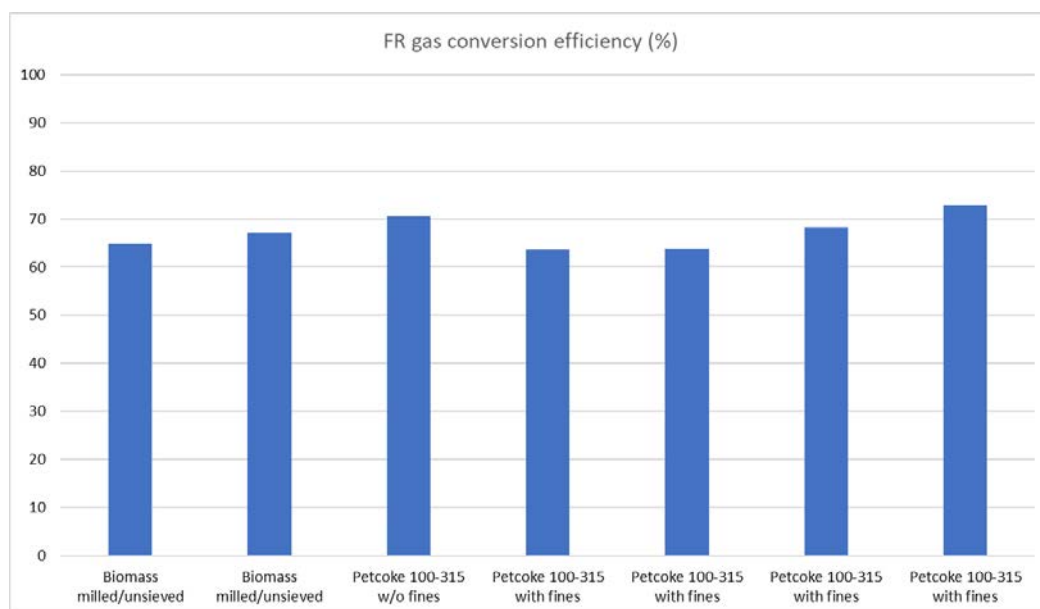


Figure 6-21: FR gas conversion efficiency, SINTEF ER with Mn-ore LY as OC.

6.2.2 Oxygen carrier characterisation

The Mn-ore to be used by SINTEF ER had to be additionally sieved before it could be used. The resulting size after this sieving is mainly in range 60 – 200 µm, with some fraction of both smaller and larger particles (cf. chapter 3.2). SEM and EDS pictures of the fresh material before use is shown in Figure 6-22. Most particles are near pure Mn oxide or heterogeneous Mn oxide and glassy phase mix. Some Fe oxide particles can also be seen. In addition, there are some Si oxide particles, plus minor amounts of some other oxides (cf. Table 3-2).

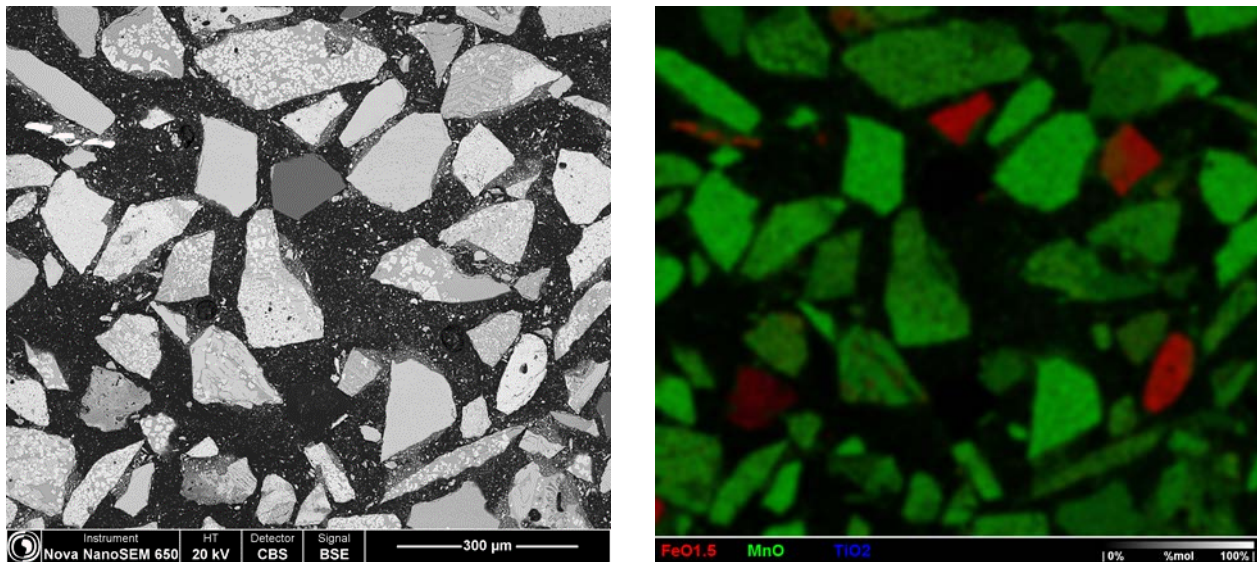


Figure 6-22: Fresh Mn-ore LY about 60 – 200 μm . SEM (left) and EDS of Fe, Mn, Ti oxides (right).

SEM and EDS of OC samples taken from AR reactor, AR bucket and AR chamber are shown in Figure 6-23. Compared to the fresh material, the reactor samples show clearly increased internal porosity, and surface enrichment in Mn in the heterogeneous Mn oxide plus glassy phase mix particles. The samples from the bucket and chamber show similar composition as the reactor sample, but smaller particle size and many fines. The amount of fines is largest in the chamber since this is a very low-velocity volume in order to settle small particles.

The samples from the FR are shown in Figure 6-24. They show much of the same as the AR samples. The increased internal porosity and surface enrichment in Mn in the heterogeneous Mn oxide plus glassy phase mix particles are very clearly seen in the magnified view in Figure 6-25. The porosity increase is most marked in the pure Fe oxide particles. The amount of OC fines in the bucket and chamber samples are less than what was found for the AR.

The FR chamber sample contains quite many small and hollow fuel particles. This is more clearly seen in the enlarged picture in Figure 6-26 where the fuel particles are the dark grey particles in between the brighter OC particles. In the results evaluation it was found that the carbon balance between gaseous carbon leaving the system (AR+FR) and the carbon input with fuel was only about 70 – 72 % for the Mn-ore cases when operating with petcoke 100 – 315 μm containing 40 % fines (< 100 μm). When operating petcoke 100 – 315 μm without fines, the carbon balance was OK. It is anticipated that the fines in the petcoke fuel may very easy escape with the centre gas flow of the FR without being fully converted.

The hollow structure is similar to the petcoke chars found in [6] where small petcoke particles were exposed to high heating rate devolatilization when being fed to a drop tube reactor at 1300 °C.

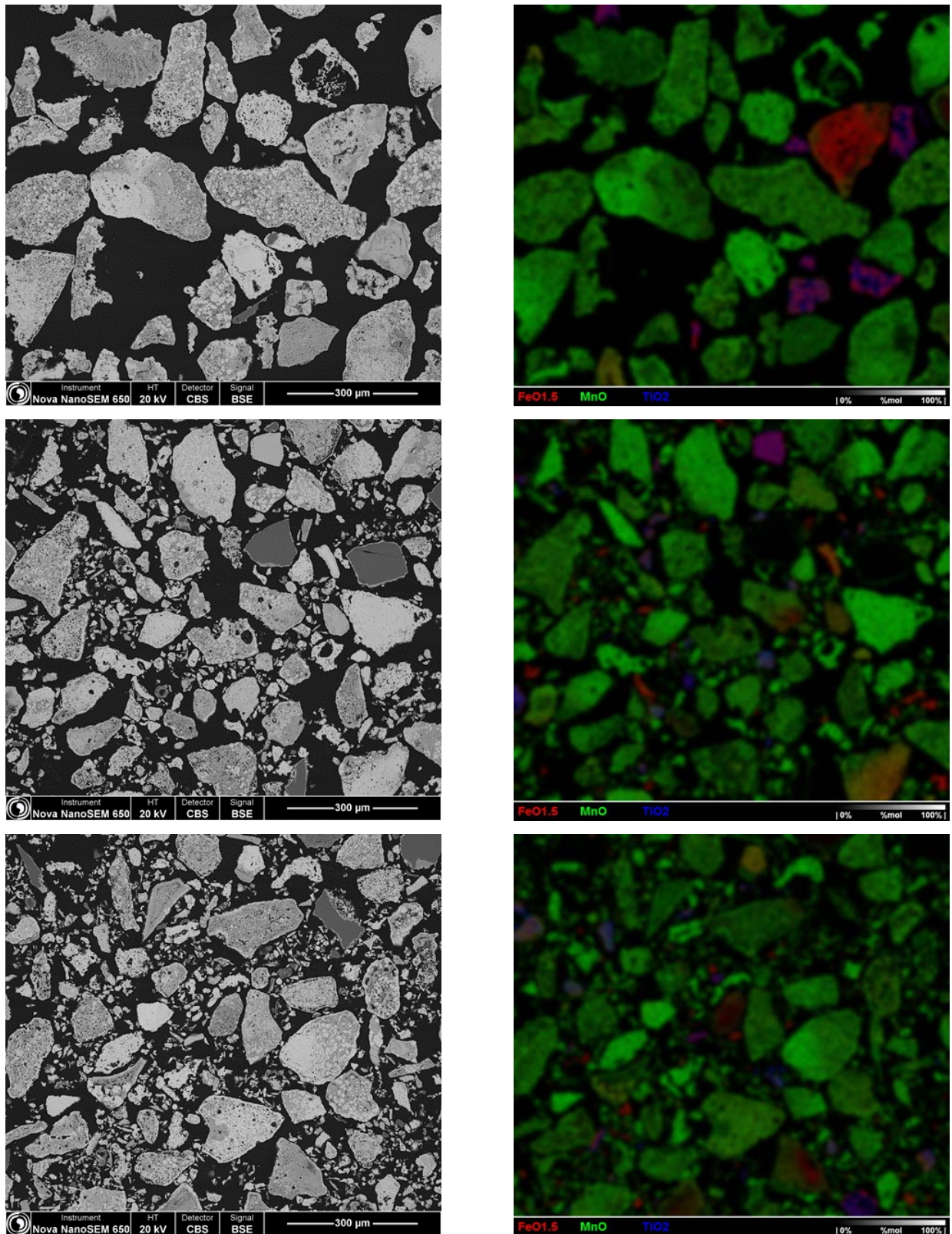


Figure 6-23: SEM (left) and EDS (right) of Mn-ore sample from AR reactor after last test with petcoke (top), from AR bucket (middle), and from AR chamber (bottom).

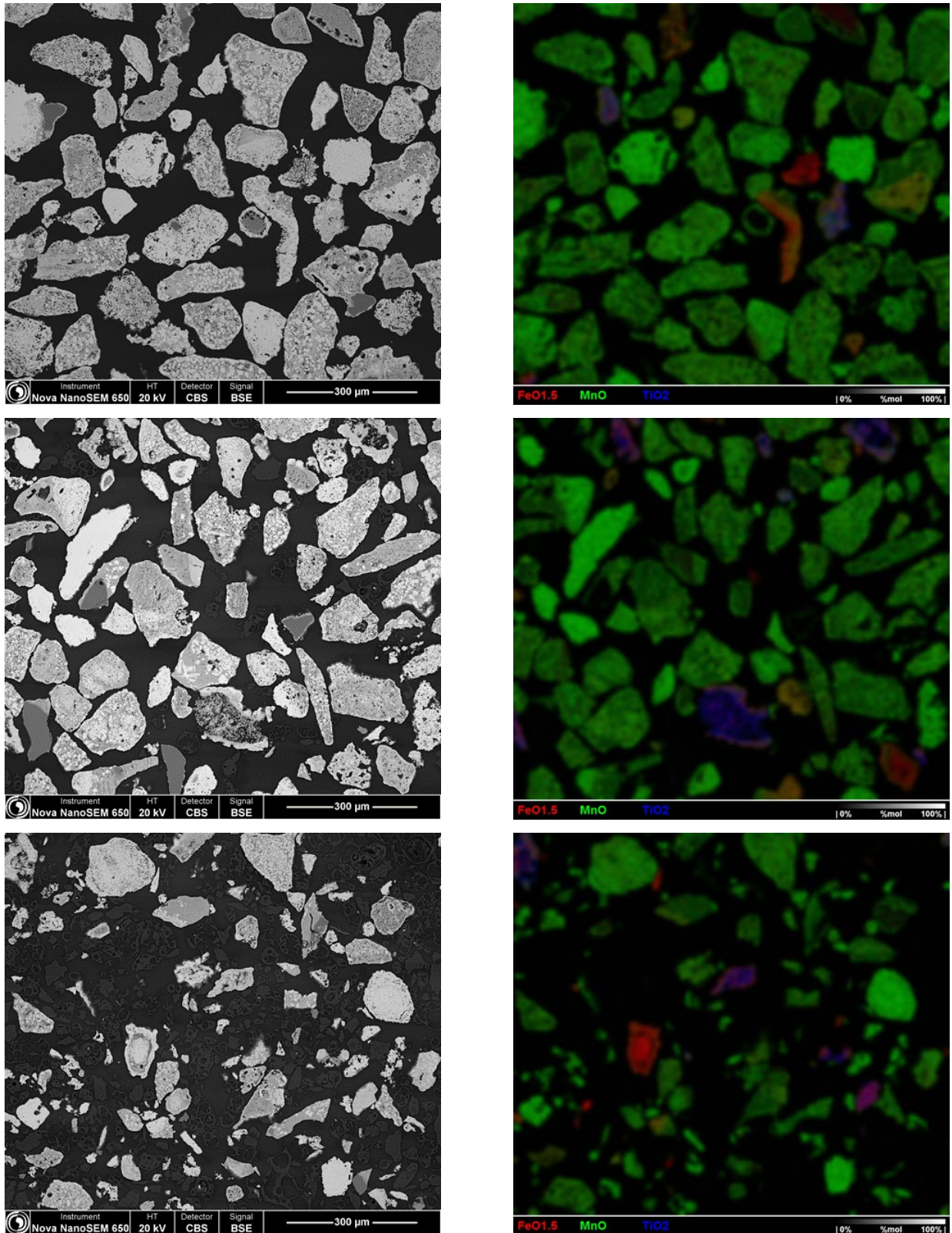


Figure 6-24: SEM (left) and EDS (right) of Mn-ore sample from FR reactor after last test with petcoke (top), from FR bucket (middle), and from FR chamber (bottom).

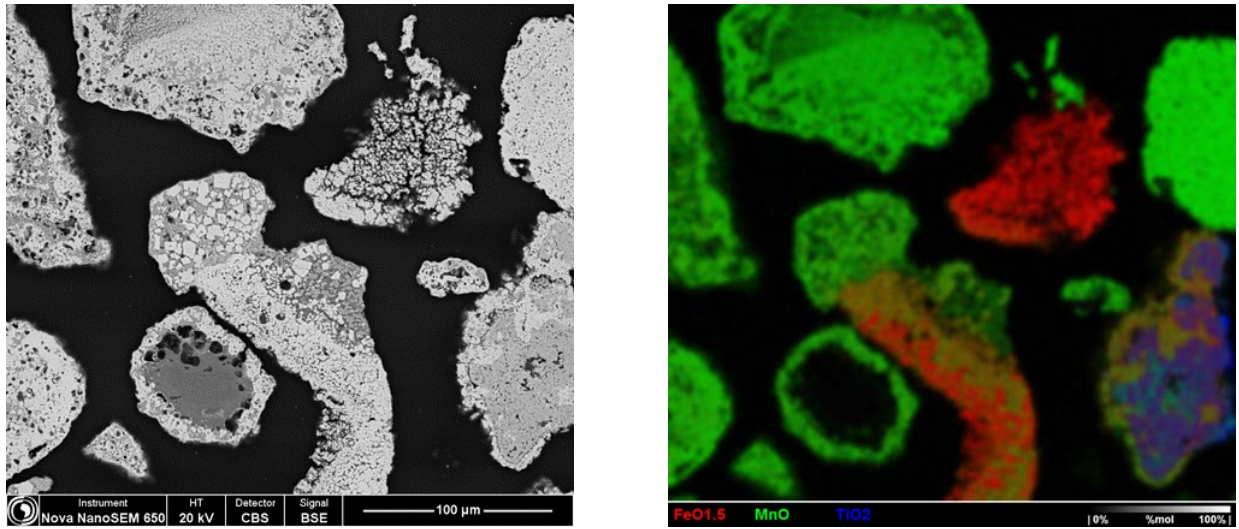


Figure 6-25: SEM (left) and EDS (right) of Mn-ore sample from FR reactor (same as above but larger magnification).

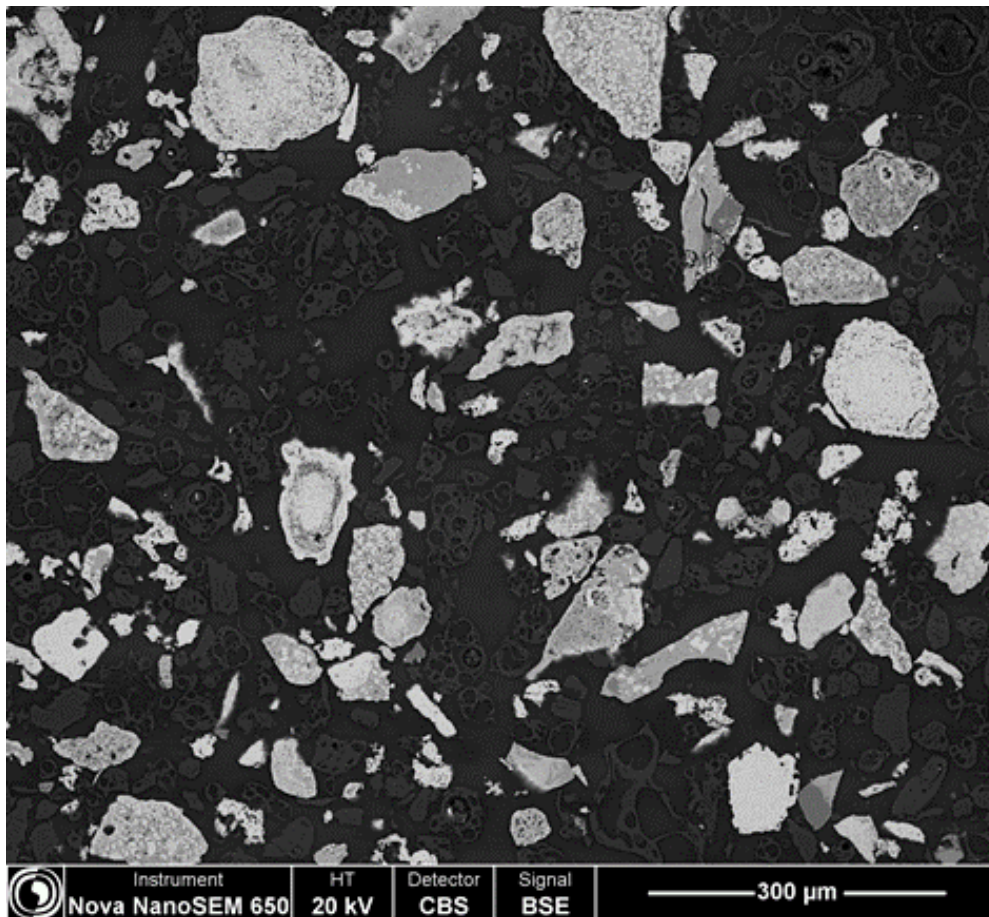


Figure 6-26: Enlarged SEM of Mn-ore sample from FR chamber, showing many small and hollow fuel particles.

6.2.3 Agglomeration and operability

The operability of the Mn-ore LY was not different from ilmenite T1, after it was sieved more properly. Fluidisation was easy to achieve and the "flowability" of the material was even better after some time in the reactor system, where the small share of remaining fines after sieving (about 15 wt-%) had been lost. Some instabilities and problems with plugging in the AR cyclone/downcomer was observed also for this OC, however, this is a problem that is most likely a consequence of the design and not the OC. The same problem is observed also for other OC's, such as the ilmenite T1.

No indication of serious agglomeration was observed during the experiments, however, after the last test the reactor system was emptied, some small lumps of material were found. As seen in the picture in Figure 6-27 it looks very metallic, and it was analysed with SEM and EDS to check its structure and composition.



Figure 6-27: Metallic lump taken out from FR after last test with Mn-ore LY.

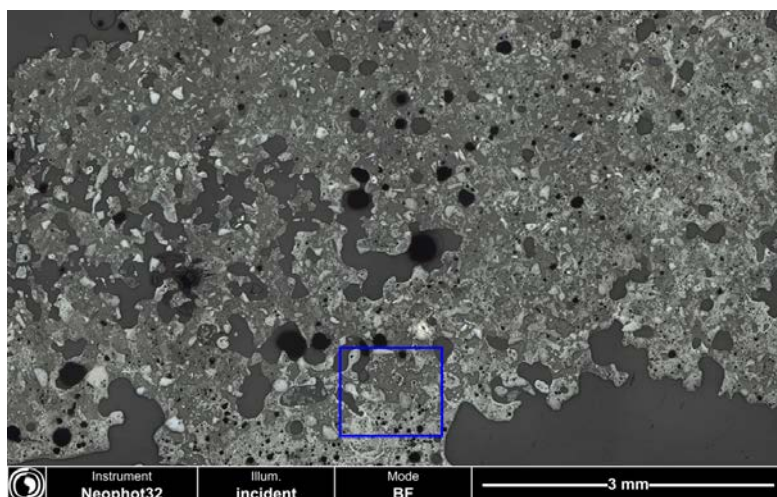


Figure 6-28: Optical view (bright field) of metallic lump taken out from FR.

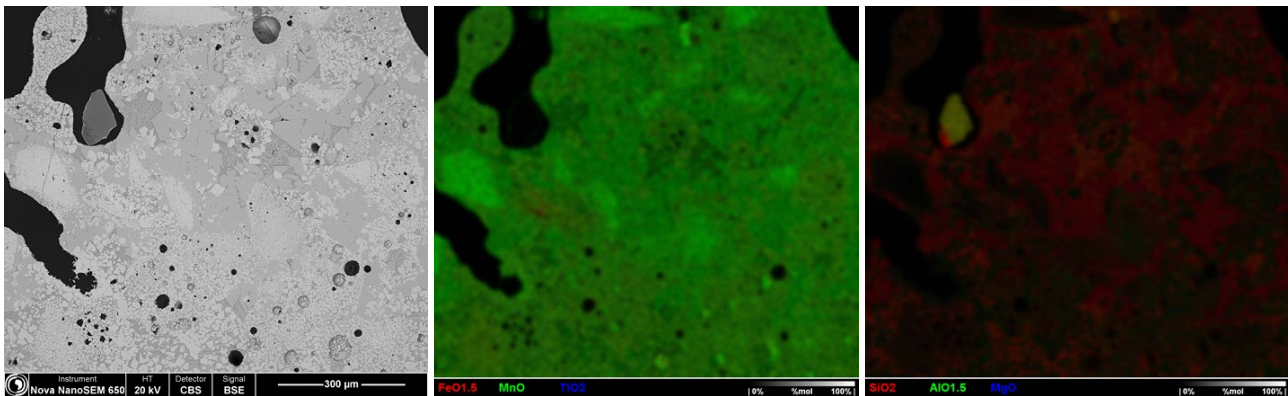


Figure 6-29: SEM (left) and EDS (middle and right) of lump from FR.

The optical view of the cross-cut lump in Figure 6-28, and the magnified SEM and EDS in Figure 6-29, show it is a compact agglomerate, with many of the original OC particles still clearly apparent. It consists mostly of Mn oxide and mixed Mn/glassy phase.

It was very few lumps that were seen when emptying the reactor and during operation they did not cause any notable problems. Since the tests had limited duration, it is unsure if this is a problem that can build up. On the other hand, this rather heavy small lumps will most likely be extracted through the normal ash extraction system.

6.2.4 Summary from operation of Mn-ore LY in 150 kW unit

Operation with Mn-ore LY in the SINTEF ER pilot unit went smooth without any tendencies to serious process upsets needing shut-down. Based on qualitative judgement the operability was about the same as for ilmenite T1. The pilot unit is prone to have some clogging in the AR cyclone and downcomer. These upsets can normally be handled by activation of some flushing nozzles, however, in the worst cases they will cause shutdown. There was no noticeable difference in the tendencies to such clogging with Mn LY compared to ilmenite T1.

The CO₂ capture rate is very high when using biomass, i.e., low loss of unconverted fuel particles from FR to AR. With petcoke the situation is quite different, a high loss of unconverted fuel particles from FR to AR causes a low capture rate. These trends are the same as for ilmenite T1.

The results show that with biomass, no fuel particles leave the FR, all is leaving in gaseous form. However, the gas is not fully converted since the FR gas conversion efficiency is only 65 – 67 %. The additional oxygen needed will have to be supplied in the oxygen polishing step. It should be noted that the low FR gas conversion may be a result of low solid circulation, bringing too little oxidised OC to FR, and low fuel power and fluidisation of FR, causing too little particle entrainment up the FR.

The FR gas conversion efficiency is about the same in the petcoke cases, 63 – 72 %. In these cases, there is also a loss of fuel particles with the exhaust gases out of the FR. Close to 30 % of the fuel feed. This will increase the amount of oxygen needed in the oxygen polishing step.

OC samples from the reactors (taken after tests) and from AR and FR exhaust (taken during tests) were analysed with SEM-EDS. In general, they show increased internal porosity and surface enrichment in Mn in the heterogeneous Mn oxide plus glassy phase mix particles. The porosity increase is most marked in the

pure Fe oxide particles. No agglomeration tendencies were seen in the exhaust gas samples analysed. However, some highly metallic lumps were found in the FR after the test.

It should be noted that the SINTEF ER pilot unit does not have a carbon stripper and the residence time in the FR is relatively short. The low capture rate for petcoke, as well as a high share of unconverted fuel particles out from FR, is mainly a consequence of this, and not the oxygen carrier itself.

7 RESULTS WITH THIRD OXYGEN CARRIER – ILMENITE T2

This is also a Norwegian ilmenite but compared to the ilmenite T1, this one (which we here call ilmenite T2) has larger particle size. The size fraction of this material is much more beneficial with respect to the needed particle size for the demo unit in China (cf. section 3.3). It has almost exactly same composition as the ilmenite T1, except it was completely dried before being used in the pilot units. Early-stage testing of T2 showed serious problems with agglomeration and it was in fact rejected as a candidate. However, more recent tests at IFPEN showed that adding a small steam flow during heating up and OC activation could potentially avoid the agglomeration issue. The benefit of the more optimal particle size distribution is large and further testing was decided, as will be described below.

7.1 IFPEN

7.1.1 Ageing tests results

The two ilmenites have been aged with methane as reducing gas at 900°C in the batch unit.

a. Reactivity comparison

It has been observed that ilmenite material consumes a high amount of oxygen during its heating under air. Figure 7-1 (a) presents the evolution of methane conversion as a function of the number of cycles for the 10 tests performed on the two ilmenites T1 and T2. Figure 7-1 (b) shows the evolution of the oxygen carrier's $R_{O\Delta X}$ as a function of the cycle number.

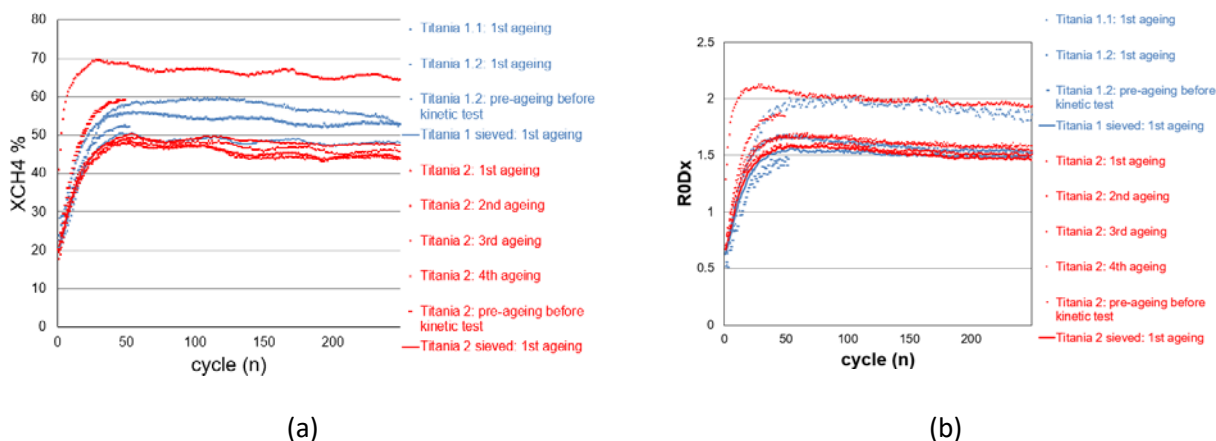


Figure 7-1: Experimental results of the ageing tests performed on ilmenite materials. (a) evolution of the methane conversion with the number of cycles, (b) evolution of the oxygen carrier's $R_{O\Delta X}$ value over the cycle number for the 10 tests performed with ilmenite oxygen carriers

According to Figure 7-1 (a), the ilmenite materials show a very strong activation over the first 50 cycles. Indeed, for similar cycle operating conditions, the methane conversion increases from 20% to between 45 and 70%. Besides, the $R_{O\Delta X}$ value varies from 0.5 % to between 1 and 2 %. There is a disparity between the test results of a same material (e.g., T2), this is mostly due to a level of experimental uncertainties and in some cases to reactor pollution from previous tests.

b. Agglomeration

Tests have been performed to determine if there are differences in terms of reactivity or stability between T1 and T2. It appears that T2 has a greater tendency to agglomerate than T1. For all the tests performed with T2, a ring of agglomerated particles has formed at the bottom of the reactor (see Figure 7-2). The reason of this ring formation was at that stage not fully elucidated since T1 and T2 have almost the same properties. Due to the agglomeration problem, T2 was originally rejected as a candidate, to reduce as much as possible the agglomeration occurrence in low fluidization zones of the larger units (L-valves and loop seals in the IFPEN 10 kW_{th} pilot and CHEERS 3 MW_{th} unit). However, T2 has been re-investigated further at a later stage in the project (see section 7.1.3).



Figure 7-2: Agglomerated ring of ilmenite T2.

c. Ilmenite morphological evolution

The two ilmenite samples have been characterized before and after the 250 cycles ageing tests with methane fuel, with a special focus on morphological evolution.

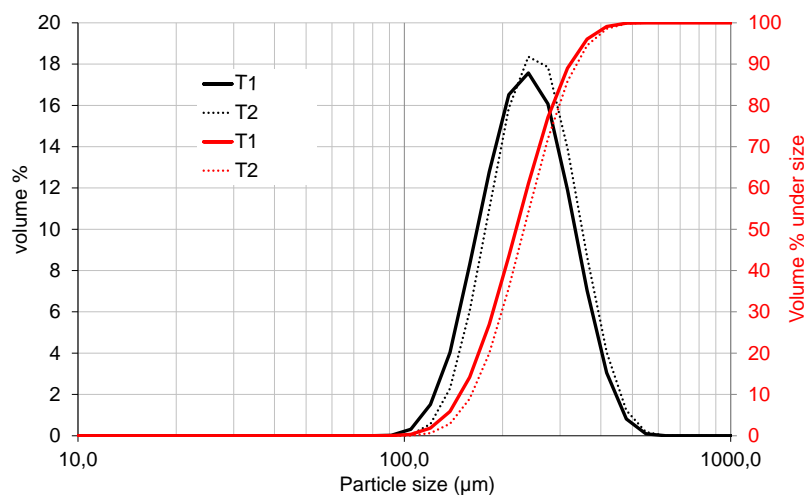


Figure 7-3: Particle size distribution of fresh ilmenite T1 (batch delivered to IFPEN, i.e., after sieving to 180-300 µm) and T2 (directly delivered after drying), measured by laser granulometry.

T1 and T2 come from the same mine, and as such, do not differ much, except T2 has been dried, and is delivered at larger particle size and with narrower particle size distribution. In Figure 7-3 is shown particle size distributions measured by laser granulometry of T1 (batch delivered to IFPEN, i.e., sieved to 180-300 μm), and T2 (as delivered without sieving). The mean particle size (D_v^{50}) of this T1 batch is 252 μm , and that of T2 is 267 μm . Some small elemental analysis variations between T1 and T2 have been measured by the supplier, which can be attributed to compositional variations in the ore itself as well as to measurement accuracy.

XRD analysis confirms there is little difference between both samples, FeTiO_3 (ilmenite) and Fe_2O_3 (hematite) being the predominant detected phases, along with silicate-based impurities. The particles are very angular (Figure 7-4 and Figure 7-5), and literally non porous (0 ml/g porous volume, as measured by Hg porosimetry).

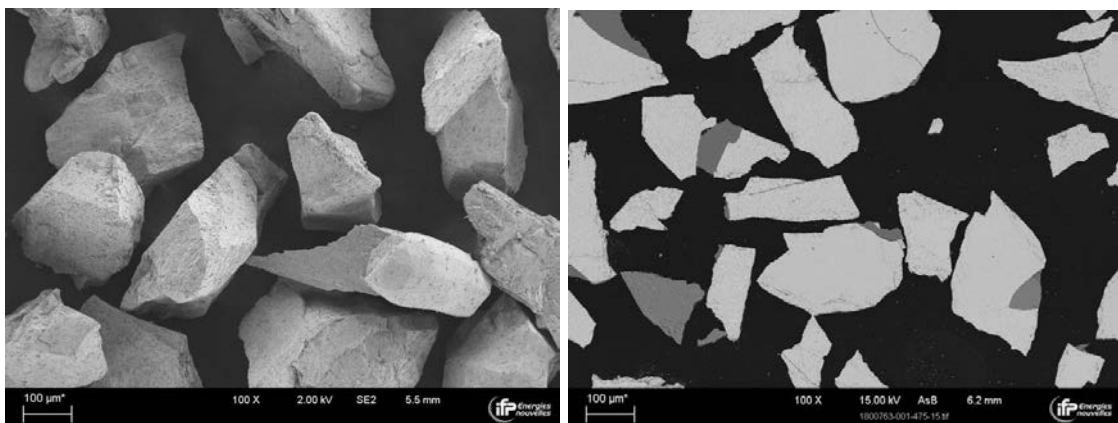


Figure 7-4: SEM pictures of fresh ilmenite T1 particles (left: direct observation; right: polished cross-section)

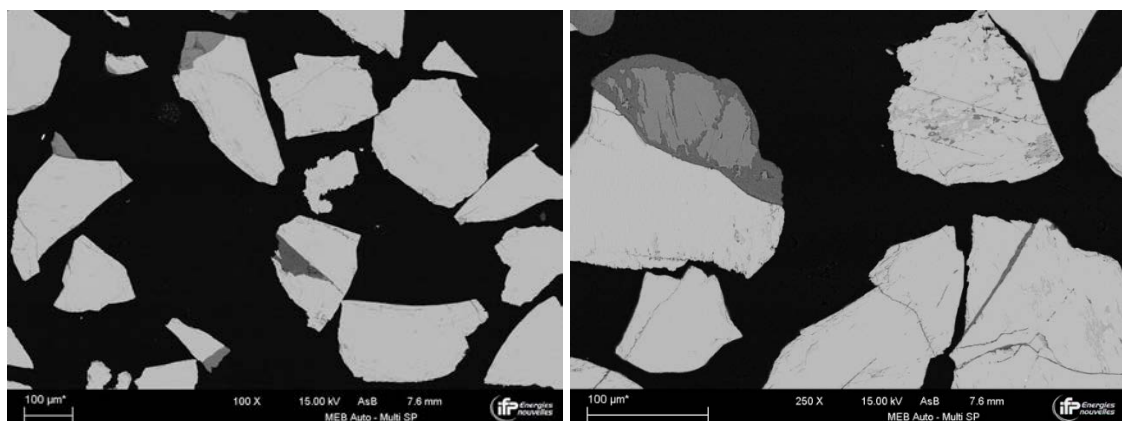


Figure 7-5: SEM pictures on polished cross-section of fresh ilmenite T2 particles

The brighter areas in the polished cross-section pictures in Figure 7-4 and Figure 7-5 are constituted mainly of Fe and Ti oxides, while the darker areas are made of Si oxide mixed with other impurities. Based on the available characterization data, it is not possible to differentiate T1 from T2, except for the very small difference in particles size distribution (between the two batches delivered to IFPEN, not the original materials). It is hence difficult to understand their different behavior with regards to agglomeration during the ageing tests.

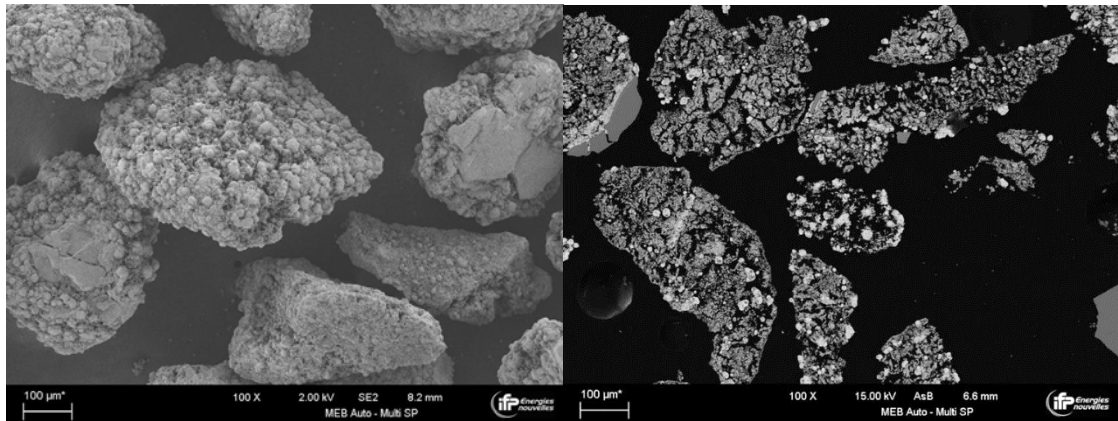


Figure 7-6: SEM pictures of T1 after 250 redox cycles (left: direct observation; right: polished cross-section)

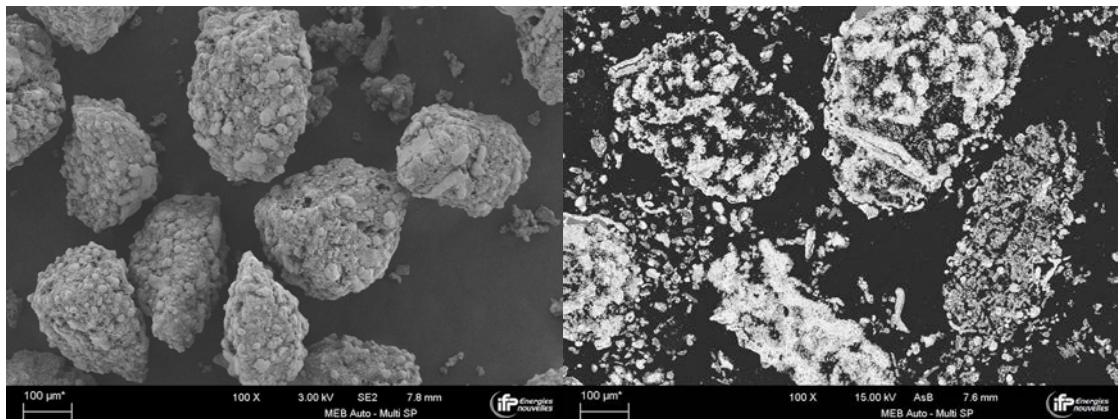


Figure 7-7: SEM pictures of T2 after 250 redox cycles (left: direct observation; right: polished cross-section)

After 250 redox cycles in batch fluidized bed, the morphological evolution of T1 and T2 is similar (Figure 7-6, Figure 7-7): In both samples, a large porosity increase of the particles is observed, which probably accounts for the reactivity increase observed during the first 50 cycles. EDS cartography of the aged particles (Figure 7-8) shows that Fe and Ti are segregated within the particles, with iron forming round shaped nodules both inside and at the surface of the particles.

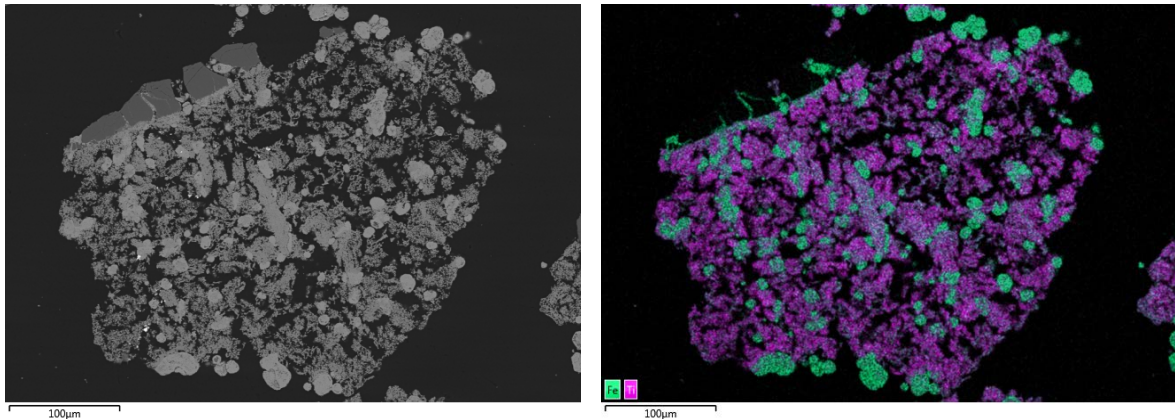


Figure 7-8: SEM (left) and EDS (right) pictures of T1 after 250 redox cycles, showing Fe and Ti distribution

7.1.2 Kinetic screening

After 50 redox cycles pre-ageing of samples with methane, petcoke is injected in the oxygen carrier bed. In the presented study, a petcoke from TOTAL has been used since no Chinese one had been selected yet. Figure 7-9 shows the gaseous components profiles at the reactor outlet during the pet-coke conversion stage. This particular curve has been obtained at 940°C with 50% of steam in the inlet gas.

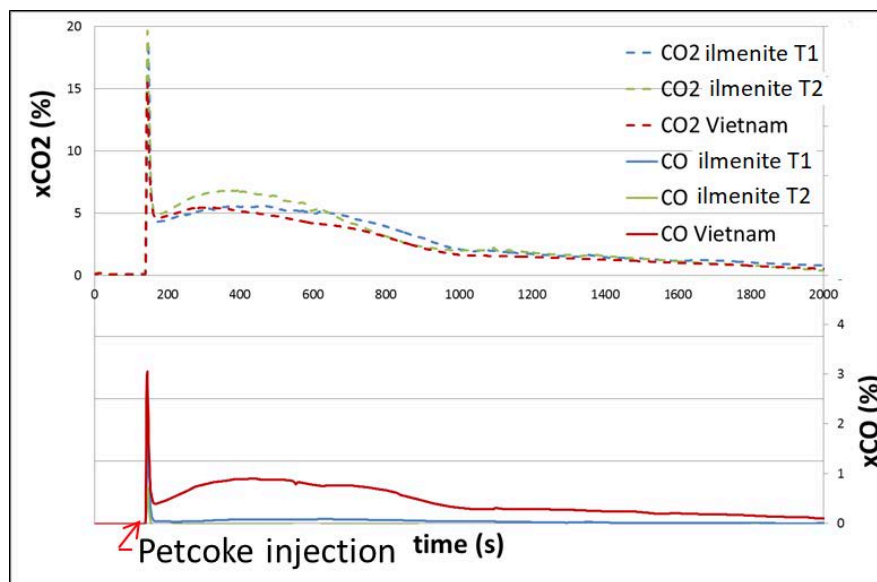


Figure 7-9: CO₂ and CO concentration evolution at the reactor outlet during petcoke conversion in the batch fluidized bed reactor with ilmenite T1 and T2 (plus a Vietnam ilmenite).

When petcoke is injected in the reactor, volatiles are instantly released and burnt. After that, the gasification reaction takes place during several minutes. From these results, it is clearly visible that the limiting step of petcoke conversion is its gasification rate. It does not change when one ilmenite or another is used as oxygen carrier, and no differences have been observed between T1 and T2. According to Figure 7-10, the higher the

temperature and the steam concentration, the higher the petcoke gasification rate. Similar results have been obtained with T1.

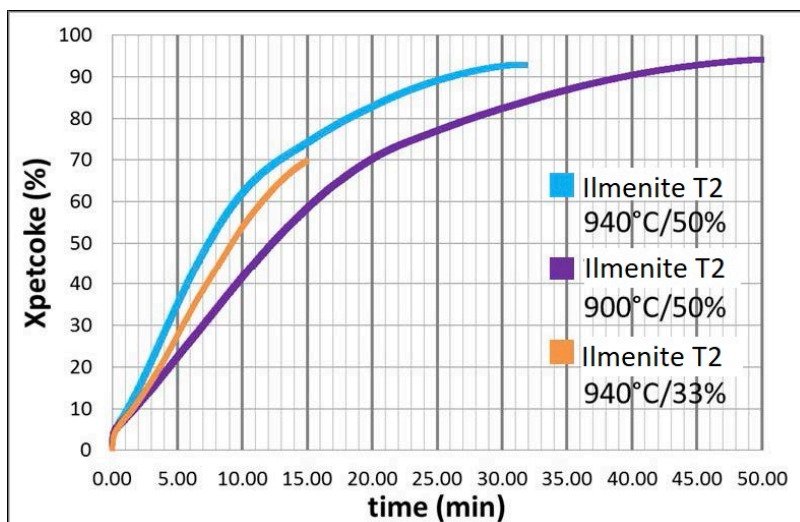


Figure 7-10: Impact of temperature and steam concentration on petcoke conversion in the batch fluidized bed unit. Test with petcoke from TOTAL and Ilmenite T2 as oxygen carrier.

7.1.3 Ilmenite T2 test with water addition

The previous tests conducted on ilmenites T1 and T2 have demonstrated a good capacity for fuels conversion but they have a tendency to agglomerate in areas of poor fluidization. IFPEN batch unit tests showed that in general, ilmenite T1 leads to less agglomeration than ilmenite T2. As previously stated, the main differences between these two materials (from the same mine) are the particle size distribution and the water content (Ilmenite T1 having more dispersed PSD and more water content than T2). Since the PSD does not impact a lot the agglomeration phenomena, the hypothesis is therefore that the presence of water could avoid the agglomeration phase, which seems to occur during the temperature rise phase under air conditions (first oxidation). Therefore, the influence of steam addition on Ilmenite T2 tendency to agglomerate was studied in the IFPEN batch fluidised unit.

7.1.3.1 Test procedure

During the test, the batch reactor temperature is set at 900 °C. The flowrates of CH₄, air, H₂O and N₂ are given in Figure 7-11. Water addition account for 30 % of the total volume of the gas phase. First, since the agglomeration phenomena seems to occur during the temperature rise, around 10 cycles are carried out. This is the first test performed with steam addition.

Then, a second test has been performed over 250 cycles where steam account for 8.6 % of the total gas volume. This test aims to get close to the conditions that will be operated in the CHEERS demonstration unit where the heating of the two reactors is carried out with flue gas from natural gas and lignite combustion.

The results obtained from these two tests and the comparison with the results of the ageing test of ilmenite T2 without any addition of water is discussed below.

Phase	inertage	reduction	inertage	oxydation
CO (NI/h)	0	0	0	0
H ₂ (NI/h)	0	0	0	0
CH ₄ (NI/h)	0	75	0	0
Air (NI/h)	0	0	0	93
H ₂ O (g/h)	46	46	46	46
H ₂ O (NI/h)	57	57	57	57
N ₂ (NI/h)	133	58	133	40
CO ₂ (NI/h)	0	0	0	0
total (Nm ³ /h)	0,190	0,190	0,190	0,190

Figure 7-11: Flow rates during each phase of a cycle (inerting, reduction and oxydation)

7.1.3.2 Mechanical behavior

Over 250 cycles and with 8.6 %vol of water in the gas phase, no agglomeration has been observed contrary to the test with no water addition (under equivalent operating conditions). This confirms the hypothesis that the water content of ilmenite T1 is enough to limit the agglomeration.

7.1.3.3 Performances

The effect of steam addition (8.6 %v and 30 %v) on the methane conversion and oxygen transfer capacity (RODX) of the ilmenite T2 is shown on Figure 7-12. The influence is clear: RODX is reduced when the concentration of steam increases. Consequently, the same effect is observed with the methane conversion during the test. The trend of the test under 30 % steam addition seems to confirm this influence.

To confirm this inhibition of reactivity, the steam addition has been stopped for 10 cycles just before the cycle 180 (see red dots of Figure 7-12) and then resumed until the end of the test. During those 10 cycles, the methane conversion and the oxygen mobility are found close to the values obtained without adding water.

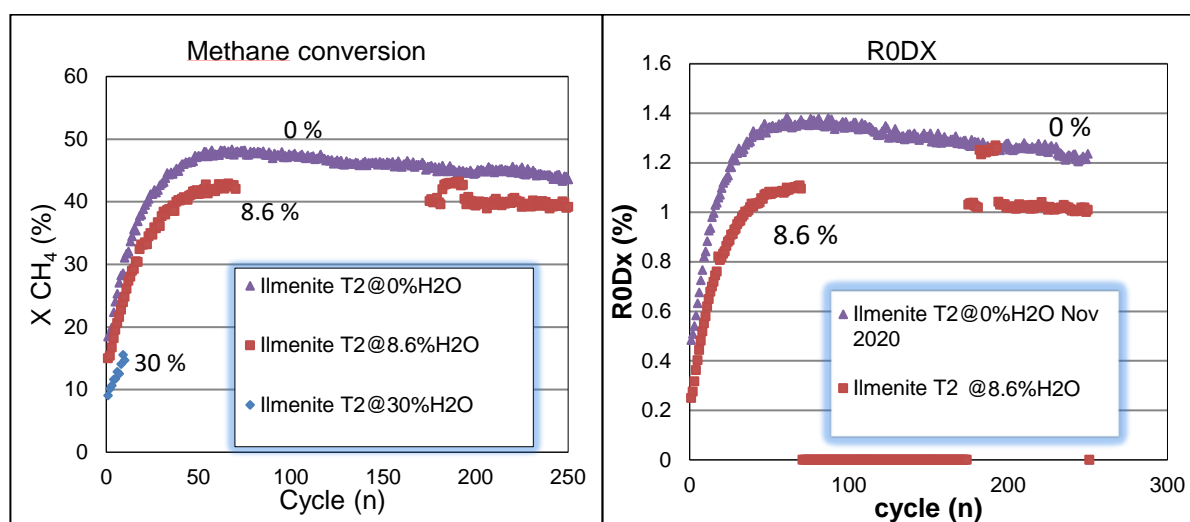


Figure 7-12: Evolution of methane conversion and oxygen mobility of ilmenite T2 over the number of cycles with 0 % (triangle), 8.6 % (red squares) and 30 % addition of steam (diamonds).

The lack of data between the cycle 70 and 175 is due to the presence of a public holiday that does not allow the change of the protective filter trapping water upstream of the gas analyzer. Given the large addition of water during these tests, the pump supplying the gas analyzer has been shut off during this time.

7.1.3.4 Ilmenite T1 test with water addition

To compare the influence of the water addition on ilmenite T1 and T2 ageing tests, same operating conditions are reproduced to study the impact of steam addition on ilmenite T1 ageing test, see Figure 7-13.

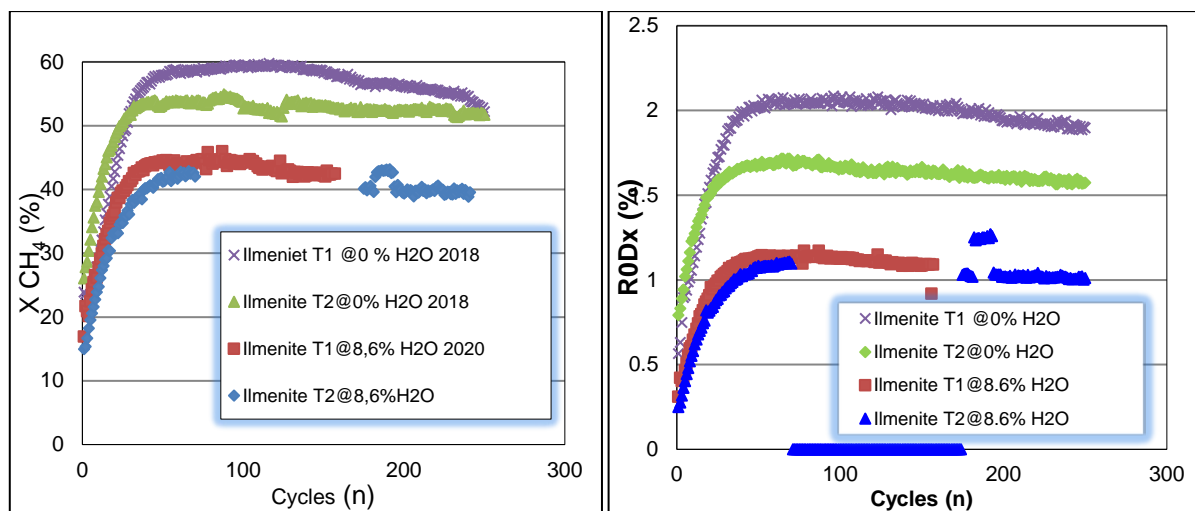


Figure 7-13: Comparison of the evolution of methane conversion and oxygen mobility of ilmenite T1 and T2 over the number of cycles with 0% and 8.6% steam addition

Like the test of Ilmenite T2 with water addition, the test of ilmenite T1 with steam leads to an inhibition in the methane conversion and oxygen mobility. Furthermore, methane conversion and RODX over the two tests of ilmenite with steam addition are in the same order of magnitude.

However, their mechanical behaviour is strongly different. As visible on Figure 7-14, an important formation of fines was formed during the test of ilmenite T1 with steam addition. This leads to an increased pressure in the reactor, reaching the maximum security pressure. Fluidisation has been lost and an agglomerated ring has also formed in the bottom part of the reactor.

This poor mechanical performance, when water is added to the system, was not observed with T2 under water addition. This favours the use of the ilmenite T2 over T1 as oxygen carrier in the 3 MW_{th} demo unit.



Figure 7-14: Left : outlet of the reactor (upper part) ; right : bottom part of the reactor after the test of ilmenite T1 with water addition

7.2 SINTEF MK

7.2.1 Attrition testing of ilmenite T2 (vs Mn-ore LY)

Hot attrition testing was performed in a 3 kW dual circulating fluidized bed chemical looping unit at SINTEF MK. The unit has a fuel and an air riser reactor, and two down-comers after the hot separation cyclone. The reactor tubes are dynamically gas-separated by loop-seals. The reactors have rather small inner diameter of 34 mm (9 cm²) giving fast transport of materials and low residence time for the particles. The cyclone, which has an inlet of 1 cm², gives nearly 10 times higher gas velocities for the particles in the cyclone. The cyclone is not built for high separation of gas/oxide but more for high velocity to increase attrition of the particles.



Figure 7-15: 3 kW rig with dual filter system to measure fines in filters. The system is also combined with a pressurised air system to return separated OCM back into the reactor to maintain mass circulation.

The unit is filled with OCM materials at room temperature. After filling of the reactor through the air reactor inlet, particles are distributed in the whole rig. The distribution process is monitored by the pressure distribution and fluctuation in the different part of the rig. This will need around 10-15 L/min in the air and fuel reactor, depending on OCM's tap density, sphericity, and particle size. The gas velocity regime is adjusted so that the particles circulate through the rig until the cyclone releases a rather low amount of materials to the filtering systems. Afterwards, the hot attrition test was performed at 900 and 950°C. Under CLC condition, air and 4% H₂ were used in the air and fuel reactor, respectively. The fuel and air reactor gases are pre-heated to 600°C by in-line heaters. Replaceable filter system is installed on both the air and fuel reactors' outlet lines. The pore size of the installed filters is 5 µm. Fines are continuously collected in the filters and are manually measured every 1 or 2 hours depending on the amount of fines collected. The filtration system is equipped with a particle return system, which allows the user to return large particles back to the reactor. These are large particles that have left the reactor due to imperfection of the cyclone separation.

For the hot attrition of ilmenite T2, 1085 g of materials was used to measure the attrition rate at 900 and 950°C, similar to the temperatures for pilot testing. It is clearly shown from Figure 7-16 that the materials

have a faster attrition rate at the beginning of 900°C and become slower and even level out as testing continues. As temperature increases to 950°C, there is no increase in attrition rate for ilmenite T2, indicating that ilmenite has good mechanical strength under CLC conditions.

For the hot attrition of LY-Mn ore, 937 g of material was used for measuring attrition rate only under hot air condition, i.e., air was used for both fuel and air reactors. The LY-Mn shows very high attrition rate even under hot air, which is around 4-5 times higher than ilmenite T2 (c.f. Figure 7-16). The fines are easy to agglomerate as shown in Figure 7-17. Considering such a high attrition rate, we had to stop the testing to prevent the fines to be accumulated inside the reactors and other parts of the rig.

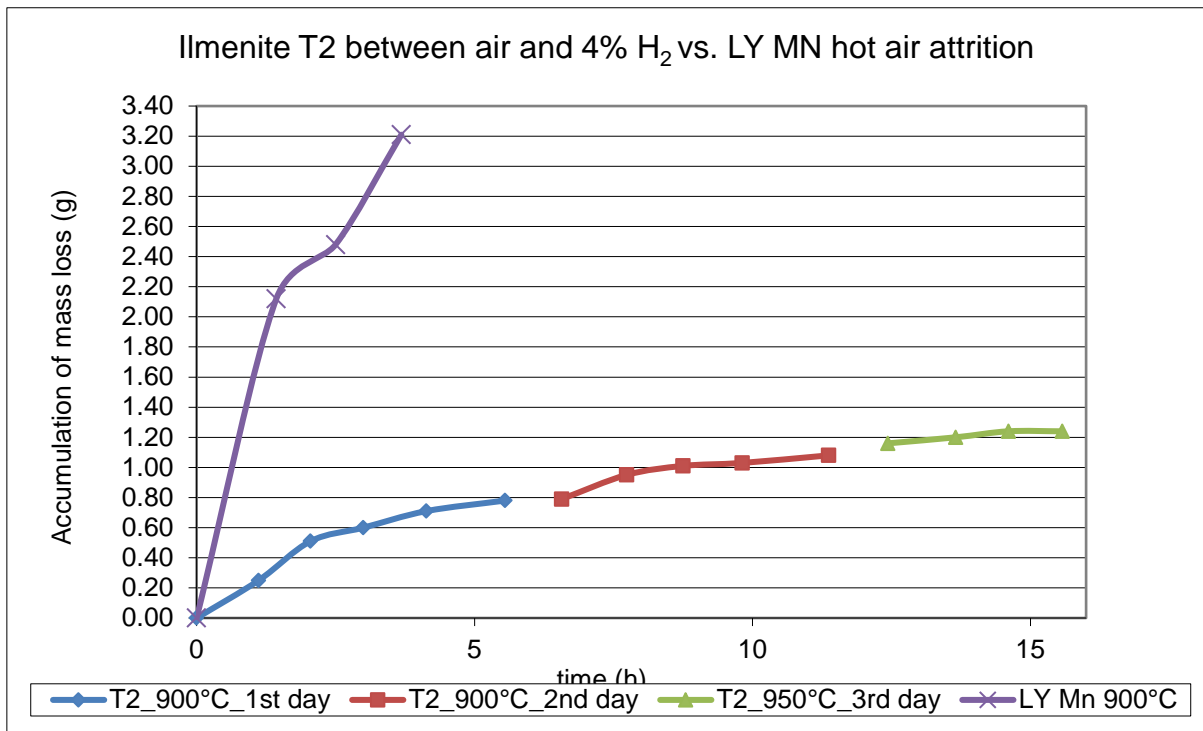


Figure 7-16: Accumulated fines for LY-Mn and ilmenite T2 as a function of time.



Figure 7-17: Agglomeration of LY-Mn fines in a filter.

7.2.2 Kinetics of ilmenite T2 vs other candidate materials

When evaluating redox performance of ilmenite using TGA, the oxygen release rate was also derived. For ilmenite T1 and T2, the rates are equal, and comparable to other Fe-rich and Mn-rich ores, as shown in Figure 7-18. Detailed information can be found in deliverable D3.1.

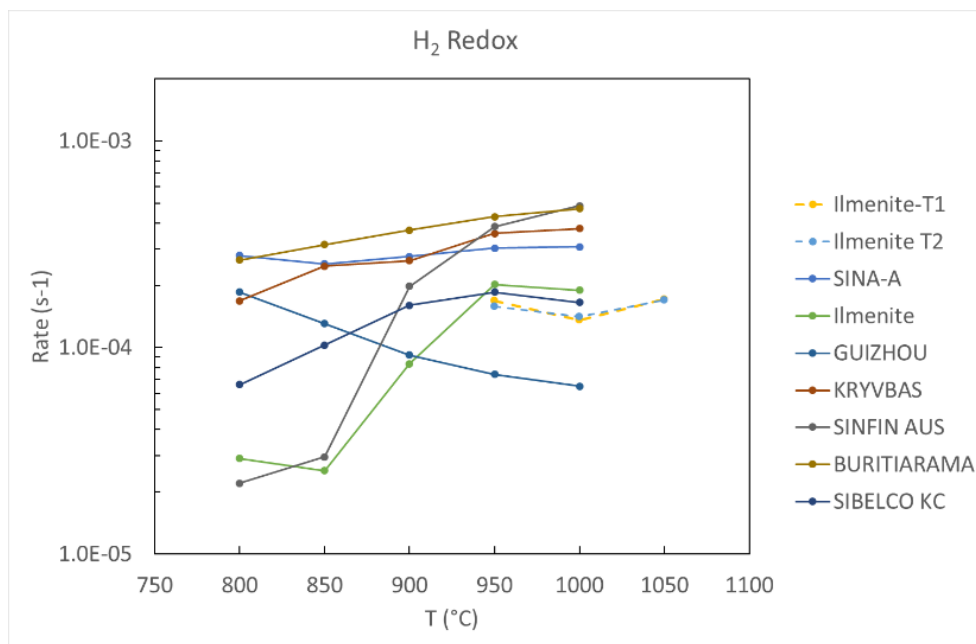


Figure 7-18: Oxygen release rate of Ilmenite T1 and T2 in size fraction range 210-300 μm , between 5% H₂ and 20% O₂ as a function of temperature, compared to other and similar minerals in size range 125-180 μm .

7.3 SINTEF ER

7.3.1 Main test results

Tests were also carried out using the so-called ilmenite T2, which is similar to the ilmenite T1 that has been extensively tested in the reactor before, but with a larger particle size fraction (d_{50} around 210 μm). Because of the size of the particles, it was uncertain if it was possible to obtain the needed particle circulation in the reactor system. The reactor system requires a minimum of particle circulation, not only to transport the oxygen needed for the combustion, but also to transport heat from the exothermic AR to the FR, so the FR temperature is maintained at a level where the reaction rates is sufficiently high (above 950°C). The temperature development in the system can easily come into a negative spiral if the temperature starts to drop in the FR because this leads to reduced fuel conversion, which leads to a lower degree of reduction of the metal oxide, which again leads to lower heat release in the AR since less oxidation can take place.

Both milled wood pellets and petcoke was tested as fuels, in a one-day experiment, where the first 2.5 hours of testing were used to gradually activate the ilmenite. The experiment was run with a higher surplus of air than normally used, which led to an AR superficial velocity of around 5 m/s compared to 3 – 3.5 m/s which is normally used. It was then possible to obtain fuel conversion and capture rates comparable to what was found for the ilmenite T1 previously tested. However, when using milled wood pellets as fuel, it was necessary to add around 1 kg/h (around 12.8 kW) of propane to air reactor, to prevent the temperature from dropping. Combustion in the air reactor consumes oxygen and can thus hinder the oxidation of the oxygen carrier. However, because of the large surplus of air, this effect is believed to be negligible. When using petcoke as fuel, there was no need for any propane addition to the air reactor. This is because the residence time in the FR is not long enough to completely gasify the petcoke, which leads to transport of char/unconverted petcoke to the AR. The char combusts in the AR and release heat.

The main operating conditions are shown in Table 7-1 and the main performance results are shown in Table 7-2. FR gas conversion efficiency using biomass is at about 80 %, which is at the same level as found when operating with ilmenite T1, and somewhat higher than for Mn-ore LY which had about 65 – 67 %. The capture rate with biomass is very high, 98 %, about same level as obtained with biomass and Mn-ore LY, indicating very little carbon is transported to the AR. For the test with biomass the carbon balance indicates that 10,9 % more carbon is leaving FR and AR as gaseous components than the amount of carbon fed with the fuel. This is not physically correct (indicated with red fonts) and is a consequence of uncertainties mentioned in section 2.1.4. Biomass cases with deviation within about 10 % is included as test results since there are several uncertainties that can affect the results.

Table 7-1: Main operating conditions SINTEF ER pilot unit test with ilmenite T2.

Test No.	Type of fuel	Fuel feed rate (kg/h)	Fuel power (kW)	AR top / bottom temp. (°C)	FR top / bottom temp. (°C)	AR riser mass flow (*) (kg/s)	FR inventory (kg)	Specific FR inventory (kg/MW)
T2-1	Bio milled unsieved	23.7	125.3	1020 / 1015	936 / 949	7.6	28.5	227
T2-2	Petcoke with fines	13.9	116.3	1010 / 1004	942 / 965	9.9	35.5	305

(*) Analytically calculated theoretical riser mass flow as described in Ch.2.1.3.

Table 7-2: Main performance results from SINTEF ER pilot unit test with ilmenite T2.

Test No.	Type of fuel	Fuel carbon conversion X_{fuel-C} (*) (% of total fuel carbon)	Carbon leaving AR (as CO ₂) (% of total fuel carbon)	Carbon out as FR and AR gas components (% of total fuel carbon)	Carbon balance = carbon out FR as particles (% of total fuel carbon)	FR gas conv. efficiency (%)	CO ₂ capture rate (%)
T2-1	Bio milled unsieved	109.8	1.1	110.9	-10.9	79.6	98.9
T2-2	Petcoke with fines	17.5	57.7	75.2	24.8	79.9	42.3

(*) Fuel carbon conversion is equivalent to amount of fuel carbon leaving FR as gas components.

The petcoke case with ilmenite T2 shows somewhat higher CO₂ capture rate than for petcoke using ilmenite T1, 42 vs 33 %, while FR gas conversion efficiency is lower, 80 vs 95 %. The fuel carbon conversion is only 17.5 % which is slightly lower than for the Mn-ore petcoke cases with about 20 %. However, the quality of the outflowing FR gases is better than for the Mn-ore cases, with a FR gas conversion efficiency of about 80 % compared to 63 – 72 % for the Mn-ore petcoke cases.

In the petcoke case, the ratio of the gaseous carbon leaving the system to the carbon fed to the system is 75,2 %. This indicates a loss of 24,8 % unconverted petcoke fines out with the FR exhaust gases. This high amount of loss is clearly observed in the particle sample analysis below. After test T2-2 with petcoke, some samples from the FR wet exhaust scrubber were dried and put in a muffle oven to burn away any organic matter (the oxidation of OC is not considered, meaning that the actual loss of organic matter is even slightly higher than the weight reductions shown below):

- The sample from the FR wet scrubber overflow showed 73 % weight reduction.
- The sample from the FR wet scrubber bottom showed 25 % weight reduction.

This clearly indicates the high amount of very fine petcoke particles that goes out from the FR in this case.

7.3.2 Oxygen carrier characterisation

The ilmenite T2 was used as received, i.e., the size was in the range 150 – 350 µm. SEM and EDS pictures of the fresh material is shown in Figure 7-19. The material is homogeneous in Fe and Ti oxides, with only very few inclusions of other oxides.

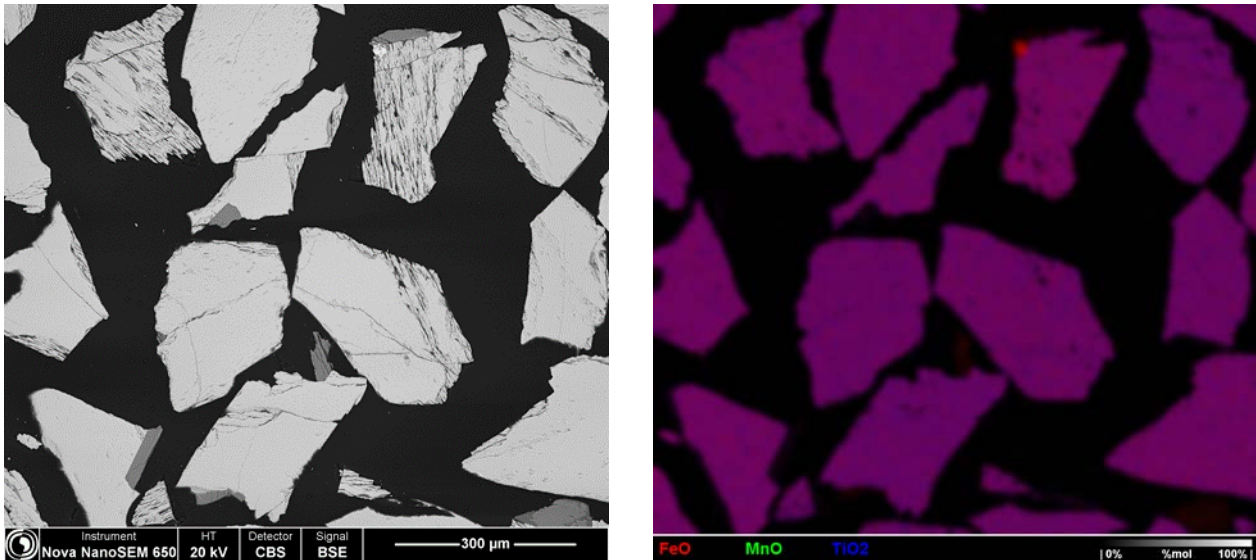


Figure 7-19: Fresh ilmenite T2 used in pilot unit at SINTEF ER, SEM (left) and EDS (right).

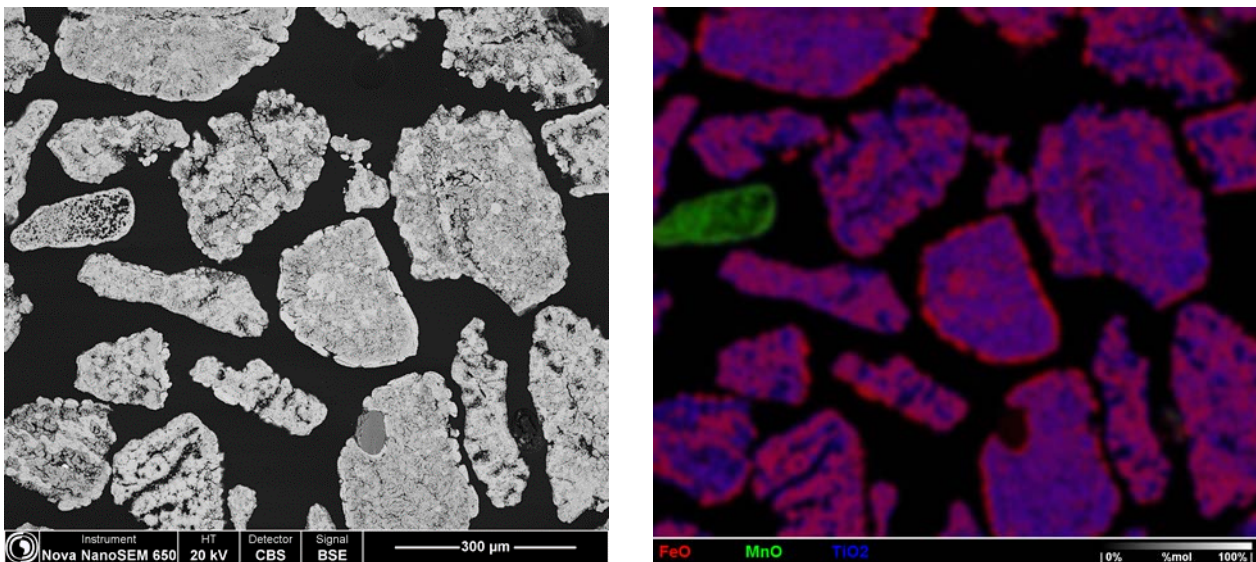


Figure 7-20: SEM and EDS of samples from AR reactor taken out after test.

SEM and EDS of samples taken out from AR reactor after test (Figure 7-20) show high level of microporosity, but particles remain mostly coherent. Iron and titanium oxides mostly dissociated, iron enrichment to surface. This is same development as for ilmenite T1 and typical for ilmenite oxygen carriers. In Figure 7-21 is shown SEM and EDS of samples from FR bucket and chamber. It shows high level of microporosity in large particles and presence of many "fines" and small average particle size. There are also some non-ilmenite particles present. The samples contain much organic matter, i.e., unconverted petcoke particles, as can be seen as dark grey particles in between the brighter OC particles. This is more clearly seen in the magnification shown in Figure 7-22. This verifies the carbon balance of 75 %, indicating that a significant fraction of unconverted fuel particles leaves the FR.

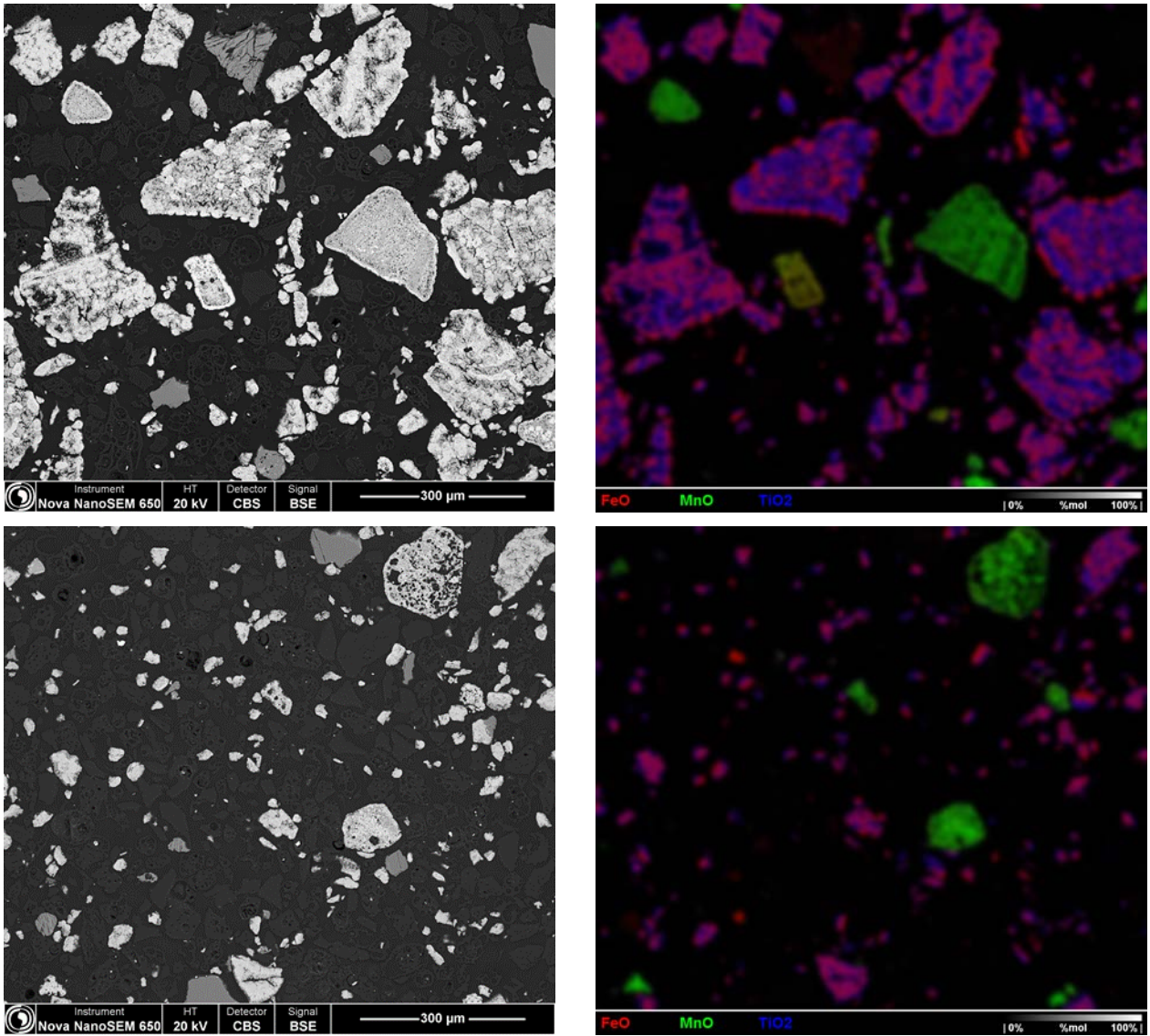


Figure 7-21: SEM and EDS of sample from FR bucket (top) and FR chamber (bottom) after petcoke test.

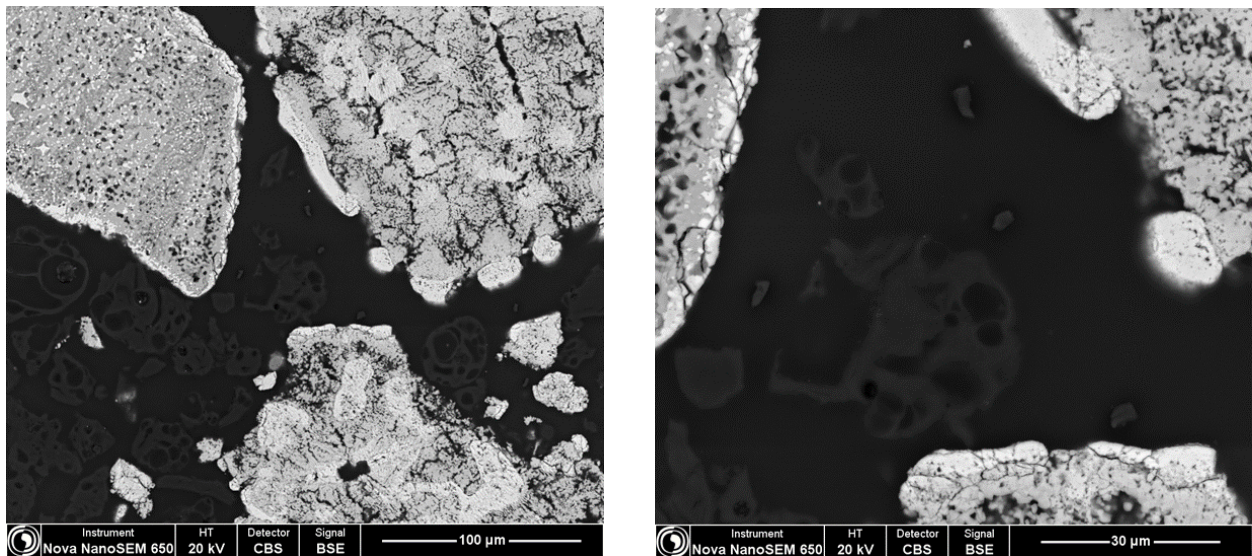


Figure 7-22: Magnified SEM picture of sample from FR bucket after petcoke test.

7.3.3 Agglomeration and operability

After the test, some lumps were found in the FR reactor. From the SEM and EDS pictures (Figure 7-23) it is seen this is a loose agglomerate of large particles. Mostly composed of ilmenite, only partially dissociated into Fe and Ti oxide. The surface of the particles is enriched in Fe oxide, with a titanium oxide rich sublayer. The particles seem fused through the iron oxide layer.

During operation, there were no signs of agglomerates causing process upsets. The ilmenite T2 were easy to operate as long as enough fluidisation air was available in the AR. From this rather short test it is difficult to draw conclusions, but from qualitative judgement the operability was at least as good as for ilmenite T1 and Mn-ore LY. Less AR cyclone/downcomer upsets were observed, indicating that larger particles than used earlier may be beneficial to this issue.

The ilmenite T2 tests were operated with a large reactor inventory and a high AR riser mass flow. A relatively small fraction of the OC oxygen capacity was therefore utilized. As discussed in chapter 5.1.4, the oxygen carrier particles will not be very "stressed" and far from fully reduced. A highly reduced material is more prone to agglomeration. Such a condition will be more likely in the demo unit with much larger residence times and less overall oxygen surplus. The design of the IFPEN pilot unit is more equal to the demo unit in that respect.

The high amount of fluidisation air needed causes a large excess air ratio, in the range 1.35 – 1.5. This is not wanted from a process efficiency point of view. The SINTEF ER pilot unit is originally not designed for such large OC particles as ilmenite T2. The test with T2 was mainly to check if it could work at all in this unit, if there were clear operational differences from ilmenite T1, and if we could see a higher tendency to agglomeration. Except for the needed air excess, the test revealed no clear differences from T1 operation.

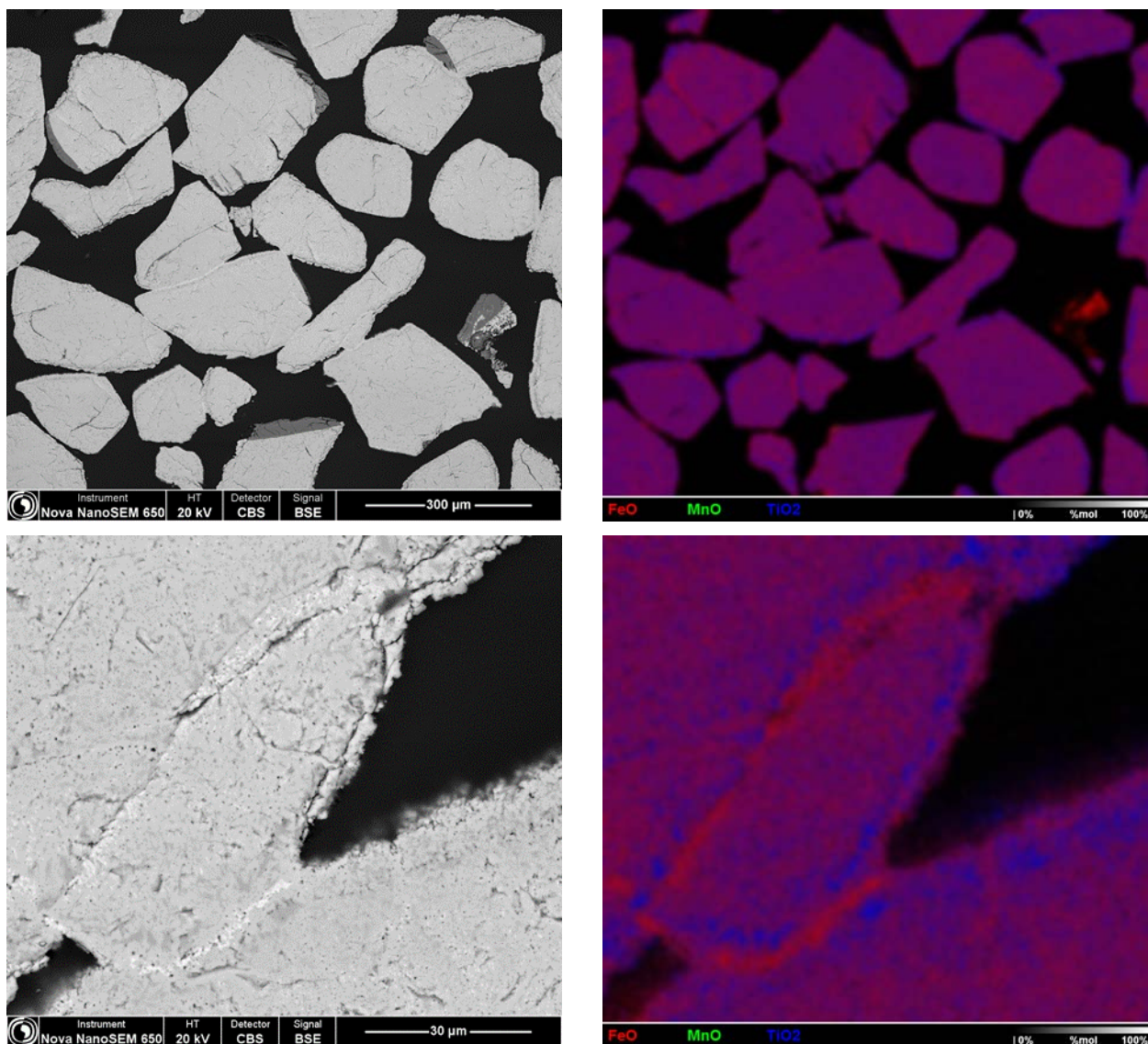


Figure 7-23: SEM and EDS of lump from FR reactor (top), with magnified view (bottom).

7.3.4 Summary from operation of ilmenite T2 in 150 kW unit

Operation with ilmenite T2 in the SINTEF ER pilot unit was smooth as long as enough air was available for fluidisation of these large particles. No agglomeration problems were observed during operation, however, after testing, some lumps were found in the FR. SEM-EDS revealed they were loose agglomerates of large particles.

As for both ilmenite T1 and Mn-ore LY, the CO₂ capture rate is high for biomass (about 98 % at the best), whereas it is low for petcoke fuel (less than 50 %). Again, it should be noted that the SINTEF ER pilot unit does not have a carbon stripper and the residence time in the FR is relatively short. The low capture rate for petcoke is mainly a consequence of this, and not the oxygen carrier itself.

For biomass, no fuel seems to leave the FR as unconverted fuel particles. All is in gaseous form and the gas is about 80 % fully converted. This is higher than for Mn-ore LY which showed about 65 – 67 % gas conversion

(but the Mn-ore LY value may also be attributable to low solid circulation and low fuel power/FR fluidisation). The ilmenite T2 gas conversion is at same level as for ilmenite T1 with biomass.

With petcoke, the FR gas conversion efficiency is the same as for biomass, about 80 % converted. This is higher than for Mn-ore LY which showed about 63 – 72 %. In addition, some unconverted fuel particles go out with FR exhaust, about 25 % of the fuel feed. This is lower than for Mn-ore LY where it was 28 – 30 % of the fuel feed.

SEM and EDS of OC samples taken out after test, show high level of microporosity, but particles remain mostly coherent. Iron and titanium oxides are mostly dissociated, with iron enrichment to surface. This is the same development as for ilmenite T1 and typical for ilmenite oxygen carriers. After the test, some lumps were found in the FR reactor that was shown to be loose agglomerates of large particles. Mostly composed of ilmenite, only partially dissociated into Fe and Ti oxide. The surface of the particles is enriched in Fe oxide, with a Ti oxide rich sublayer. The particles seem fused through the Fe oxide layer.

8 CONCLUSIONS

Results based on IFPEN studies both in batch and continuous unit have shown that the reactivity of LY Mn ore is high enough to convert the gases produced by petcoke gasification. In IFPEN's 10 kW pilot unit with high solid residence time, a petcoke conversion of up to 89% was observed without any recycle of unburnt petcoke. It was observed that LY Mn ore has a high initial $RO\Delta X$ value ($RO\Delta X=0.8$), which lead to shorter activation period in comparison to the campaign with Ilmenite T1.

A parametric study has confirmed the tendencies observed in IFPEN's batch unit for both LY Mn and Ilmenite T1:

- Fuel reactor temperature: as expected, fuel reactor temperature significantly increases solid fuel conversion and oxygen transfer capacity of the oxygen carrier.
- Petcoke flowrate: it has a significant effect on reduction potential of oxygen carrier in the fuel reactor, where it is possible to double the $RO\Delta X$ value by adjusting the petcoke flowrate.
- Oxygen carrier flowrate affects $RO\Delta X$ value significantly, since it determines the oxygen availability for the combustion of gas released by petcoke gasification.

Regarding LY Mn ore, the mean value of inventory loss under methane exposure is 0.30%/h (or 0.12 kg/h) which leads to a particle lifetime of approximately 331 hours. With petcoke, the inventory loss is around is 0.21%/h, leading to a particle lifetime of 482 h. Fragmentation of LY Mn ore seems to be more important with methane as fuel. In addition, in conditions of higher petcoke flowrate, operation at high $RO\Delta X$ values is possible. These are encouraging results regarding large scale operation with LY Mn ore as an oxygen carrier.

Similarly, Ilmenite's reactivity is high enough to convert the gases produced by petcoke gasification. In IFPEN's 10 kW pilot unit, a petcoke conversion up to 73% was observed without any recycle of unburnt petcoke. A parametric study has confirmed the same tendencies observed with LY Mn ore. In terms of mechanical performance, ilmenite structure is stressed a lot by redox cycling, and cracks are observed in the activated particles. The mean inventory loss is 0.07%/h for a $RO\Delta X$ value of 1.4% which corresponds to a bed lifetime of approximately 1430h.

Hot attrition testing by SINTEF MK in a 3-kW dual fluidized bed reactor, clearly shows the higher attrition rate and fines production when operating Mn-ore LY compared to ilmenite. From the filter samples it was also seen that fines easily agglomerated.

The pilot unit operation in SINTEF ER 150 kW unit rely on auto-thermal operation, and operating conditions varies between the different cases and OCs. Especially for ilmenite T2 where inventory and fluidization air had to be considerably increased to circulate enough of the larger particles. However, some clear trends can be seen. Capture rate of 90 % and higher is obtained for the tested biomass fuels, whether whole pellets, milled and sieved, or milled and un-sieved. This holds for both Mn LY and the ilmenites (T1 and T2). For petcoke fuels, the capture rate is considerably lower. Except one very special case (capture rate 18.3 %), the petcoke cases show 33 – 52 % capture rate. The higher values are for Mn LY, which is also consistent with a slightly higher petcoke conversion for the Mn LY, 21 – 22 % compared to 17.5 % for ilmenite T2. Even though the Mn LY cases were operated with much less circulation and FR inventory.

The FR gas conversion efficiency for Mn LY was lower than for ilmenite for both biomass and petcoke fuels. In the range 63 – 72 % compared to 80 – 90 % for the ilmenites T1 and T2. It should be noted that the Mn LY cases had lower OC circulation and FR inventory, and low OC particle entrainment up the FR. However, also the ilmenite T2 cases had low particle entrainment up the FR, even though the global circulation was higher.

Much of the OC is instead returned to the AR via the lifter. Even though, the FR gas conversion efficiency was 80 % for both the biomass and petcoke case.

The fuel conversion and capture rate of the SINTEF ER unit are hampered by rather low residence time and not having a carbon stripper, especially for a slow reacting fuel as petcoke. On the other hand, the unit has very few parts with dense bed of OC where particles in reduced state can agglomerate. No severe agglomeration needing shut-down was observed during operation. However, some lumps and agglomerates were found inside the system at the end of the different tests. The IFPEN 10 kW unit is more equal to the 3 MW demo unit in that respect, and the tests clearly show that dense bed volumes and low-velocity zones need special precautions.

The ilmenites T1 and T2 showed equal performance in the IFPEN batch unit and in SINTEF ER pilot unit. However, the initial batch unit tests showed severe agglomeration using T2, and more limited agglomeration with T1. The ilmenite T2 is delivered completely dry whereas T1 contains some water. When some steam was added to the batch unit during heat-up and methane activation of T2, the agglomeration tendency was considerably reduced. In the 3 MW demo unit, the heat-up sequence will be done with natural gas and lignite, giving a water content about equal to what was applied in the batch unit test. In the SINTEF ER pilot unit, no severe agglomeration was observed with the ilmenite T2. One reason might be the high circulation, keeping the OC material from not being highly reduced. In addition, the heat-up sequence under air conditions, and the first period of red-ox cycling is done with propane and hydrogen fuel gas already from about 300 °C upwards. This introduces a significant amount of water which, according to the batch unit tests, may also help to reduce the agglomeration.

Given the almost similar performances of ilmenites and LY Mn ore, the higher attrition rate and fines production of LY Mn ore, and the interesting price of ilmenites compared to LY Mn ore, ilmenite seems to be the best candidate. The additional batch unit tests of T2 with water addition, and the T2 being already at the wanted particle size, orient the choice of the OC for the 3 MW demonstration unit towards ilmenite T2.

9 REFERENCES

- [1] Øyvind Langørgen, Inge Saanum, Nils Erland L. Haugen. Chemical looping combustion of methane using a copper-based oxygen carrier. 13th Conference on Greenhouse Gas Control Technologies (GHGT), 14 to 18 November 2016, Lausanne, Switzerland, Energy Procedia 114 (2017) 352 – 360.
- [2] Ø. Langørgen, I. Saanum, N.E. Haugen, Chemical Looping Combustion of biomass in a 150 kWth CLC pilot unit, 5th International Conference on Chemical Looping, 24-27 September 2018, Park City, Utah.
- [3] Markström, P., C. Linderholm, and A. Lyngfelt, Operation of a 100 kW chemical-looping combustor with Mexican petroleum coke and Cerrejón coal. Applied Energy, 2014. 113: p. 1830-1835.
- [4] Markström, P. and A. Lyngfelt, Designing and operating a cold-flow model of a 100 kW chemical-looping combustor. Powder Technology, 2012. 222: p. 182-192.
- [5] C. Linderholm, P. Knutsson, M. Schmitz, P. Markström, A. Lyngfelt, Material balances of carbon, sulfur, nitrogen and ilmenite in a 100 kW CLC reactor system. International Journal of Greenhouse Gas Control, 27 (2014), pp 188-202
- [6] K.S. Milenkova et al., Devolatilisation behaviour of petroleum coke under pulverised fuel combustion conditions. Fuel, 82 (2003) 1883–1891

Page 80:

Linderholm et al. 2014; Linderholm et al. 2016; Linderholm, Lyngfelt et Dueso 2013; Linderholm et al. 2012

A MODIFICATIONS DONE AT SINTEF ER PILOT UNIT

The CLC reactor system was originally designed for gaseous fuels, and modifications have been done to be able to use solid fuels. Most of these were made before the CHEERS project. However, during the first part of the CHEERS project, additional improvements have been made to better suit the use of petcoke as fuel:

- New screw feeder for solid fuel feeding to FR. The old solid fuel feeding screw was a rather large and rough one, ideal for feeding e.g., pellets. However, for small fuel particles and powder it was not applicable. A smaller and much more appropriate volumetric screw feeder from Coperion K-Tron was installed instead. The installation is made so that we can change between the two screws with some small amount of mechanical work.
- Installation of a small steam generator and a new coriolis steam mass flow meter to measure the steam flow to the FR. For efficient petcoke gasification it is important to introduce enough steam. A small steam boiler was acquired and installed, including necessary modifications to the pipe system to be able to feed steam to the FR fluidisation nozzles.
- Installation of thermal mass flow controllers for N₂ fluidisation of loop seals and lifter. The old valves for controlling the loop-seals and lifter fluidisation were no longer working properly. These small fluidisation streams need to be controlled accurately, and especially the lifter fluidisation which is very important for the circulation in the system. Five thermal mass flow controllers were installed, all of which old ones taken down from an earlier reactor system.
- Installation of two heater cables for reactor heating. 10 kW heating cables were mounted, one on each reactor, including necessary electric power supply and insulation work.
- Particle settling chambers for recycling of OC loss from cyclones. The reactor system had from earlier a bucket for OC sampling just after the cyclones. Just downstream of these, a low velocity particle settling chamber was mounted for each reactor exhaust flow. Almost all particles lost through the cyclones are now captured by these chambers.
- Dust minimisation at fuel bin filling. The petcoke fuel is from HSE considerations more severe than the biomass fuels that has been operated earlier. The fuel filling bin was therefore equipped with an evacuation system to ensure a small under-pressure during filling. This measure reduced the dusting to almost zero.
- Installation of a new on-line gas analyser on fuel reactor exhaust line. The earlier Teledyne analyser showed poor repeatability and the CO cell broke down. It was therefore replaced by an Emerson Rosemount X-stream analyser for CO₂, CO and O₂ measurements on the FR exhaust stream.
- Installation of continuous flushing system of pressure transducer tubing. Because of pressure fluctuation in the reactor, OC particles tends to get pushed into the tubes to the pressure transducers and cause plugging. This results in erroneous pressure measurements. The flushing system consists of sonic nozzles (0.4 mm) that ensures a small flow (4 NI/min) of gas through each of the tubes, unaffected by pressure variations in the reactor system. This flushing is preventing particles from entering the pressure measurement line, while at the same time, the flow is slow enough to not influence the pressure measurement.



Figure A-1: Steam boiler



Figure A-2: Thermal mass flow controllers for loop seal and lifter fluidisation



Figure A-3: Reactor heating cable



Figure A-4: Particle settling chamber



Figure A-5: Volumetric fuel feeding system

B SUMMARY OF MAIN RESULTS SINTEF ER PILOT UNIT

Test No.	Type of fuel	Fuel feed rate (kg/h)	Fuel power (kW)	AR top / bottom temp. (°C)	FR bottom temp. (°C)	AR riser mass flow (*) (kg/s)	FR inventory (kg)	Specific FR inventory (kg/MW)	Fuel carbon conversion X_{fuel-c} (*) (% of total fuel carbon)	Carbon leaving AR (as CO ₂) (% of total fuel carbon)	Carbon out as FR and AR gas components (% of total fuel carbon)	Carbon balance = carbon out FR as particles (% of total fuel carbon)	FR gas conv. efficiency (%)	CO ₂ capture rate (%)
T1-1	Biomass pellet		108.6	1019/ 1011	996	7.4	27.5	253.2					81.9	88.3
T1-2	Biomass milled/ sieved 1		99.7	1010/ 1000	976	3.4	12.2	122.4					80.2	92.3
T1-3	Biomass milled/ sieved 2		113.0	998/ 989	961	3.8	10.0	88.8					78.3	91.1
T1-4	Biomass milled/ un-sieved		120.3	991/ 983	954	2.9	15.4	127.8					79.4	93.5
T1-5	Mix b/p 75/25		80.5	998/ 989	973	4.7	20.0	248.6					89.1	64.8
T1-6	Mix b/p 50/50		93.1	1001/ 990	974	4.8	22.6	242.8					90.9	47.5
T1-7	Petcoke 315–500		126.6	1041/ 1015	1011	3.9	23.5	185.6					95.7	33.2
T1-8	Mix b/p 50/50 w/fines		109.4	999/ 991	966	4.8	28.7	262.3					85.5	57.6

Test No.	Type of fuel	Fuel feed rate (kg/h)	Fuel power (kW)	AR top / bottom temp. (°C)	FR top / bottom temp. (°C)	AR riser mass flow (*) (kg/s)	FR inventory (kg)	Specific FR inventory (kg/MW)	Fuel carbon conversion X_{fuel-c} (*) (% of total fuel carbon)	Carbon leaving AR (as CO ₂) (% of total fuel carbon)	Carbon out as FR and AR gas components (% of total fuel carbon)	Carbon balance = carbon out FR as particles (% of total fuel carbon)	FR gas conv. efficiency (%)	CO ₂ capture rate (%)
MnLY-1	Bio milled unsieved	22.0	115.9	1008 / 1006	954 / 967	2.1	15.1	130	109.0	3.7	112.6	-12.6	64.8	96.3
MnLY-2	Bio milled unsieved	22.0	115.9	1015 / 1013	960 / 973	1.9	17.0	147	108.9	3.2	112.1	-12.1	67.1	96.8
MnLY-3	Petcoke w/o fines	10.0	83.3	1038 / 1025	956 / 975	1.3	15.4	185	19.9	81.7	101.6	-1.6	70.5	18.3
MnLY-4	Petcoke with fines	12.0	100.3	1002 / 998	939 / 945	1.4	16.3	163	21.2	50.9	72.2	27.8	63.6	49.1
MnLY-5	Petcoke with fines	12.0	100.3	1021 / 1018	945 / 958	1.4	16.3	162	18.8	52.1	70.9	29.1	63.8	47.9
MnLY-6	Petcoke with fines	12.0	100.4	1013 / 1011	945 / 957	1.6	18.7	186	20.5	51.0	71.5	28.5	68.2	49.0
MnLY-7	Petcoke with fines	12.0	100.2	1012 / 1009	955 / 970	2.1	20.5	204	21.8	48.0	69.9	30.1	72.8	52.0
T2-1	Bio milled unsieved	23.7	125.3	1020 / 1015	936 / 949	7.6	28.5	227	109.8	1.1	110.9	-10.9	79.6	98.9
T2-2	Petcoke with fines	13.9	116.3	1010 / 1004	942 / 965	9.9	35.5	305	17.5	57.7	75.2	24.8	79.9	42.3